Funded by
the European Union

Collaborative project

Project acronym: SNM

Project full title: "**Single Nanometer Manufacturing for beyond CMOS devices**"

Grant agreement no: 318804

Deliverable: D7.6 ("Measurements on SNM patterned material using TEM, AFM & FIB")

Name of the coordinating person: Prof. Dr. Ivo W. Rangelow, Email: ivo.rangelow@tu-ilmenau.de

List of participants:

Participant no.	Participant organisation name	Part. short name	Activity Type	Country
1 (Co)	Technische Universität Ilmenau	**TUIL**	HER	Germany
2	EV Group E. Thallner GmbH	**EVG**	IND; End-user	Austria
3	IMEC	**IMEC**	RES	Belgium
4	Mikrosistemi Ltd	**µS**	SME; End-User	Bulgaria
5	Universität Bayreuth	**UBT**	HER	Germany
6	Technische Universiteit Delft	**TUD**	HER	Netherlands
7	Spanish National Research Council	**CSIC**	RES	Spain
8	IBM Research GmbH	**IBM**	IND; End-user	Switzerland
9	École polytechnique fédérale de Lausanne	**EPFL**	HER	Switzerland
10	SwissLitho AG	**SL**	SME; End-User	Switzerland
11	Oxford Instruments Nanotechnology Tools Ltd	**OINT**	IND; End-user	UK
12	Imperial College London	**IMPERIAL**	HER	UK
13	The Open University	**OU**	HER	UK
14	Oxford Scientific Consultants Ltd	**OSC**	SME	UK
15	VSL Dutch Metrology Institute	**VSL**	IND	Netherlands

16	University of Liverpool	**ULIV**	HER	UK

SNM Work Package 7 Deliverable: D7.6 ("Measurements on SNM patterned material using TEM, AFM & FIB")					
Lead beneficiary number	9	**Nature**	R	**Dissemination level**	CO
Estimated Person-months	51.50				
Person-months by partner for the Deliverable	TUIL: 6,375; VSL: 11.5; EPFL: 12; IBM: 4; OSC: 14; CSIC: 4; OINT: 2; OU: 2 Sum: 55.85				
Estimated Delivery Date	Mx: 12/2016	**Delivery Date**	10/03/17 05/09/17 revised version		
Author	• Andras Kis, Richard Koops, Philip Prewett, Marcus Kästner, Armin Knoll				
Reviewed by:	• WP7 Leader: Marijn van Veghel • WPG2 Leader: Mike Cooke • Coordinator: Ivo W. Rangelow				
Criteria and Achieved Results	**Criteria**	**Achieved result**			
	Critical dimension measurements possible on SNM patterns.	SNM patterns have been characterised using TEM, AFM, He-ion microscope.			

TUIL	VSL	EPFL	IBM	OSC	CSIC	OINT	OU
6,375	11.5	12	4	14	4	2	2

Funded by
the European Union

Description of the Deliverable

Executive Summary

- EPFL: Transmission electron microscopy (TEM) measurements on electron-beam induced deposition (EBID) patterns

TEM imaging allows monitoring the etching process of small nanostructures, patterned with EBID. EPFL was able to image lines before and after etching with high resolution scanning TEM (STEM) and reveal the main features of our patterns:

- Pt/C composition of initial EBID patterns.
- Dimensions of the deposited EBID patterns,
- Change of high angle annular dark field (HAADF) intensity, corresponding to etching process
- Comparison between HAADF and energy-dispersive x-ray (EDX) maps shows, that after etching Si is thicker on the parts, masked with Pt deposits. This confirms, that etching indeed took place.
- Impact of etching on the EBID patterns. The redistribution of Pt has been seen. Also, we could not reveal the carbon presence in the written lines after etching, which might imply that there is interaction between plasma etching and Pt/C EBID patterns, which destroys them in some way. Optimization of etching process in future might allow to avoid this damage.

- EPFL: Transmission electron microscopy (TEM) measurements on SPL-patterned samples
  - Graphene was deposited on Si3N4 membranes to create a robust, transparent and electrically conductive substrate, required for TEM imaging of SPL-patterned samples
  - The sample was patterned using SPL and measured via AFM
  - TEM imaging of the patterned areas could not resolve the pattern, presumably due to low contrast of the patterned area where TEM should have to resolve the difference between the 20 nm thick Si_3N_4 with and without the low molecular weight resist

- VSL: Atomic force microscopy (AFM) measurements on EVG Nanoimprint Lithography (NIL) samples

NIL samples were manufactured by EVG and measured independently by two different AFM systems. Since the measurement setup at EVG was not optimized for accurate measurements, the samples were shipped to VSL. The VSL measurements were performed with a calibrated system and known probe shape enabling the correction of probe shape effects and calculation of the measurement uncertainty to enable quantitative comparison of data. The results with a calibrated measurement system show a more consistent result, within the measurement uncertainty, for the pitch, line width and depth compared to the data reported in D10.2.

- VSL: AFM measurements on TUIL Scanning Probe Lithography (SPL) samples

Measurements on the line width, line width roughness (LWR), line edge roughness (LER), profile depth and profile shape were performed successfully on the etched SPL pattern from TUIL. Comparison of measurement results on these samples is challenging since the results depend on the exact measurement position and instrumental settings and probe characteristics. Since the TUIL data were provided only for the depth and without measurement uncertainty a quantitative comparison is not possible but the results on the depth measurements are similar.

- VSL AFM measurements on Nanowire sample from UBT

These measurements were performed to study the potential application of this type of nanowire as reference structures for height and diameter calibration purposes. It was found that the measured height of the nanowire structure is dependent on the measurement settings of the AFM. The apparent height varies between (1.4 ± 0.3) µm and (2.8 ± 0.3) µm for a range of the AFM tapping mode setpoint parameter values that result in stable imaging. Application of these nanowires as reference structures is therefore not very likely since the choice of the setpoint parameter value is arbitrary within the range of stable imaging.

- OSC Measurements using a helium ion microscope (HIM)

OSC conducted HIM measurements on SPL patterned calixarene resist and on helium ion beam patterned novel fullerene resist from WP5. Free surface energy effects were imaged and analysed in the gold anti-charging layer of the SPL samples. For the fullerene samples, HIM was capable of distinguishing optimal lithography conditions. Measurements of line edge roughness and the shot noise limits of the lithography were also successful.

- TUIL AFM measurements

For investigation of resist materials, their morphology, aging and dewetting behavior the resist surface was investigated by AFM methods.

In order to characterize FE-SPL patterned features, as well as its etching result (cryogenic plasma etching, ALE, etc.), regular AFM topographic measurements (AM-AFM) were carried out. In this context, for automatic extraction of geometric feature data (line width, line depth, etc.) from AFM images an analysis program was programmed.
TUIL has patterned a 10 nm hp dense line/space feature into novel UBT8:C60 molecular glass resist. In order to compare the AFM characterization methods TUIL has initially measured the pattern (pitch, line width & patterning depth) and subsequently sent the sample to VSL for comparative measurement. Here, the VSL system is traceable (calibrated by national standards). The VSL measurement results are described in section 2.2, wherein also the measurements of TUIL and VSL are compared.

Three samples prepared by FE-SPL and subsequently etched by atomic layer etching (OSC) or cryogenic plasma etching (TUIL) the line width and line depth were measured by using three different methods, in particular AFM (TUIL), SEM (TUIL) and xTEM (IMEC). The quantitative comparison of the measurements should address the applicability of these methods for sub-10nm feature analysis. Comparable results for pitch measurements were obtained by SEM, AFM and xTEM. Line width measurements of SEM, AFM and xTEM agreed within

	measurement uncertainty. The line depth values were comparable for AFM and xTEM measurements. • IBM: line edge roughness in t-SPL processed samples IBM concentrated on measuring the line edge roughness (LER) of line patterns obtained after amplification and transfer using the SiO2 hardmask stack technology. The patterns are imaged in a JEOL SEM using a pixel pitch of <1 nm and fitting contour lines to a fixed brightness value in the SEM image. The LER analysis is based on the measurement of the deviation of the line edge profile from a straight line (for details see section 5 of the report). Consistently we measure 3 sigma LER values of 2 to 3 nm (data is shown for 11 nm half pitch lines transferred into a HM8006 hardmask polymer and 20 nm thick Au lines with a critical dimension of 17.6 nm). The dimensions of the structures is at the resolution limit of SEM. To better understand the capabilities of tSPL patterning, Si nanowire arrays with 13.7 nm half pitch were fabricated and subsequently analyzed by cross sectional TEM revealing a true width of the Si nanowires of 7 nm. *The detailed report follows below.*
Explanation of Differences between Estimation and Realisation	Since TUIL's contribution to the sub-5 nm methodology D7.2 were less than estimated TUIL transferred the unused PMs to measurement and metrology activities for this deliverable. OSC spent 14 PM of staff effort on D7.6 against a revised allocation of 15 PM for this deliverable and 16.5 PM for WP7 as a whole. OSC's total effort spent on WP7 was only 15.3 PM. The spare effort of 1PM from D7.6 and 0.2PM from D7.8 was transferred to WP5 in order to maximize the benefits of the new HM-01 fullerene resists.
Metrology comments	Measurements on various fabricated nanostructures were performed by different consortium partners. In order to provide traceability and enable provide comparability to results from other instruments for a selected number of samples these samples were measured by a fully calibrated AFM at VSL. Providing a measurement uncertainty remains a critical issue when comparability of measurements is required.

Funded by
the European Union

Detailed description of the deliverable

1. EPFL: TEM – based measurements on EBID-deposited patterns

At EPFL, we investigated the patterns, deposited at TU Delft by Electron Beam Induced Deposition (EBID) of Pt patterns before and after etching, which was performed at Oxford Instruments (OINT). Below are the details of measurements and conclusions.

1.1. Setup

The schematic of the sample and measurement setup is presented on Figure 1. Si_3N_4 with thickness of 20 nm serves as a substrate, on which 20 nm Si was evaporated. Furthermore, Pt is patterned with EBID. Measurements are performed in scanning transmission electron microscope (STEM) at 80kV. High angle annular dark field (HAADF) detector is used for detection of scattered electrons. In this way, the intensity *I* of each pixel is sensitive to the the atomic number Z of material with relationship $I \propto Z^{1.7}$.

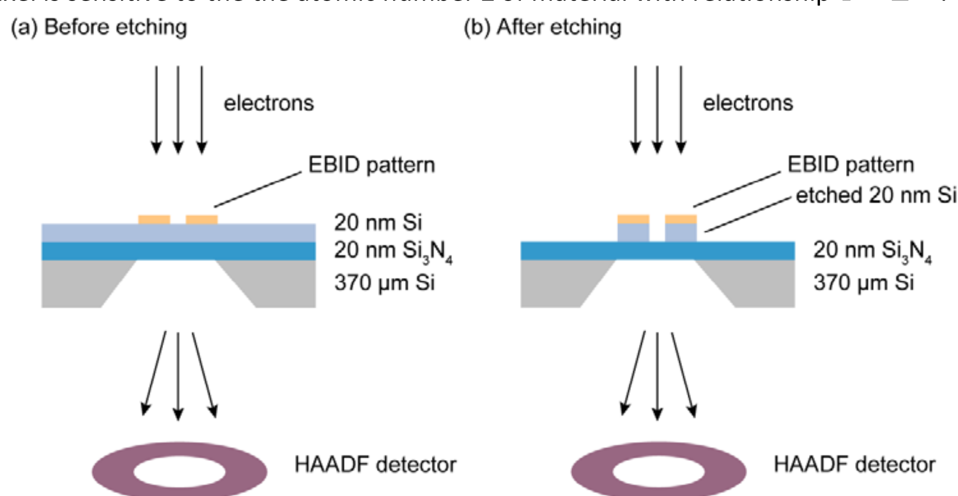

Figure 1. Schematic of experimental setup. High energy electrons pass through the membrane on which EBID patterns are written (a) before and (b) after etching. Depending on the atomic number of elements electrons are inelastically scattered and detected by HAADF detector.

1.2. Etching process details

Etching was performed at Oxford Instruments. Etching parameters are listed below:
S1: 16s Ar preclean + 25 cycles of Cl_2/Ar ALE, etch depth on OINT a-Si ~17nm
S2: 16s Ar preclean + 20 cycles of Cl_2/Ar ALE, etch depth on OINT a-Si ~12-13nm
Further in the report we will concentrate on the sample S1.

1.3. Sample before etching

1.3.1. HAADF STEM imaging

Overview of the sample under investigation is shown in Figure 2. The bright EBID patterns are visible at dark Si/Si_3N_4 background. Furthermore, we performed high resolution imaging of EBID patterns.

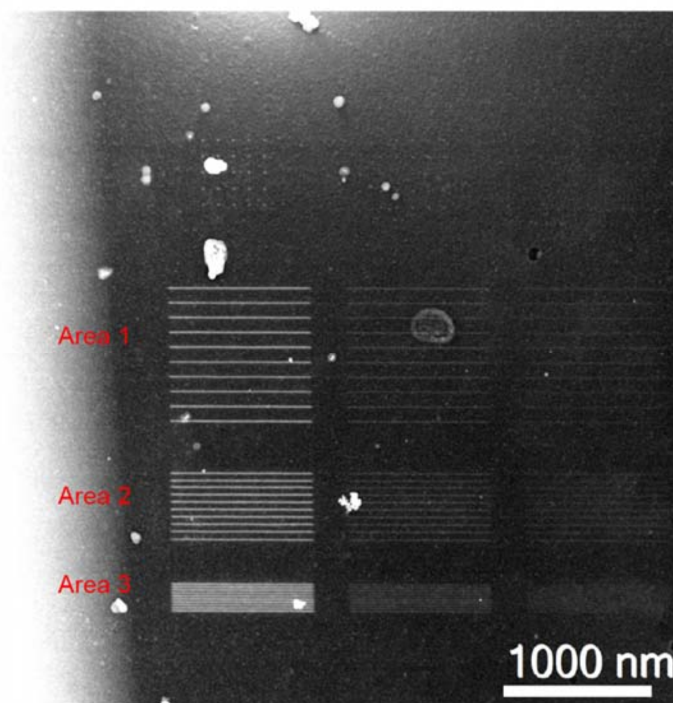

Figure 2. HAADF-STEM at 80kV. Overview of the sample under investigation. Areas of interest are labeled 1-3.

Three types of patterns, labeled in Figure 2 Area 1-3 were examined. Summary of these measurements at higher magnification is shown on Figure 3. The spacing between the lines during patterning was set to be 100 nm, 50 nm and 20 nm for Area 1-3 respectively. We measured intensity profiles perpendicular to written lines and extracted the distance between intensity maxima. Furthermore, we measured at full width at half maximum (FWHM) fitting line profile using a Gaussian function. Summary of these measurements is shown in Table 1. We notice, that FWHM will not be the ultimate width of etched trenches, because any Pt particle should be work as an etch mask for Si underneath. Area 3 in particular shows that the lines with spacing of 20 nm merge and thus etching between them will probably not be possible. However, the experimentally measured spacing is in a very good agreement with the values set during writing process.

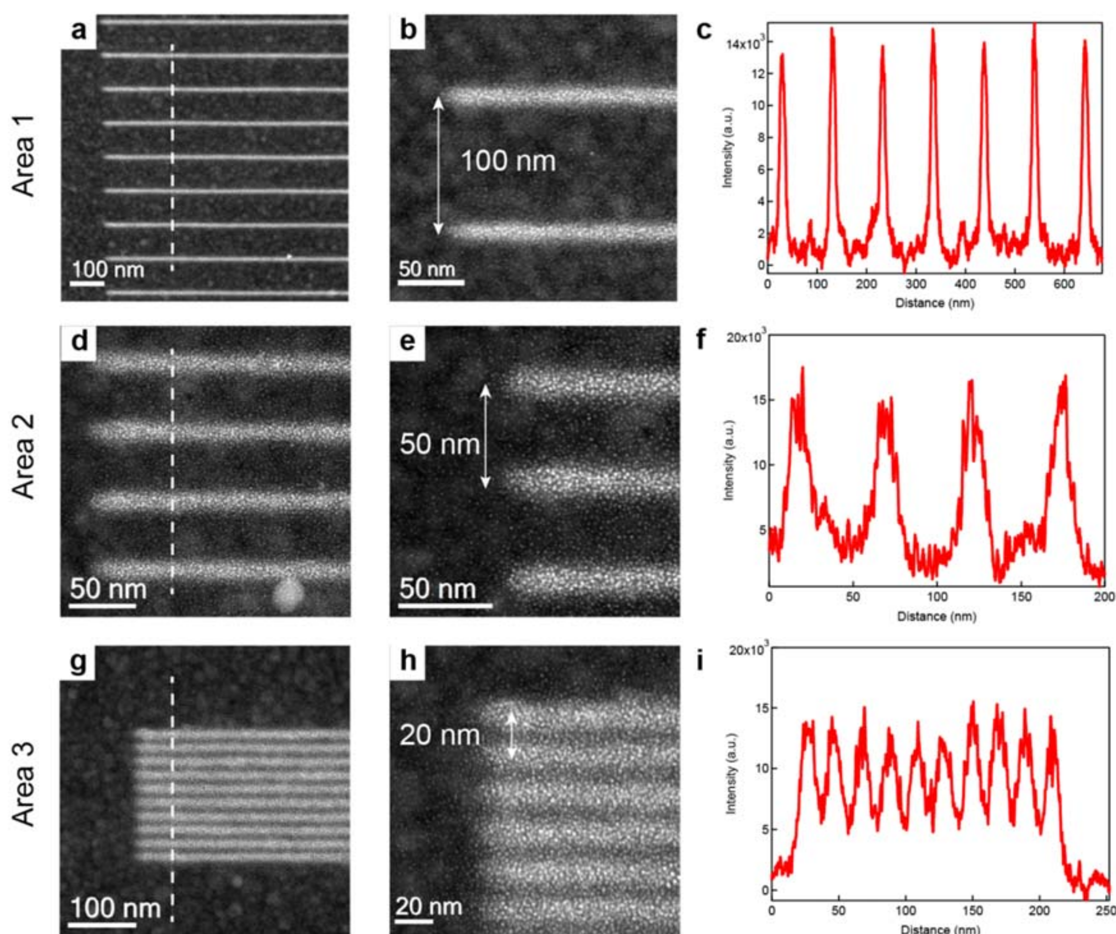

Figure 3. EBID patterns at different magnification. Area 1 (a-c), Area 2 (d-f), Area 3 (g-i). Distance between the lines is extracted from plots of integrated HAADF intensity across the line cut (a, d, g) and plotted as a function of distance in (c, f, i), respectively.

Area #	Separation between lines (nm)	Line width (FWHM with Gaussian fit) (nm)
1	101.5±1.9	17.2±1
2	52.0±0.5	18.8±3.4
3	20.2±1.3	18.4±4.1

Table 1. Summary of separation and line width for Areas 1-3.

A closer look on the EBID patterns reveals that they contain of small Pt grains, as shown on Figure 3. These grains have typical dimensions of several nm (particle size analyses is limited due to the contrast of our STEM images) and are located not only on the written lines, but also on the substrate around, where their density is relatively small. The grains beyond the written pattern are qualitatively smaller than the ones on the pattern itself.

1.3.2. EDX analysis

Energy-dispersive X-ray spectroscopy (EDX) provides information on elemental distribution of atoms inside our deposits. It is useful, as soon as HAADF provides only intensity variation information, while EDX

allows to locally judge on the film composition. It was of fundamental interest to understand the composition of Pt/C deposits and thus we acquired spectra of the representative region area 1, which is shown in Figure 4 (a-c). In the HAADF STEM image (Figure 4(a)) brighter lines correspond to EBID patterns, while Figure 4(b,c) show distribution of carbon and Pt respectively. Although carbon is known to be present in small quantities as contamination layer even in high vacuum of the sample chamber of the TEM, increase of intensity at the lines is visible. Furthermore, Pt is found only in the EBID lines.

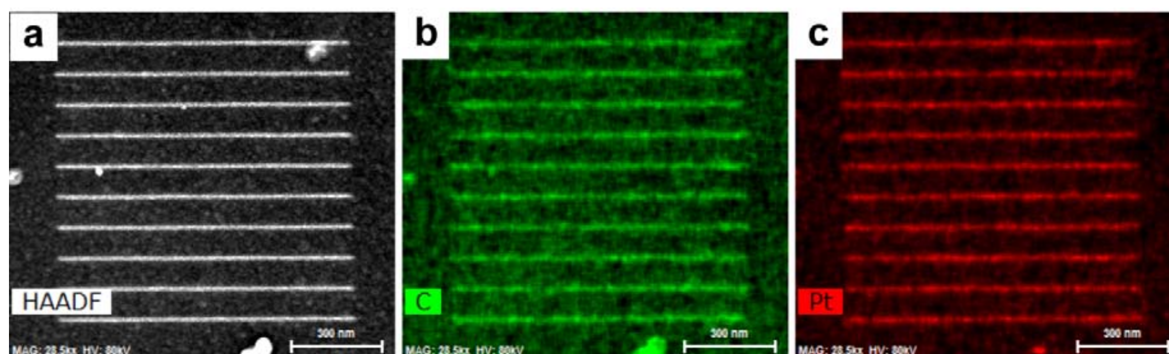

Figure 4. EBID patterns: lines ~20 nm wide with ~100 nm spacing before etching. (a) HAADF STEM image of patterned area with lines visible as brighter regions. (b) EDX map of C distribution. (c) EDX map of Pt distribution. (a), (b) and (c) images are acquired simultaneously.

1.4. Sample comparison before/after etching

After etching similar measurements have been performed. We employed the combination of HAADF-STEM and Energy-dispersive X-ray spectroscopy (EDX) to get an idea how the etching process impacts the films and the elemental distribution on the substrate.

1.4.1. HAADF STEM imaging

We performed standard HAADF STEM imaging of the sample after etching. All investigated samples appeared to be intact with the variation of contamination level. On Figure 5 we plot EBID patterns on exactly the same area before and after etching with corresponding intensity slices. Since our films consists of 20 nm Si_3N_4 (the average Z_{SiN} = 10) and 20 nm Si (Z_{Si} = 14) initially and current of the electron beam was varied (150 pA before etching and 200 pA after etching) we recalculate the intensity ratio before and after etching and extract the thickness information, taking a linear relation into account. The result roughly corresponds to 40% (8 nm) of Si film thickness to be removed. This is smaller than estimated for the same process on a-Si calibration sample at Oxford Instruments (17 nm). However, we point on the fact that Pt is redistributed all over the film (see further EDX analyses) and provides additional contribution to overall intensity, thus increasing the overall contrast and providing underestimation of etched thickness. This fact can be seen comparing Figure 5 (a) and (b). Figure 5 (b) contains lots of small particles. As it will be clear from EDX analysis, they consist of Pt.

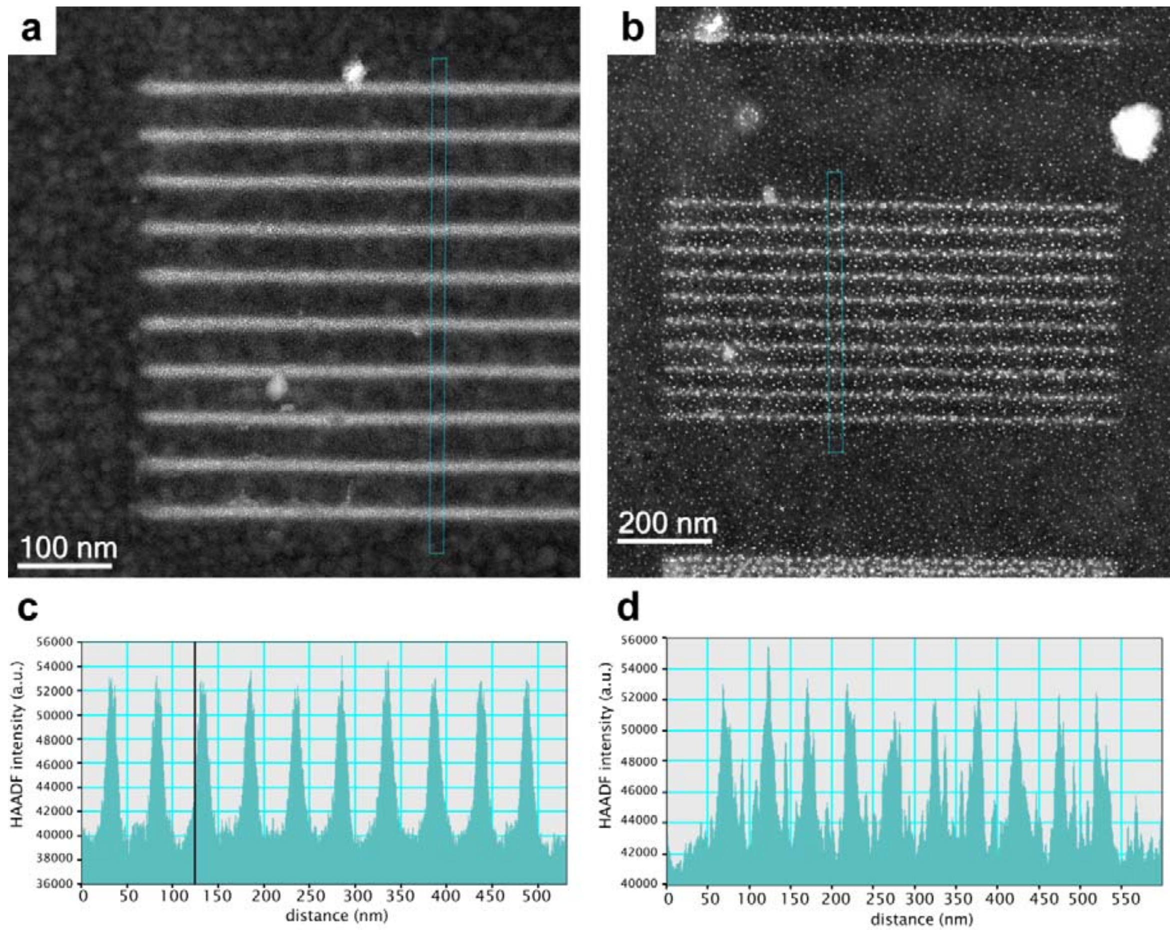

Figure 5. EBID patterns of area2: lines ~20 nm wide with ~50 nm spacing before and after etching. HAADF STEM images (a) before, (b) after etching and corresponding intensity profiles slices (c, d).

1.4.2. EDX analysis

On Figure 6 EDX analyses is performed on the example of area 2 with 20 nm lines and 50 nm spacing. We find that lines still look brighter than the surrounding (Figure 6(a)). EDX maps further confirm that etching has happened. We plot silicon distribution on Figure 6(b). Here brighter intensities correspond to brighter regions in Figure 6(a). We notice, that in fact all layers of our membrane contain Si and thus such intensity variation implies overall thickness variation.

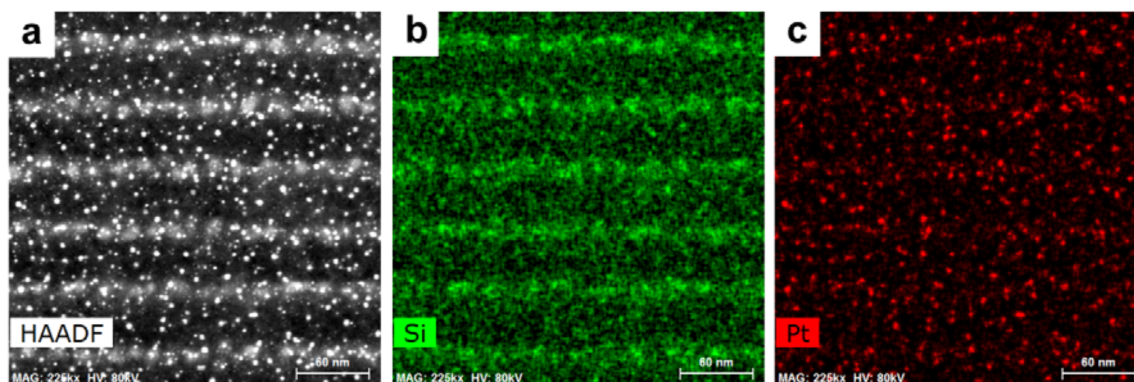

Figure 6. EBID patterns: lines ~20 nm wide with ~50 nm spacing after etching. (a) HAADF STEM image of patterned area with lines visible as brighter regions . (b) EDX map of Si distribution. (c) EDX map of Pt distribution. (a), (b) and (c) images are acquired simultaneously.

Pt distribution, however, is less pronounced. We believe that etching process impacts in some way the Pt/C EBID pattern. It is clear on Figure 6(c) that Pt particles are homogeneously distributed around the pattern with tiny variation of intensity in the etched voids between the lines. This was not the case before, where more clear lines could be seen before etching. We also notice, that we could not confirm the pronounced presence of carbon in etched lines, as shown on Figure 7. We speculate, that carbon matrix of EBID pattern has been impacted in some way by the etching process.

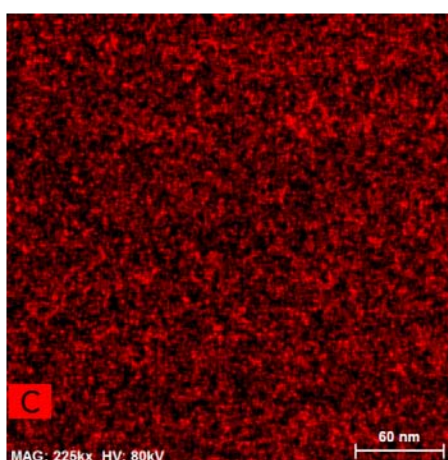

Figure 7. Carbon distribution after etching, map is acquired simultaneously with Figure 6.

Quantitative analyses from EDX data can be complicated, as soon as we are dealing with multiple layers of material, in particular $Pt/Si/Si_3N_4$ stack. However, qualitative data on HAADF intensities and Si distribution confirms that etching took place.

1.5. Conclusions – TEM imaging of EBID patterns

We have shown in this report that it is possible to monitor etching process of small nanostructures, patterned with EBID. We were able to image lines before and after etching with high resolution STEM and reveal the main features of our patterns:

- Pt/C composition of initial EBID patterns.

- The dimensions of the deposited EBID patterns, see Table 1 for details. The line width and separation, measured by STEM are in good agreement with the ones used for patterning.

- Change of HAADF intensity, corresponding to etching process. The thickness of 8 nm etching depth, extracted from these measurements is lower than on reference sample, but other factors could influence it.

- Comparison between HAADF and EDX maps shows, that after etching Si is thicker on the parts, masked with Pt deposits. This confirms, that etching indeed took place.

- Impact of etching on the EBID patterns. The redistribution of Pt has been seen. Also, we could not reveal the carbon presence in the written lines after etching, which might imply that there is interaction between plasma etching and Pt/C EBID patterns, which destroys them in some way. Optimization of etching process in future might allow to avoid this damage.

- The TEM-based investigation, requiring the use of thin, insulating Si_3N_4 membranes proved difficult to reconcile with SPL methods, requiring the presence of conductive layers in the substrate in order to either electrostatically actuate the probe or to induce an electric field.

2. EPFL: TEM – based measurements on SPL-patterned samples

2.1. Substrate preparation process flow and setup

Process flow for substrate preparation is illustrated on Figure 8a. The starting Si wafer, 370 µm thick, is covered with 20 nm of SiN is patterned at the back side by means of photolithography to etch through silicon and leave a suspended 20 nm SiN membrane, which will serve as a platform for TEM investigations (step 2). Since the SPL technique used by TU Ilmenau requires conductive substrates, while TEM requires good electron transparency, we grew graphene by means of chemical vapor deposition (CVD) and furthermore transferred it on top of our SiN membranes (step 3) in order to create a robust, transparent and electrically conductive substrate. During the last step, the resist was patterned on top.

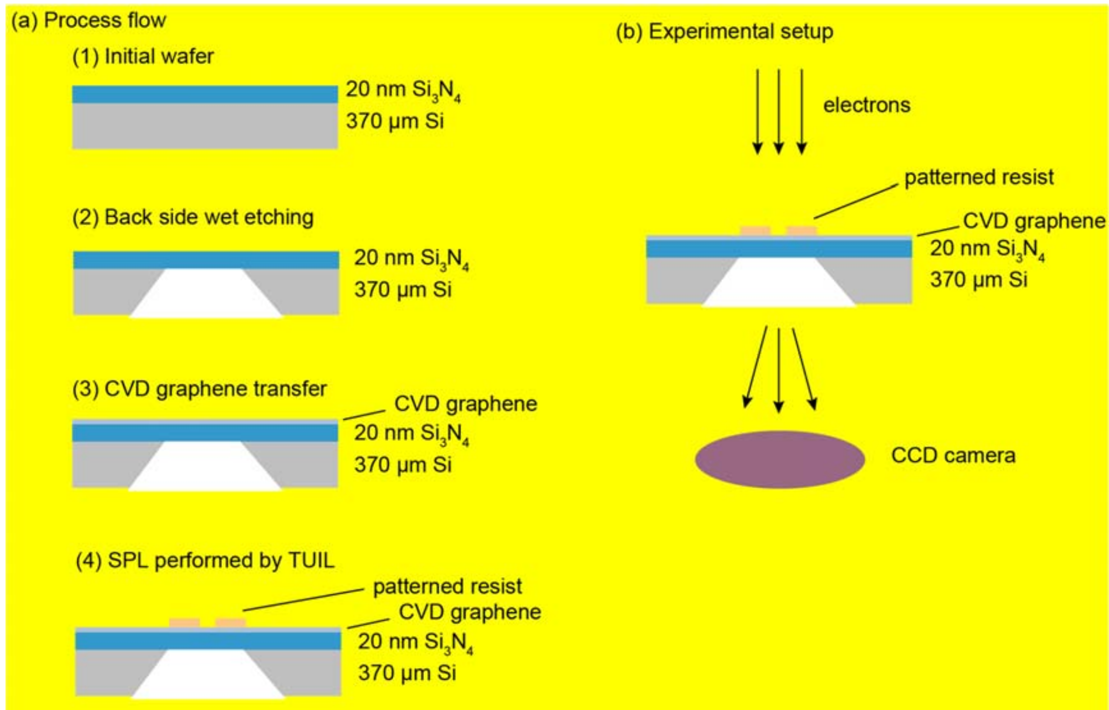

Figure 8. Process flow and schematic of experimental setup used. (a) Process flow used to fabricate the samples. (b) Experimental setup - transmission electron microscope.

Figure 8b shows the experimental setup used. We employ transmission electron microscopy (TEM) to investigate the created patterns. The only limitation here is the membrane transparency (thick membranes will not allow observations with good resolution), as well as contrast of created structures.
Figure 9 shows the sample during the patterning process at TUIL. On Figure 9b patterns written in the resist could be identified using an AFM.

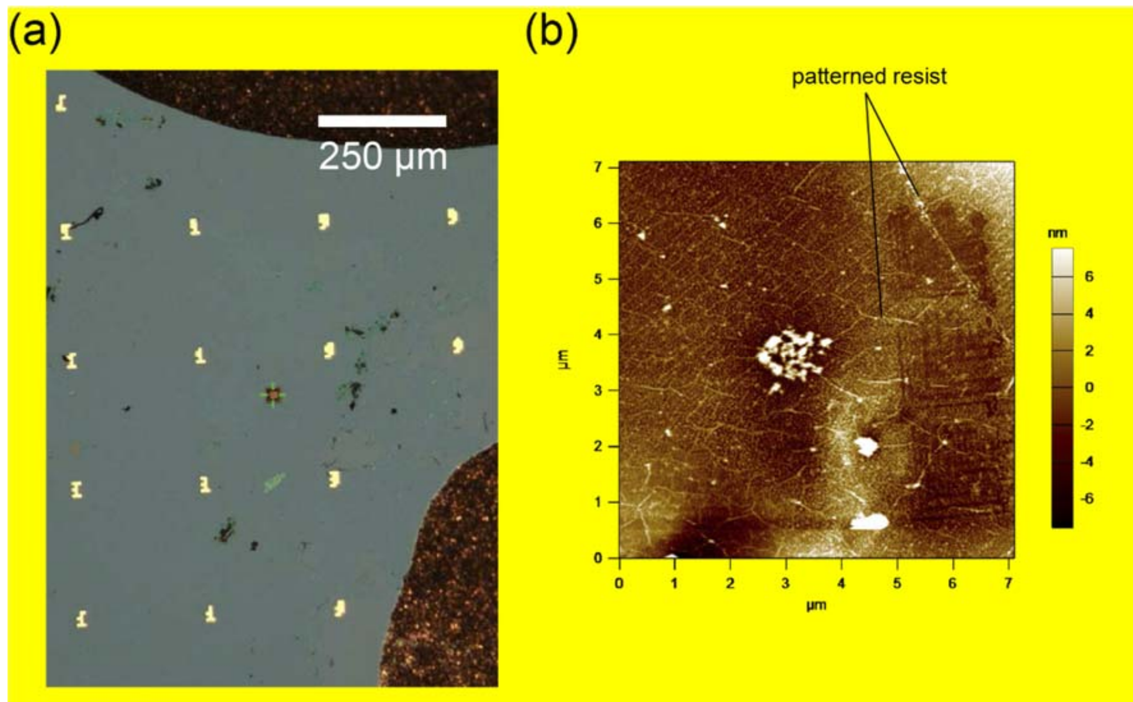

Figure 9. Patterning of the sample. (a) Optical micrograph and (b) AFM micrograph after patterning.

2.2. Substrate conductivity

We performed two-contact measurements after deposition of graphene to verify the conductivity of deposited layer. Cracks and other defects which occurred during the growth or after transfer could significantly decrease the conductivity and thus prevent successful SPL.

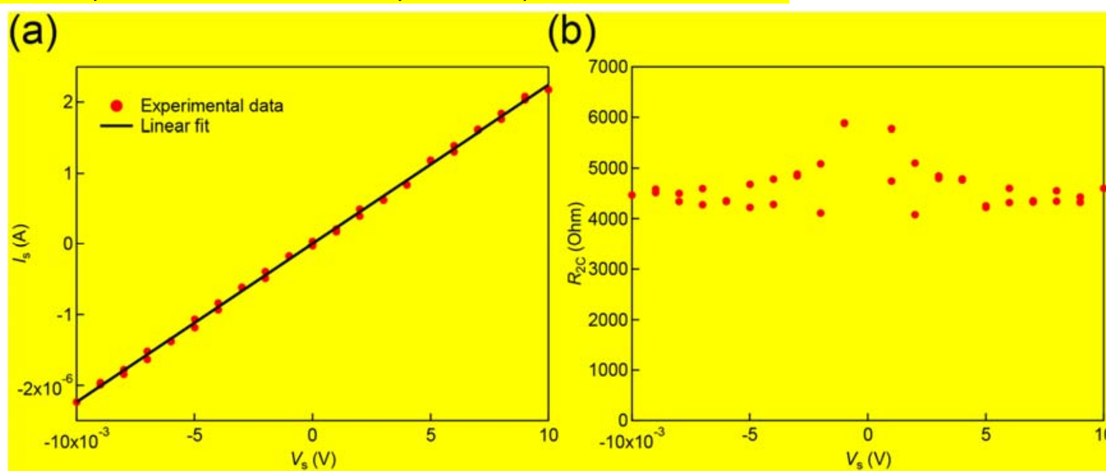

Figure 10. Electrical measurements on TEM membrane #1. (a) I_s-V_s curve, recorded on the region, surrounding the membrane. (b) Two-contact resistance R_{2C} as a function of applied voltage.

Figure 10 shows electrical measurements on the membrane, on which SPL was later performed. Two metal needles are placed on the distance of 250 µm between each other and the voltage is swept. Current-

voltage characteristic I_s-V_s is shown on Figure 10a, showing linear behavior and relatively low resistance of 5 kOhm (Figure 10b). Such electrical conductivity furthermore allowed TUIL to perform SPL.

2.3. TEM imaging after patterning

Overview of the sample under investigation is shown on Figure 11. Optical image is shown on Figure 11a. On Figure 11b the membrane is shown under the electron beam. Bright square corresponds to the membrane area, while dark areas around correspond to thick silicon, which is not transparent for electron beam.

Figure 11c shows a magnified view of one of the areas. Although we cannot perform atomically resolved imaging, collecting the diffraction pattern on the 2 µm × 2 µm area allows us to observe the clear hexagonal diffraction pattern from graphene (Figure 11d), which corresponds to (0-110) direction of graphene lattice. Although we could see defects in graphene (darker lines on Figure 11c) as well as contamination, we could not identify and inspect the patterned areas. The reason might be low contrast of the patterned area (the contrast of which could be roughly understood as difference between the contrast of SiN with resist+SiN contrast). These observations suggest that resist or etching mask which will interact with electron beam in a strong way (one example of which is the electron beam deposited Pt patterns) will be a better option for TEM observations.

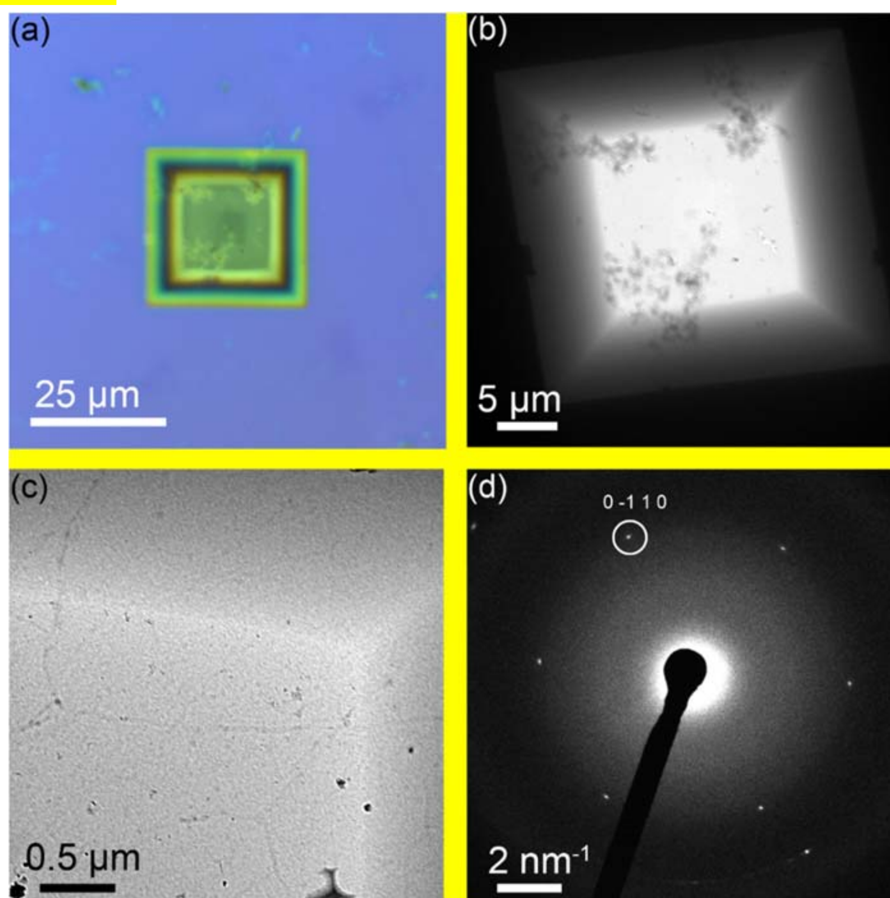

Figure 11. TEM imaging of TEM membrane #1. (a) Optical image of the membrane after patterning. (b) Low magnification TEM micrograph of the membrane. (c) Higher magnification TEM image, where polycrystalline graphene could be identified. (d) Selected area diffraction pattern from 2 µm area on the membrane is shown, confirming the presence of graphene. The only crystalline material here is graphene, which shows a hexagonal diffraction pattern.

2.4. Conclusions - TEM imaging of SPL patterns

In this report, the process flow for fabrication of electron transparent thin membranes was shown. Due to the fragile membrane structure FE-SPL patterning was challenging. Only 1 out of 3 membrane samples could be patterned. TUIL found during this study that the applicable exposure parameter range was limited due to the graphene bottom layer. This lead only to a partial exposure of the resist and to a low-contrast in the TEM images. The suggested solutions (for our metrology technique) is to use the masks that contain heavy elements and have relatively large thickness, allowing to differentiate between the substrate and the pattern.

3. VSL: AFM measurements

3.1. AFM measurements on EVG Nanoimprint Lithography samples

Samples with identification SNM B013 IMP1, SNM B013 IMP2, SNM B014 IMP1, and SNM B014 IMP2 were shipped to VSL in order to perform additional AFM measurements.
The AFM used for these measurements is a Veeco Dimension 3100.
In order to achieve maximum fidelity of the measured profiles, a Nanotools carbon nanotube-like probe was used with the following specifications:

Parameter	
Type	M-CNT-100, High Density carbon tip
Cylinder shape length	100 nm (± 20 nm)
Cylinder diameter	10 nm (± 2 nm)
Nominal resonance	320 kHz

All samples have been measured with the same probe and with the same AFM settings with respect to scanning area and speed. The AFM scanning area was nominally 1.4 µm × 1.4 µm and was measured at a speed of 1 lines/s.

The measurement areas were located in the field below INVP62 conform previous measurements in this area as reported in D10.2 “First single step imprinting tests on small scale using SNM NIL masters”. The measurement area was nominally at the same location for each sample and the direction of the NIL structures was aligned perpendicular to the fast scanning axis of the AFM.

Before final analysis of the data, intermediate processing was performed in order to level the raw data and minimize effects from drift and residual misalignment.

The final analysis was performed semi-automatically after hand picking a suitable area for analysis. The position and height analysis was performed on the processed data without correcting for the probe shape. The line width analysis was performed on probe shape corrected data.

The images show the processed data with rectangular selection boxes for which the profiles have been analyzed. The plots show the average profiles over the selected area and the identification of the calculated parameters . The peak to peak distances are indicated by the parameters d1..dn, the valley to

valley distances are indicated by the parameters D1..Dn, the profile depths are indicated by the parameters h1..hn and the line widths are indicated by the parameters w1..wn.

The results are stated in tables for the individual lines of the selected areas as well as the average over the selected areas. The standard deviations indicate the homogeneity of the profiles.

3.1.1. Imprint sample SNM B013 IMP1

Position and height analysis

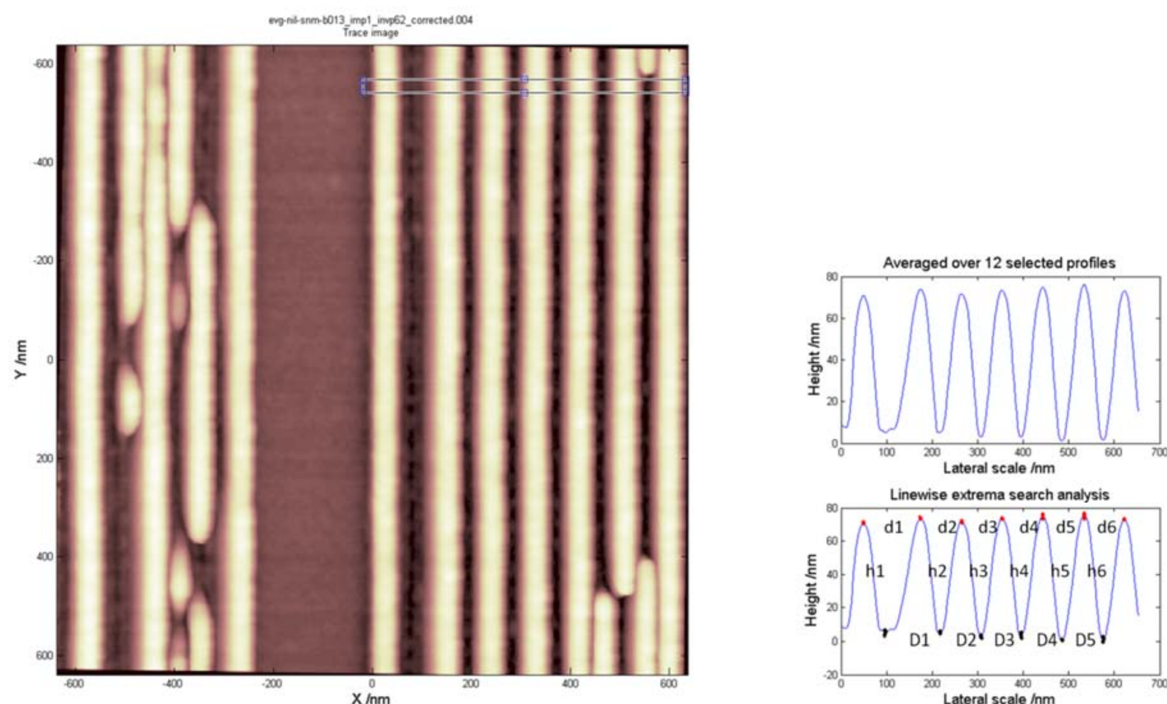

Figure 12. AFM measurement result on SNM B013 IMP1 and profile selection for spacing and height analysis.

Funded by
the European Union

Peak to peak distance in selected area based on maxima						
	d1	d2	d3	d4	d5	d6
Line no.	/nm	/nm	/nm	/nm	/nm	/nm
1	124.4	92.2	88.2	88.8	91.0	88.0
2	125.0	91.5	88.1	89.2	91.0	87.7
3	125.4	91.2	88.0	89.5	91.1	87.8
4	126.1	90.5	88.5	89.3	90.9	88.1
5	126.5	90.0	88.4	89.6	90.7	88.4
6	126.4	90.0	88.5	89.5	90.6	88.5
7	125.8	89.8	88.8	89.5	90.6	88.4
8	125.6	89.6	89.0	89.3	90.9	88.2
9	125.5	89.7	89.3	88.7	91.2	88.4
10	125.5	89.7	89.4	88.3	91.3	88.5
11	125.4	89.9	89.4	88.0	91.2	88.8
12	125.5	90.1	89.4	87.8	91.2	89.1
mean	125.6	90.3	88.8	89.0	91.0	88.3
std. dev.	0.6	0.8	0.5	0.6	0.2	0.4

Table 2. Peak to peak analysis results for sample SNM B013 IMP1

Valley to valley distance in selected area based on minima					
	D1	D2	D3	D4	D5
Line no.	/nm	/nm	/nm	/nm	/nm
1	119.1	90.2	89.0	89.2	91.7
2	120.1	89.8	88.4	89.9	91.6
3	121.5	90.2	87.2	90.1	91.7
4	122.4	89.9	87.7	89.5	91.2
5	121.3	89.5	87.6	90.2	90.8
6	120.0	89.6	87.9	90.2	90.3
7	120.2	89.9	88.1	90.1	90.2
8	119.1	89.5	88.9	89.8	90.1
9	119.5	89.9	89.0	89.6	90.1
10	120.2	90.9	88.3	89.2	90.2
11	122.7	89.7	88.4	88.8	90.1
12	121.5	90.9	88.5	88.8	90.0
mean	120.6	90.0	88.3	89.6	90.7
std. dev.	1.2	0.5	0.6	0.5	0.7

Table 3. Valley to valley analysis results for sample SNM B013 IMP1

Funded by
the European Union

Profile depth calculated as the difference between consecutive extrema						
	h1	h2	h3	h4	h5	h6
Line no.	/nm	/nm	/nm	/nm	/nm	/nm
1	66.3	70.5	67.1	68.1	75.1	74.6
2	65.6	70.2	67.1	68.5	75.4	75.2
3	65.3	69.8	67.5	68.7	75.1	75.4
4	64.7	69.5	68.1	68.5	75.2	75.2
5	64.5	68.6	68.5	69.5	74.9	75.1
6	64.7	68.6	68.6	70.1	75.1	74.4
7	64.7	69.3	69.0	70.2	74.3	74.1
8	65.0	69.0	69.5	71.4	73.8	73.7
9	65.6	68.4	69.6	71.5	73.3	73.9
10	66.3	67.9	69.7	71.6	72.6	74.6
11	67.0	67.6	70.0	71.4	72.6	74.4
12	67.2	68.1	70.1	71.3	72.8	73.7
mean	65.6	69.0	68.7	70.1	74.2	74.5
std. dev.	0.9	0.9	1.1	1.4	1.1	0.6

Table 4. Profile depth analysis results for sample SNM B013 IMP1

Line width analysis

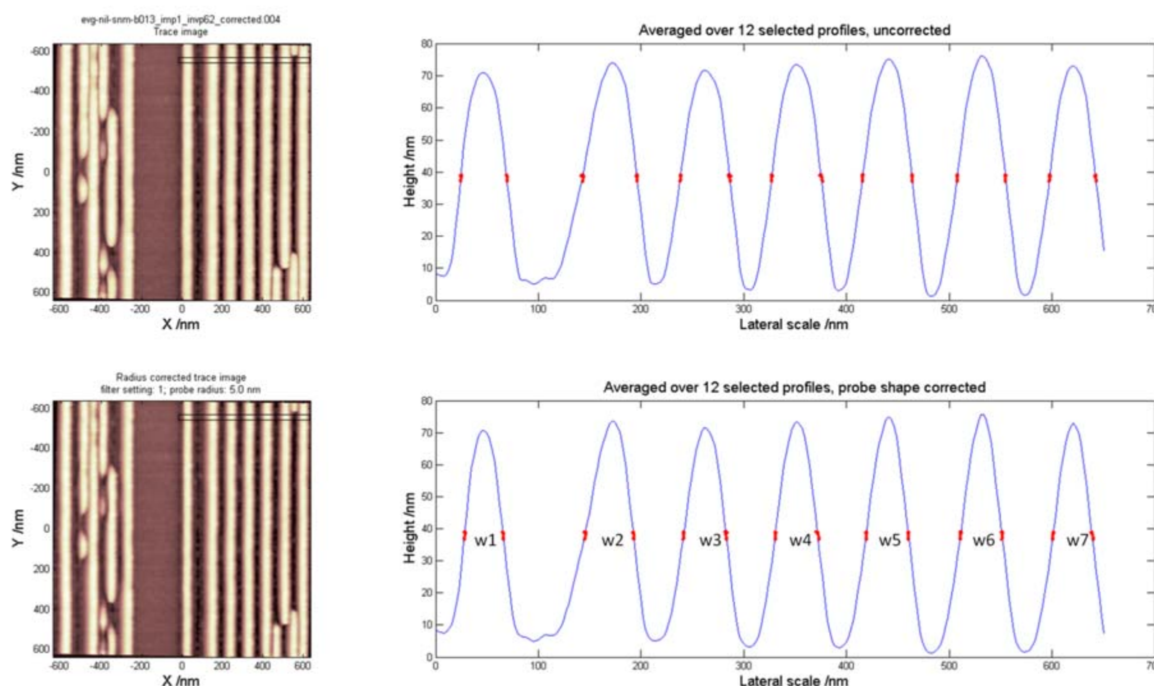

Figure 13. AFM measurement result on SNM B013 IMP1 and profile selection for line width analysis. The lower image and plot shows the results for which the probe shape has been corrected.

Line width calculated as full width at half maximum							
	w1	**w2**	**w3**	**w4**	**w5**	**w6**	**w7**
Line no.	/nm	/nm	/nm	/nm	/nm	/nm	/nm
1	37.7	47.2	42.1	39.9	40.7	40.0	36.7
2	37.8	47.2	41.6	39.7	41.3	40.3	37.1
3	37.4	47.3	41.2	39.6	41.3	40.1	37.4
4	37.4	47.5	40.6	40.1	41.2	40.2	37.6
5	36.6	47.1	40.4	40.6	41.4	40.0	37.7
6	36.7	46.5	40.2	41.0	41.0	39.8	37.4
7	37.0	46.4	40.0	40.9	40.7	39.9	37.4
8	37.4	46.4	40.3	40.9	40.9	40.2	37.6
9	37.8	46.6	40.9	41.7	41.1	40.5	38.1
10	37.8	47.1	41.8	42.4	41.2	40.4	38.9
11	38.0	47.3	42.2	42.8	41.1	40.3	39.3
12	37.8	47.8	42.4	42.8	40.9	40.3	39.5
mean	37.4	47.0	41.1	41.0	41.1	40.2	37.9
std. dev.	0.5	0.5	0.8	1.2	0.2	0.2	0.9

Table 5. Line width analysis results for sample SNM B013 IMP1

3.1.2. Imprint sample SNM B013 IMP2

Funded by
the European Union

Position and height analysis

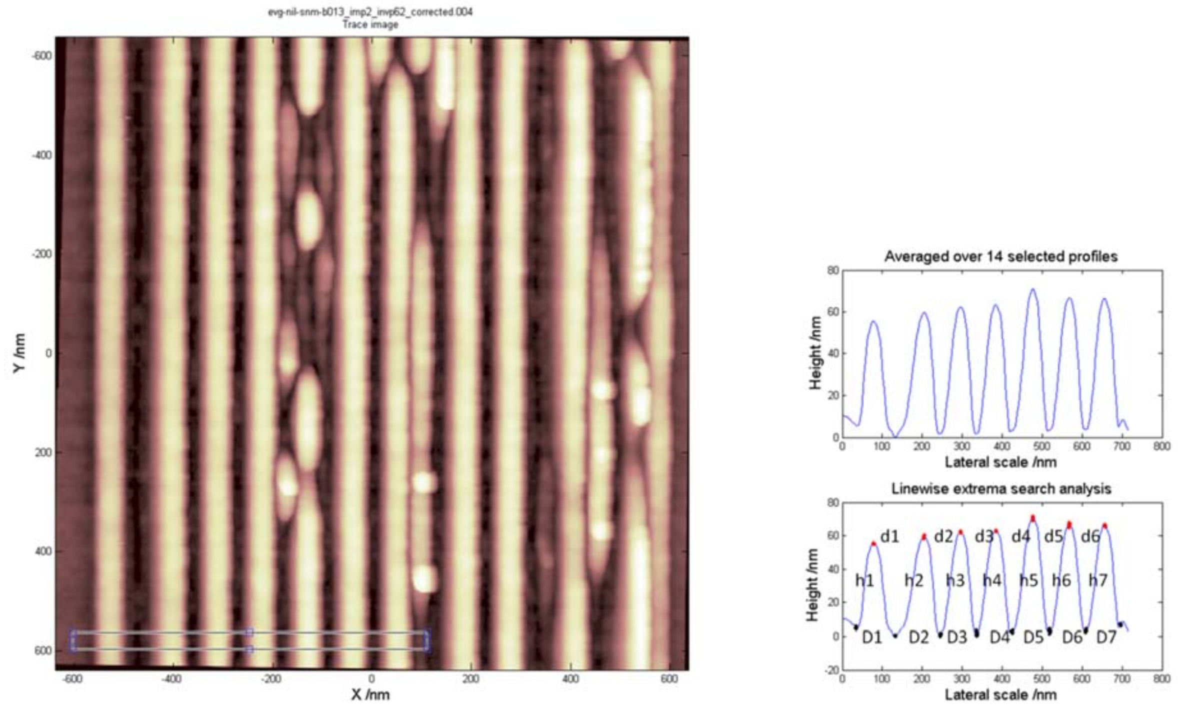

Figure 14. AFM measurement result on SNM B013 IMP2 and profile selection for spacing and height analysis

Funded by
the European Union

Peak to peak distance in selected area based on maxima						
	d1	d2	d3	d4	d5	d6
Line no.	/nm	/nm	/nm	/nm	/nm	/nm
1	124.8	92.7	87.6	93.3	91.1	88.7
2	124.9	92.7	87.6	93.1	91.6	88.1
3	125.2	92.6	87.5	93.1	91.7	87.9
4	125.4	92.5	87.3	93.2	91.4	87.8
5	126.0	92.2	87.4	93.0	91.2	87.7
6	126.9	91.6	87.5	93.0	91.1	87.6
7	127.4	91.0	87.6	93.0	91.0	87.7
8	127.4	90.5	87.8	92.8	91.2	87.9
9	127.2	90.1	88.3	92.5	91.2	88.0
10	127.0	90.2	88.4	92.4	91.2	88.2
11	126.5	90.2	89.0	92.3	90.8	88.7
12	125.9	90.4	89.2	92.5	90.2	89.3
13	125.4	90.7	89.2	92.9	89.7	89.6
14	125.0	91.0	89.4	93.1	89.6	89.7
mean	126.1	91.3	88.1	92.9	90.9	88.4
std. dev.	1.0	1.0	0.8	0.3	0.6	0.7

Table 6.Peak to peak analysis results for sample SNM B013 IMP2

Valley to valley distance in selected area based on minima							
	D1	D2	D3	D4	D5	D6	D7
Line no.	/nm	/nm	/nm	/nm	/nm	/nm	/nm
1	98.6	112.3	91.2	89.4	93.0	92.2	86.5
2	98.6	112.2	91.2	89.4	93.0	92.1	87.1
3	98.4	112.6	91.3	88.8	95.1	90.2	86.9
4	98.1	113.0	91.3	88.3	95.0	90.1	86.8
5	98.0	113.8	90.6	89.4	93.4	90.3	86.5
6	98.1	113.5	91.0	89.3	92.9	90.6	86.1
7	98.0	114.0	91.0	88.2	93.5	92.3	84.4
8	97.9	114.2	90.3	88.4	93.8	91.8	84.9
9	97.9	114.2	89.6	89.2	93.6	91.3	85.8
10	98.3	113.3	90.0	89.6	93.3	91.4	85.9
11	98.9	112.5	90.5	88.1	94.8	89.5	87.9
12	98.9	112.4	90.1	88.7	94.1	90.4	87.9
13	99.1	112.0	91.6	87.3	94.4	90.4	87.7
14	100.1	111.8	91.7	87.2	94.8	89.8	88.3
mean	98.5	113.0	90.8	88.7	93.9	90.9	86.6
std. dev.	0.6	0.8	0.7	0.8	0.8	1.0	1.1

Table 7. Valley to valley analysis results for sample SNM B013 IMP2

Profile depth calculated as the difference between consecutive extrema							
	h1	**h2**	**h3**	**h4**	**h5**	**h6**	**h7**
Line no.	/nm	/nm	/nm	/nm	/nm	/nm	/nm
1	50.7	57.6	60.5	58.7	68.1	65.2	63.2
2	50.1	57.5	60.4	60.0	67.6	65.3	62.8
3	49.8	57.9	60.5	60.5	66.9	64.4	62.7
4	49.8	58.4	60.6	61.2	67.3	64.0	62.9
5	49.8	58.8	60.7	61.4	67.3	63.7	63.0
6	49.7	59.1	61.0	62.1	67.8	63.7	62.9
7	49.7	59.7	61.1	60.9	68.1	63.5	62.2
8	49.6	60.1	60.8	61.4	68.2	63.2	61.9
9	50.0	60.2	60.9	62.4	68.1	63.4	61.6
10	50.1	60.1	61.2	62.8	68.0	63.2	61.9
11	50.4	59.7	62.1	63.2	68.1	62.8	62.9
12	50.6	59.7	62.7	62.8	67.9	63.6	63.0
13	50.7	59.8	62.9	62.3	68.1	63.0	63.1
14	50.8	59.8	63.0	62.3	68.4	62.4	62.6
mean	50.1	59.2	61.3	61.6	67.9	63.7	62.6
std. dev.	0.4	1.0	0.9	1.2	0.4	0.8	0.5

Table 8. Profile depth analysis results for sample SNM B013 IMP2

Line width analysis

Funded by
the European Union

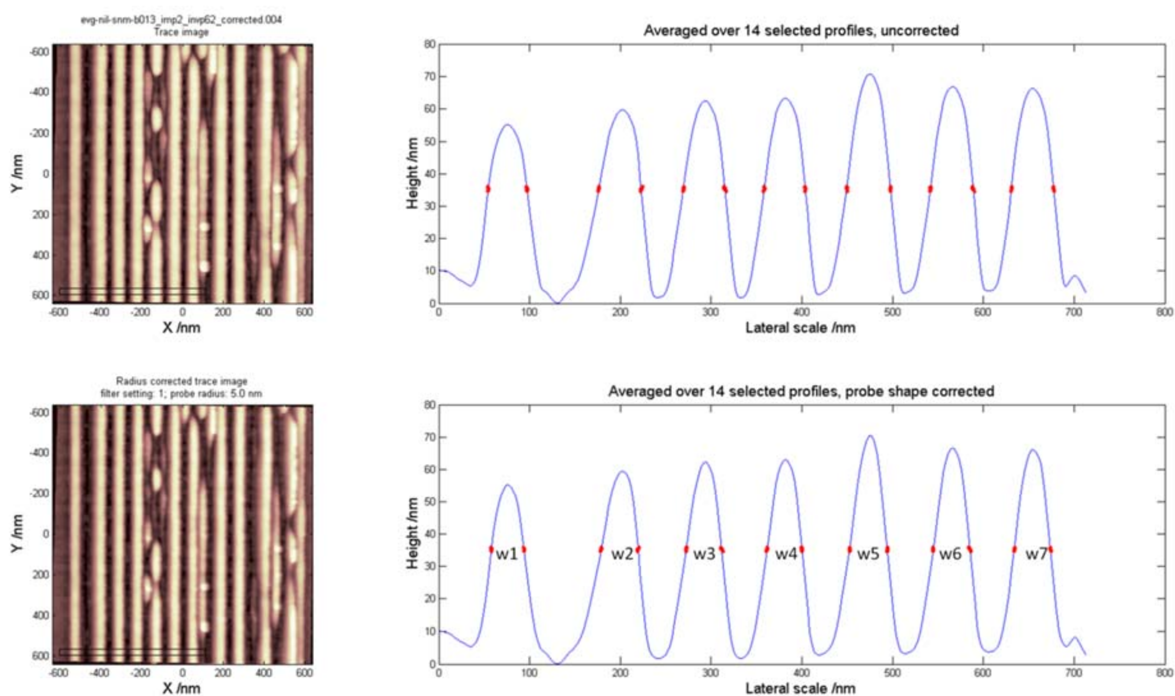

Figure 15. AFM measurement result on SNM B013 IMP2 and profile selection for line width analysis. The lower image and plot shows the results for which the probe shape has been corrected.

Line width calculated as full width at half maximum							
	w1	w2	w3	w4	w5	w6	w7
Line no.	/nm	/nm	/nm	/nm	/nm	/nm	/nm
1	35.1	40.0	39.2	38.3	40.1	40.9	40.2
2	35.4	40.1	40.3	38.9	40.7	41.5	40.7
3	36.0	40.6	41.2	39.2	41.1	41.8	40.9
4	36.0	40.4	40.9	39.0	41.3	41.3	40.5
5	36.2	40.3	40.4	38.6	41.4	40.8	39.7
6	36.3	40.5	39.6	38.2	41.2	40.2	39.3
7	36.3	41.3	38.8	38.1	41.3	39.8	39.2
8	35.9	41.7	38.1	37.9	41.5	39.6	39.1
9	35.6	41.7	37.3	37.6	41.6	39.2	39.2
10	35.6	41.5	37.3	38.0	41.8	39.3	39.4
11	35.8	41.3	37.6	38.1	41.8	39.7	39.6
12	36.3	41.0	37.9	38.3	41.7	39.7	39.9
13	35.9	40.1	37.9	38.3	42.0	39.7	39.7
14	35.4	39.1	37.9	38.0	42.1	39.5	39.2
mean	35.8	40.7	38.9	38.3	41.4	40.2	39.7
std. dev.	0.4	0.8	1.4	0.5	0.5	0.9	0.6

Table 9. Line width analysis results for sample SNM B013 IMP2

3.1.3. Imprint sample SNM B014 IMP1

Position and height analysis

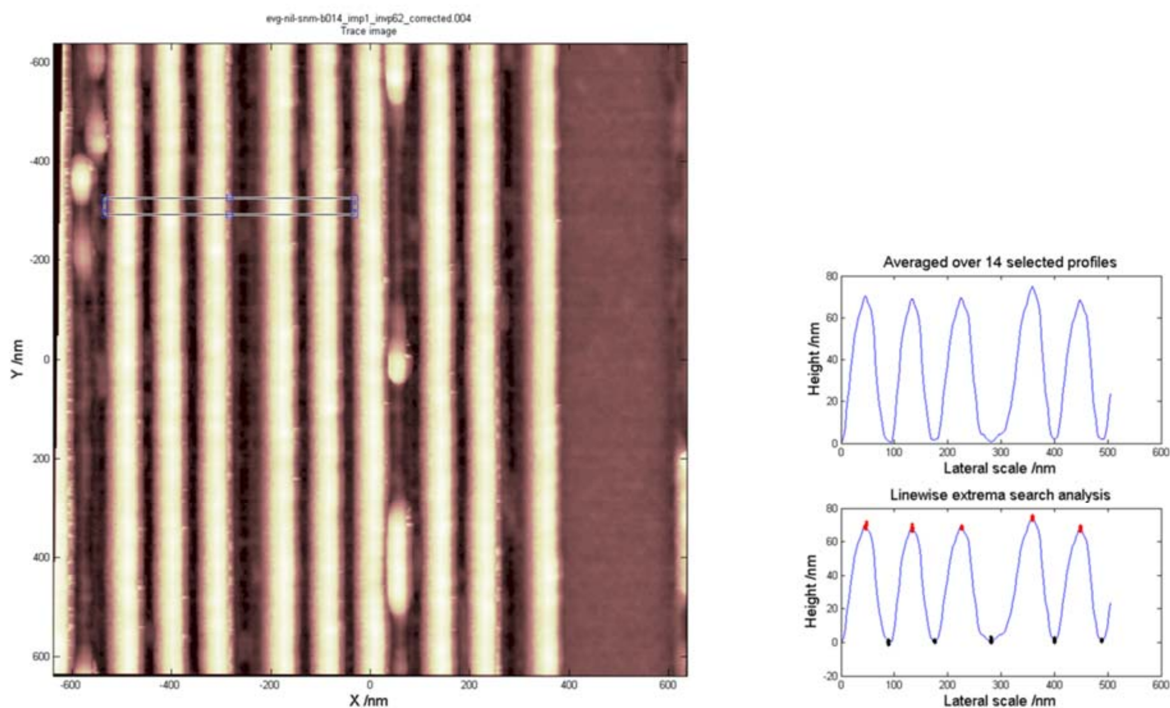

Figure 16. AFM measurement result on SNM B014 IMP1 and profile selection for spacing and height analysis

Peak to peak distance in selected area based on maxima				
	d1	**d2**	**d3**	**d4**
Line no.	/nm	/nm	/nm	/nm
1	87.6	92.7	133.3	88.9
2	87.7	92.6	133.6	89.1
3	87.8	92.6	133.3	89.7
4	88.0	92.5	133.2	89.8
5	88.4	91.9	133.3	90.0
6	88.5	92.3	132.7	90.1
7	88.3	92.4	132.4	90.2
8	87.8	92.5	132.4	90.0
9	87.6	92.3	132.6	89.7
10	87.7	91.5	133.1	89.8
11	86.9	91.7	133.0	90.1
12	86.7	91.8	132.9	89.8
13	86.6	91.6	133.0	90.0
14	86.5	91.8	133.0	90.4
mean	87.6	92.2	133.0	89.8
std. dev.	0.7	0.4	0.4	0.4

Table 10. Peak to peak analysis results for sample SNM B014 IMP1

Funded by
the European Union

Valley to valley distance in selected area based on minima				
	D1	D2	D3	D4
Line no.	/nm	/nm	/nm	/nm
1	84.6	106.3	119.5	89.1
2	84.9	107.0	118.6	88.9
3	85.7	106.9	118.6	88.5
4	85.8	106.5	118.8	88.5
5	84.9	107.5	118.6	88.6
6	85.7	106.9	118.2	88.4
7	85.2	107.6	118.1	87.9
8	85.7	107.2	118.5	87.7
9	86.9	106.0	118.7	88.1
10	87.8	105.7	118.9	88.3
11	88.3	105.3	119.0	88.2
12	86.5	105.4	119.5	88.0
13	86.6	104.1	119.8	88.6
14	88.2	103.4	119.7	88.9
mean	86.2	106.1	118.9	88.4
std. dev.	1.2	1.3	0.5	0.4

Table 11. Valley to valley analysis results for sample SNM B014 IMP1

Profile depth calculated as the difference between consecutive extrema					
	h1	h2	h3	h4	h5
Line no.	/nm	/nm	/nm	/nm	/nm
1	69.1	65.7	66.0	70.6	67.5
2	69.0	65.9	66.4	70.6	67.3
3	68.7	65.6	67.1	71.1	67.0
4	68.2	65.9	68.0	71.3	66.9
5	67.6	66.7	68.7	71.5	66.6
6	67.3	67.1	69.0	71.6	66.4
7	67.2	67.6	68.7	71.9	65.9
8	67.0	67.6	68.2	72.4	65.4
9	67.0	67.6	67.7	72.2	65.1
10	67.4	67.9	67.3	72.4	65.4
11	68.9	68.0	67.1	72.9	65.6
12	71.3	67.9	67.0	74.4	65.6
13	71.9	68.6	66.9	74.6	65.6
14	72.3	69.0	66.9	74.6	65.6
mean	68.8	67.2	67.5	72.3	66.1
std. dev.	1.8	1.1	0.9	1.4	0.8

Table 12. Profile depth analysis results for sample SNM B014 IMP1

Line width analysis

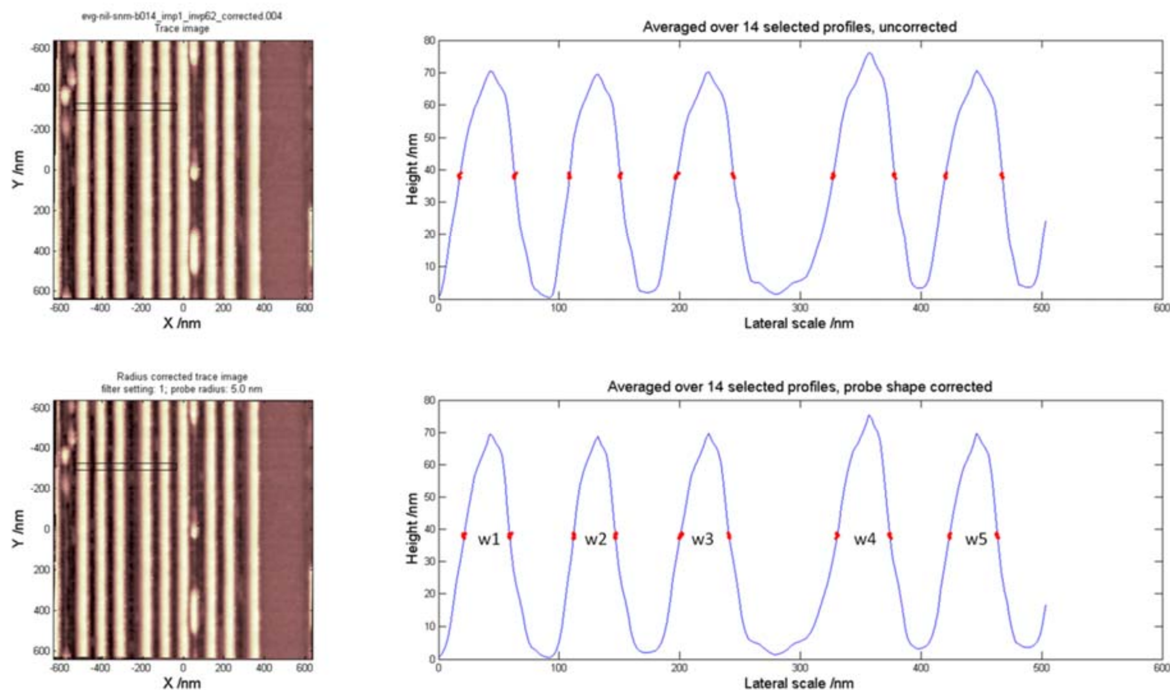

Figure 17. AFM measurement result on SNM B014 IMP1 and profile selection for line width analysis. The lower image and plot shows the results for which the probe shape has been corrected.

Line width calculated as full width at half maximum					
	w1	w2	w3	w4	w5
Line no.	/nm	/nm	/nm	/nm	/nm
1	38.1	33.7	40.2	43.7	40.2
2	37.9	33.7	40.7	44.4	40.3
3	37.4	34.2	41.8	45.6	40.5
4	37.5	35.6	41.4	45.5	40.4
5	37.6	34.9	40.8	44.7	40.2
6	37.9	34.0	41.1	43.8	40.1
7	38.4	34.7	41.2	43.5	39.8
8	38.3	33.5	40.4	42.7	39.4
9	38.6	33.8	40.1	42.4	39.3
10	39.1	34.4	39.4	42.5	39.2
11	38.6	34.9	38.5	43.1	39.2
12	38.3	35.1	38.9	43.8	39.0
13	38.2	35.3	38.4	44.4	38.7
14	38.6	35.6	38.4	44.1	38.7
mean	38.2	34.5	40.1	43.9	39.6
std. dev.	0.5	0.7	1.2	1.0	0.6

Table 13. Line width analysis results for sample SNM B014 IMP1

3.1.4. Imprint sample SNM B014 IMP2

Position and height analysis

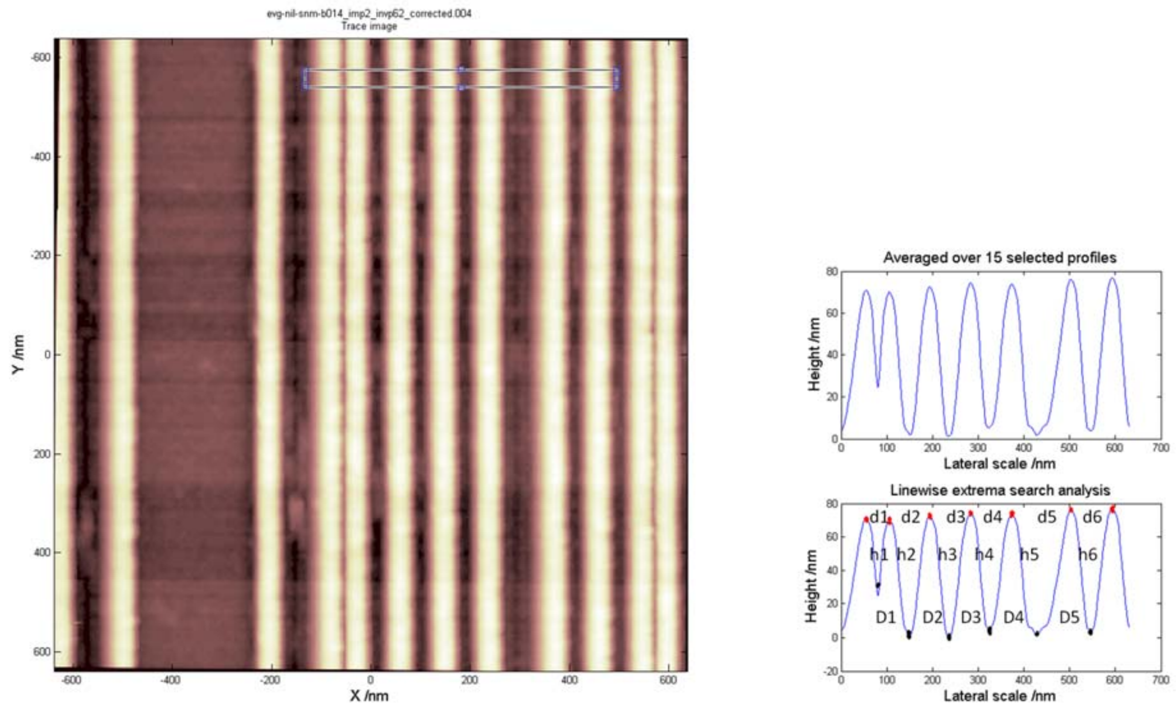

Figure 18. AFM measurement result on SNM B014 IMP2 and profile selection for spacing and height analysis.

Peak to peak distance in selected area based on maxima						
	d1	**d2**	**d3**	**d4**	**d5**	**d6**
Line no.	/nm	/nm	/nm	/nm	/nm	/nm
1	51.3	88.4	88.2	92.8	128.9	89.1
2	51.4	88.3	88.3	92.7	128.6	89.5
3	51.6	88.1	88.6	92.3	128.5	89.9
4	51.8	87.8	88.8	92.1	128.4	90.1
5	52.2	87.5	88.9	91.4	128.8	90.5
6	52.1	87.5	89.0	90.6	129.1	90.5
7	51.9	87.8	89.1	89.7	130.1	90.2
8	51.7	88.4	88.8	89.0	130.5	90.3
9	51.5	88.7	88.8	88.7	130.7	90.2
10	51.1	88.8	89.1	88.6	130.8	90.1
11	51.1	88.6	89.3	88.6	130.8	90.3
12	51.2	88.5	89.4	88.8	130.5	90.7
13	51.3	88.5	89.3	89.1	130.3	91.2
14	51.2	88.8	89.0	89.5	130.2	91.6
15	51.4	89.1	88.2	90.3	129.8	91.9
mean	51.5	88.3	88.9	90.3	129.7	90.4
std. dev.	0.4	0.5	0.4	1.6	0.9	0.7

Table 14. Peak to peak analysis results for sample SNM B014 IMP2

Funded by
the European Union

Valley to valley distance in selected area based on minima					
	D1	D2	D3	D4	D5
Line no.	/nm	/nm	/nm	/nm	/nm
1	66.6	89.3	89.7	103.4	116.6
2	67.2	88.8	89.5	104.3	115.6
3	67.4	88.5	90.0	103.6	115.8
4	68.2	87.5	89.4	104.0	115.9
5	68.6	87.0	89.6	103.3	116.2
6	68.7	87.1	89.2	103.3	116.3
7	68.6	87.9	88.5	103.4	116.5
8	67.1	88.0	88.6	103.0	117.2
9	67.0	87.9	88.7	102.4	118.0
10	66.9	88.0	88.6	102.3	118.4
11	66.8	88.0	88.5	102.7	118.1
12	66.7	87.9	88.4	103.5	117.5
13	66.6	87.6	88.7	104.3	116.9
14	65.7	88.7	88.9	104.5	116.3
15	65.4	89.1	88.9	104.9	115.8
mean	67.2	88.1	89.0	103.5	116.7
std. dev.	1.0	0.7	0.5	0.7	0.9

Table 15. Valley to valley analysis results for sample SNM B014 IMP2

Profile depth calculated as the difference between consecutive extrema						
	h1	**h2**	**h3**	**h4**	**h5**	**h6**
Line no.	/nm	/nm	/nm	/nm	/nm	/nm
1	40.4	66.6	72.5	73.0	72.3	73.1
2	39.8	67.5	73.7	71.9	72.3	72.7
3	40.3	67.9	73.9	70.5	72.7	72.8
4	40.7	68.1	73.3	70.4	73.0	73.0
5	40.9	68.3	72.3	69.7	73.1	72.9
6	39.8	68.6	71.6	69.7	72.7	72.7
7	39.0	68.9	71.8	68.9	72.4	72.4
8	38.8	69.1	71.9	69.2	71.9	72.6
9	38.7	69.2	72.1	69.4	71.1	72.8
10	38.3	69.0	72.3	69.5	70.4	73.2
11	38.6	68.4	72.3	69.5	70.3	73.8
12	39.1	67.8	71.7	70.7	70.2	74.1
13	39.5	67.7	72.0	70.8	70.3	74.1
14	39.9	67.7	71.1	70.1	70.7	73.4
15	40.2	67.9	71.1	69.8	70.9	72.4
mean	39.6	68.2	72.2	70.2	71.6	73.1
std. dev.	0.8	0.7	0.8	1.1	1.1	0.6

Table 16. Profile depth analysis results for sample SNM B014 IMP2

Line width analysis

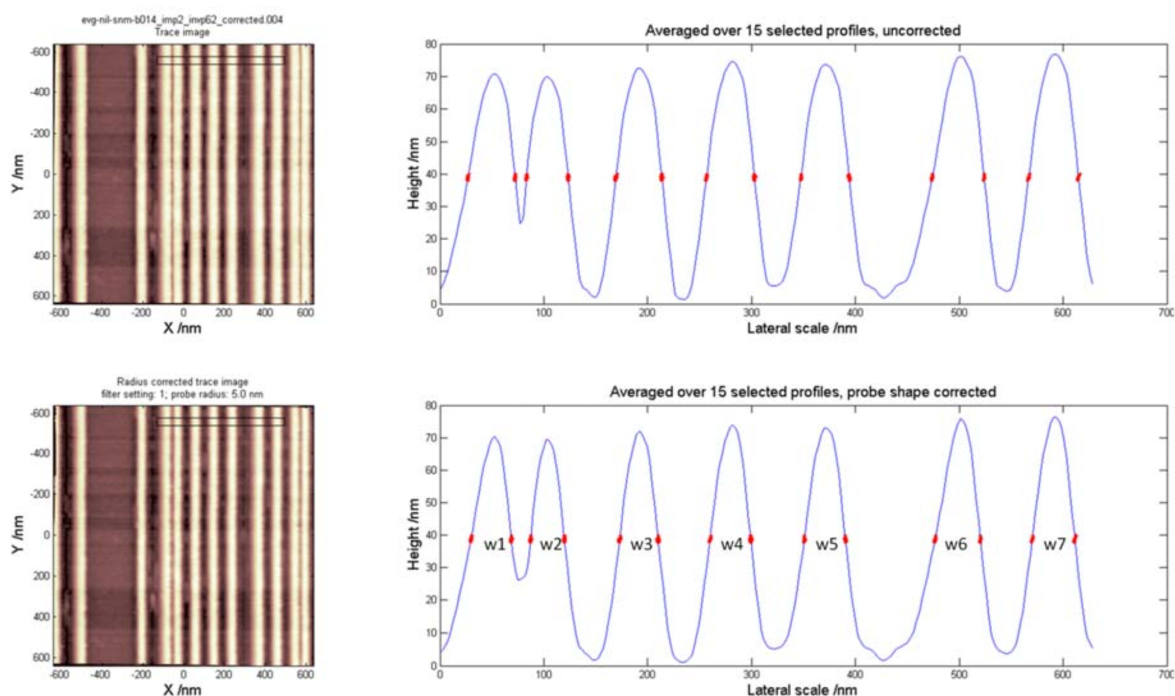

Figure 19. AFM measurement result on SNM B014 IMP2, profile selection for line width analysis. The lower image and plot shows the results for which the probe shape has been corrected.

Line width calculated as full width at half maximum							
	w1	**w2**	**w3**	**w4**	**w5**	**w6**	**w7**
Line no.	/nm	/nm	/nm	/nm	/nm	/nm	/nm
1	38.3	32.1	36.5	38.0	39.6	42.9	40.5
2	38.8	32.9	37.3	38.7	40.0	43.3	40.7
3	38.8	32.9	37.5	39.1	40.0	43.4	41.0
4	39.0	32.8	37.4	39.4	40.0	43.3	41.2
5	38.8	32.8	37.2	39.6	40.0	43.4	41.2
6	39.2	33.0	37.3	39.9	40.0	43.8	41.3
7	39.5	33.1	37.6	40.1	40.0	43.9	41.0
8	39.2	32.6	37.6	40.0	39.6	44.1	40.7
9	39.0	32.1	37.1	39.9	39.2	44.2	40.8
10	39.2	32.2	36.9	39.6	39.0	44.1	40.9
11	39.3	32.4	36.8	39.5	38.7	43.9	40.8
12	39.0	32.4	36.4	39.2	38.9	43.7	40.8
13	38.6	32.2	36.0	38.6	39.1	43.2	41.0
14	38.1	32.0	35.9	38.2	39.2	43.0	41.4
15	37.7	31.8	36.0	38.1	39.1	43.0	41.5
mean	38.8	32.5	36.9	39.2	39.5	43.6	41.0
std. dev.	0.5	0.4	0.6	0.7	0.5	0.4	0.3

Table 17. Line width analysis results for sample SNM B014 IMP2

3.1.5. Discussion

The averaged results for each sample is given in the table below. Results from deliverable D10.2 on the same samples are duplicated below for comparison. Since the regions for the profile selection sometimes contains obvious outliers in the pitch a subset with similar pitch was selected to calculate the average value and the associated standard deviation. The measurement uncertainty is based on the standard deviation and is calculated for a coverage factor k=2 corresponding to a coverage probability of approximately 95 %.

Table 18. Summary of results calculated as the averages of the above data including previously reported results obtained on the same samples with a different instrument as documented in D10.

Average results and uncertainty based on the standard deviation of the measured set						
Sample	Pitch	U95	Line width	U95	Depth	U95
	/nm	/nm	/nm	/nm	/nm	/nm
B013 IMP1	90	2	41	3	70	7
B013 IMP2	91	6	39	4	61	10
B014 IMP1	89	4	40	6	69	5
B014 IMP2	90	3	39	6	71	4

Results from deliverable: D10.2 “First single step imprinting tests on small scale using SNM NIL masters			
Sample	Pitch	Line width	Depth
	/nm	/nm	/nm
B013 master	114	70	30
B013 imprint	117	78	35
B014 master	98	67	67
B014 imprint	98	59	50

3.1.6. Conclusions

Nanoimprint lithography samples were manufactured by EVG and measured independently by two different AFM systems. Since the measurement setup at EVG was not optimized for accurate measurements, the samples were shipped to VSL. The VSL measurements were performed with a calibrated system and known probe shape enabling the correction of probe shape effects and calculation of the measurement uncertainty to enable quantitative comparison of data. Since the EVG results in D10.2 were stated without measurement uncertainty a direct comparison of this data to the ones presented above is not possible. However, using a properly calibrated instrument and a well defined sharp probe to obtain maximum fidelity of the nano imprint profiles provide a more consistent result, within the measurement uncertainty, for the pitch, line width and depth compared to the data reported in D10.2. It is recommended that for future fidelity tests only calibrated instruments and probes are used.

3.2. AFM measurements on TUIL Scanning Probe Lithography samples

Within the framework of the SNM project, samples with identification SNM_SOI_Box 7_S6 and S7 were shipped by TUIL to VSL in order to perform additional AFM measurements. A description of the samples was provided by the document ‘SNM_Samples_SOI_Box7_S6&7_After Plasma Etching_Metrology at VSL.pdf’. The current document reports on AFM measurement results and analysis performed on the corner feature test fields and meander fields on sample S6.

The AFM used for these measurements was a Veeco Dimension 3100 with a calibrated measurement space. The calibration was performed with traceable standards.
In order to achieve maximum fidelity of the measured profiles, a Bruker super sharp probe was used with the following specifications:

Parameter	
Type	TESP - SS
Tip height	10 – 15 µm
Tip radius	< 5 nm
Nominal resonance	320 kHz

The AFM measurements were corrected for a spherical probe shape effect of 5 nm.

All samples have been measured with the same probe and scanning speed. The AFM scanning area for the corner structures was nominally 2.5 µm × 2.5 µm and 5.0 µm × 5.0 µm for the meander structures in order to capture the most relevant features within the field of view. All measurements were taken at a speed of 0.1 lines/s for an image field of 512 pixels/line and 512 lines.

Before the final analysis of the data, intermediate processing was performed in order to level the raw data and minimize effects from drift and rotational misalignment. Within the measurement fields, relevant areas were selected by hand in order to exclude detrimental effects from the surrounding areas on the analysis results. The selected areas were leveled once more. Dedicated Matlab analysis scripts were used to detect all line edges and minima within the selected areas and to calculate the line width, LWR, LER and line depth. The threshold for the edge detection was set at 50 % of the maximum global depth within each selected area. The zero level was defined as the height level at the maximum of the highest peak in the histogram. The line width was calculated as average of the difference between edge points. The LWR was calculated as the standard deviation of the line width profiles. The LER was calculated as the standard deviation of the slope corrected edge profiles. The line depth was determined as the average of the collection of minima.

The results are presented as images of the scanned areas, the selected areas for horizontal and vertical lines structures including the detected edges, profiles averaged over the selected areas and tables with numerical results.

3.2.1. Sample SNM_TUIL_BOx7_S6_1stSPL

Corner feature test field

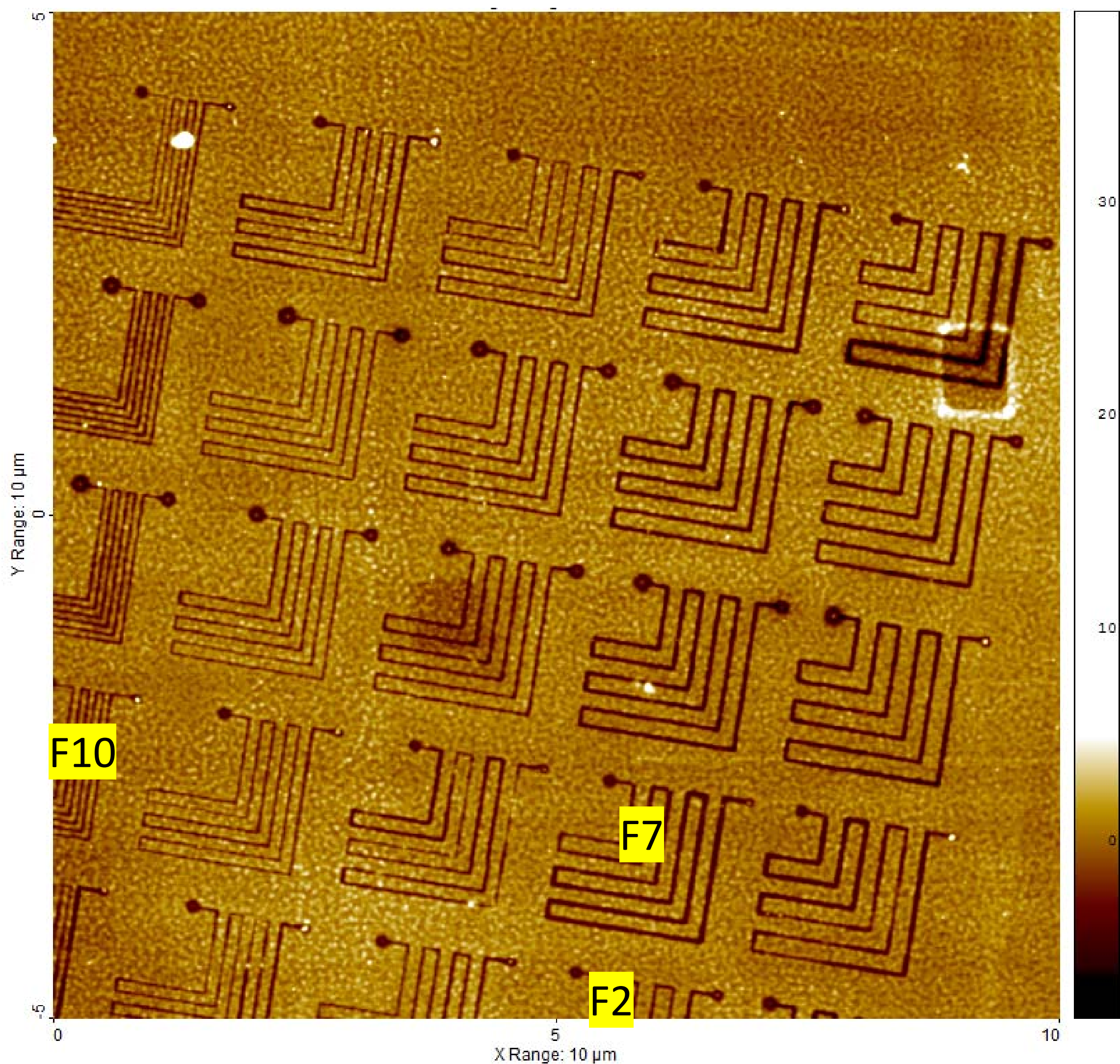

Figure 20. Overview scan of the corner feature test field in order to locate the features F2, F7 and F10.

Prior to the measurements of the features F2, F7 and F10 an overview scan was made in order to identify the orientation of the corner field. The overview of the corner field, Figure 20, shows that the base plane is textured. The analysis of the requested parameters, i.e. line width, LWR, LER and line depth, requires a well defined determination of the zero level. Once the raw AFM data has been leveled correctly, the surface is essentially planar. For the textured surface in the corner feature test field the zero level was determined by the maximum of the histogram peak that corresponds to the zero level.

Corner structure F2

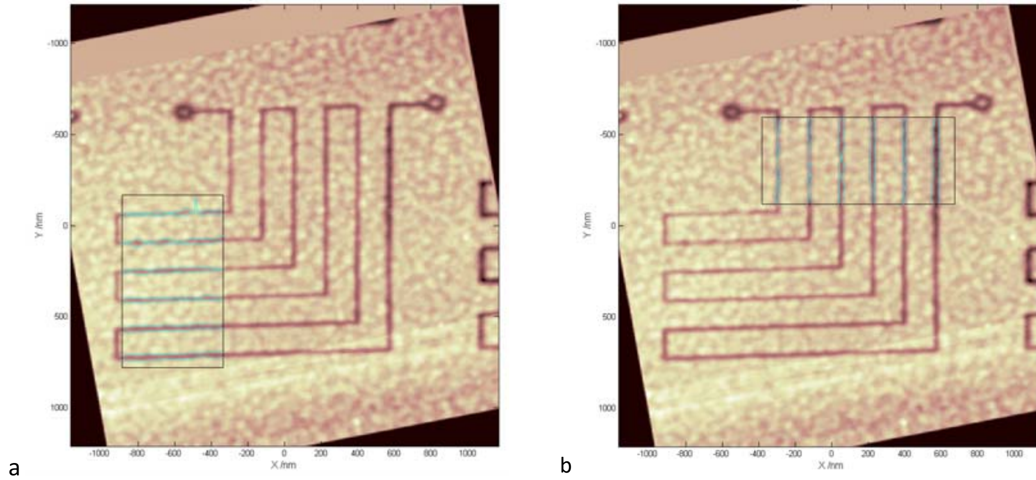

Figure 21. AFM measurement result on corner structure F2. The boxes indicate the areas in which the analysis was performed.

The analysis of the corner fields was performed for the horizontal and vertical direction separately. The areas were selected by hand and processed to extract the edges and minima for each scan line. The edge detection was based on the location of points at half the depth for each line. On rare occasions these points could not be identified because the local minimum was higher than the threshold. For these points an outlier was generated to indicate the missing edge.

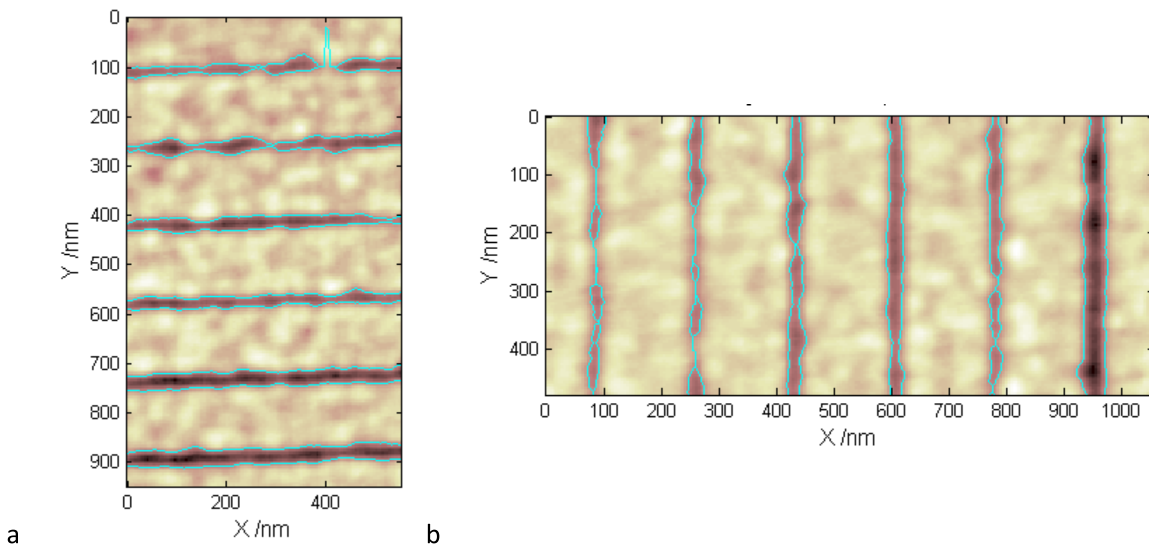

Figure 22. Selected areas on structure F2 for the analysis including the detected edges. The top curve in a) shows an outlier to indicate a missing edge.

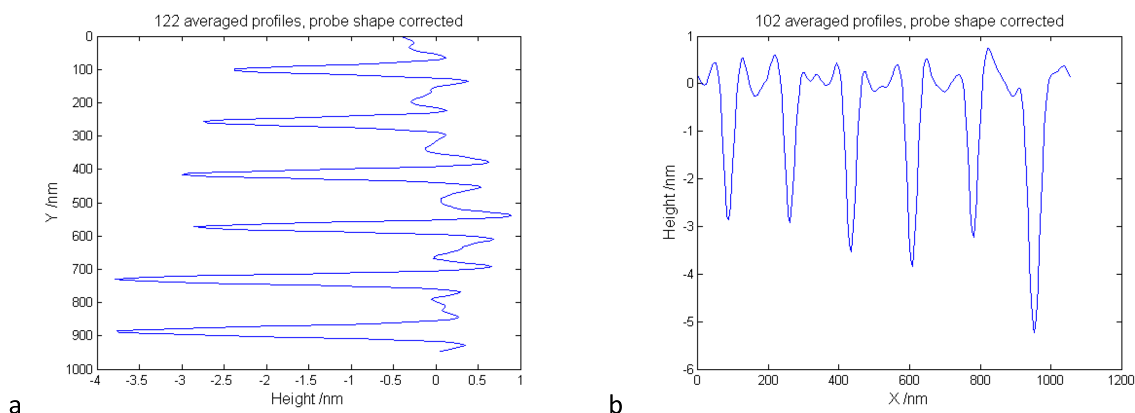

Figure 23. Averaged height profiles for the selected areas on structure F2.

	Line width /nm	LWR /nm	LER edge 1 /nm	LER edge 2 /nm	Line depth /nm
Line 01	17.6	7.8	9.8	11.4	-2.6
Line 02	22.0	7.9	4.8	4.5	-3.0
Line 03	21.8	6.2	3.7	3.0	-3.2
Line 04	20.5	3.6	2.8	2.0	-3.1
Line 05	30.2	2.6	2.4	1.8	-4.1
Line 06	32.1	3.8	2.7	2.6	-4.1

Table 18. Analysis results for the selected horizontal lines of structure F2. Line 01 corresponds to the upper line in Figure 18.

The difference between the minimum values of the average profile in the left graph of fig. 19 and the values in table 18 is due to differences in the determination of the minimum values for each profile and the minimum of the averaged profile.

	Line width /nm	LWR /nm	LER edge 1 /nm	LER edge 2 /nm	Line depth /nm
Line 01	10.5	8.6	5.1	4.6	-2.9
Line 02	10.8	9.8	4.5	5.7	-2.9
Line 03	20.1	5.8	3.9	3.4	-3.5
Line 04	23.0	4.2	2.5	2.2	-3.8
Line 05	15.8	7.1	3.8	3.5	-3.2
Line 06	37.1	5.7	3.7	1.8	-5.2

Table 19. Analysis results for the selected vertical lines of structure F2. Line 01 corresponds to the left most line in Figure 22.

Corner structure F7

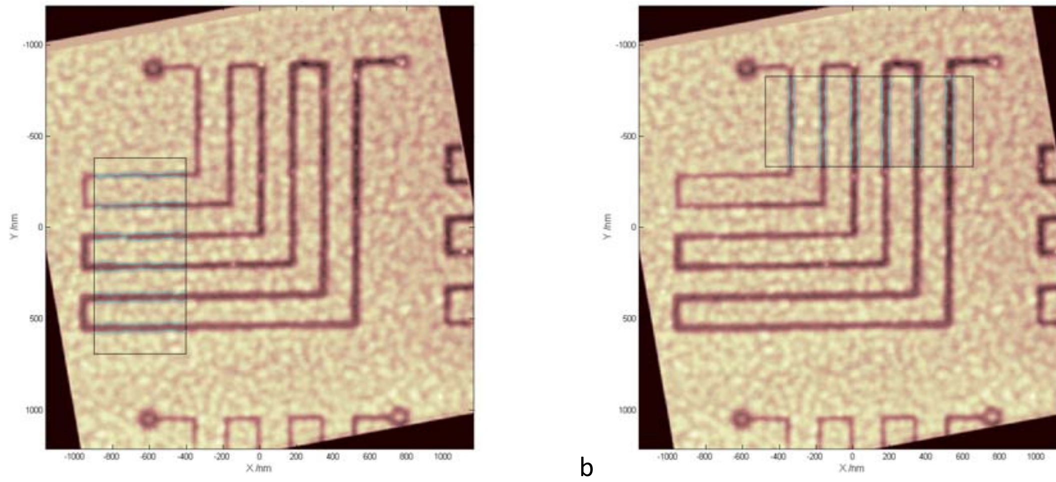

Figure 24. AFM measurement result on corner structure F7. The boxes indicate the areas in which the analysis was performed.

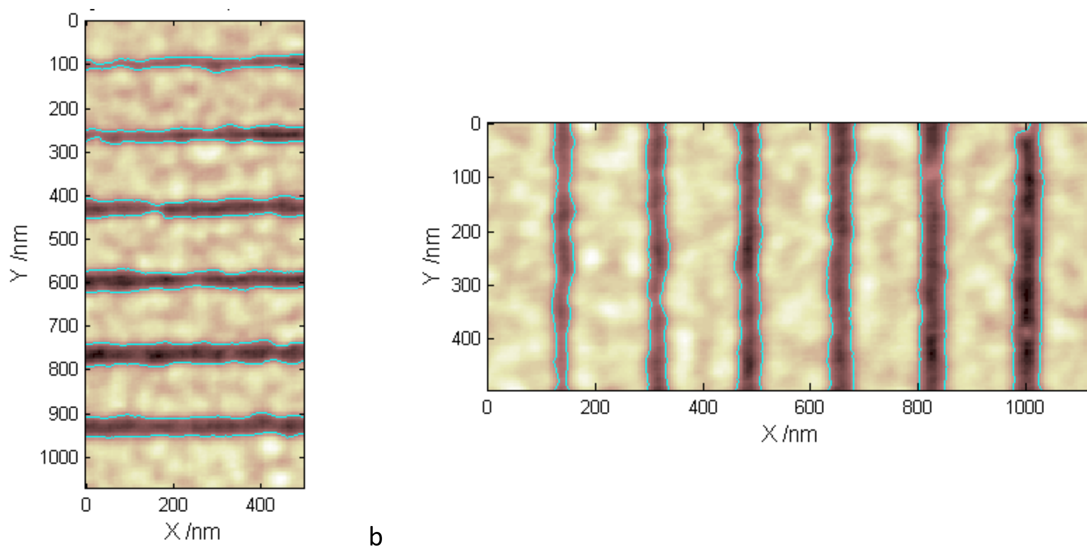

Figure 25. Selected areas on structure F7 for the analysis including the detected edges.

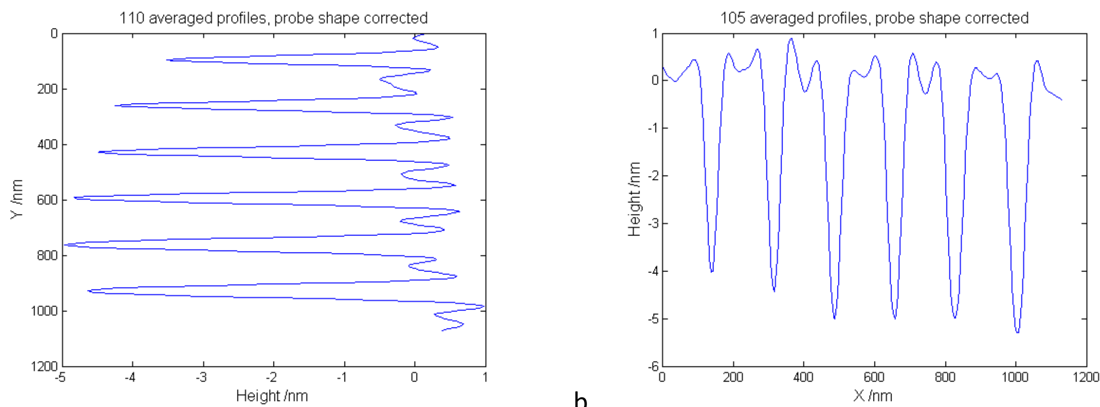

Figure 26. Averaged height profiles for the selected areas on structure F7.

	Line width /nm	LWR /nm	LER edge 1 /nm	LER edge 2 /nm	Line depth /nm
Line 01	22.5	6.0	2.9	3.7	-3.6
Line 02	29.7	6.2	2.7	3.2	-4.2
Line 03	35.9	6.9	4.0	3.9	-4.5
Line 04	39.7	6.6	3.2	3.2	-4.9
Line 05	46.7	4.7	2.7	2.6	-5.0
Line 06	43.4	3.4	3.0	2.2	-4.7

Table 20. Analysis results for the selected horizontal lines of structure F7. Line 01 corresponds to the upper line.

	Line width /nm	LWR /nm	LER edge 1 /nm	LER edge 2 /nm	Line depth /nm
Line 01	28.3	6.4	2.9	3.7	-4.1
Line 02	32.0	4.8	2.6	3.7	-4.4
Line 03	39.5	3.6	3.2	2.2	-5.0
Line 04	42.1	4.0	2.6	2.9	-5.0
Line 05	45.7	3.8	2.0	2.9	-5.0
Line 06	49.1	6.2	4.6	2.1	-5.4

Table 21. Analysis results for the selected vertical lines of structure F7. Line 01 corresponds to the left most line.

Corner structure F10

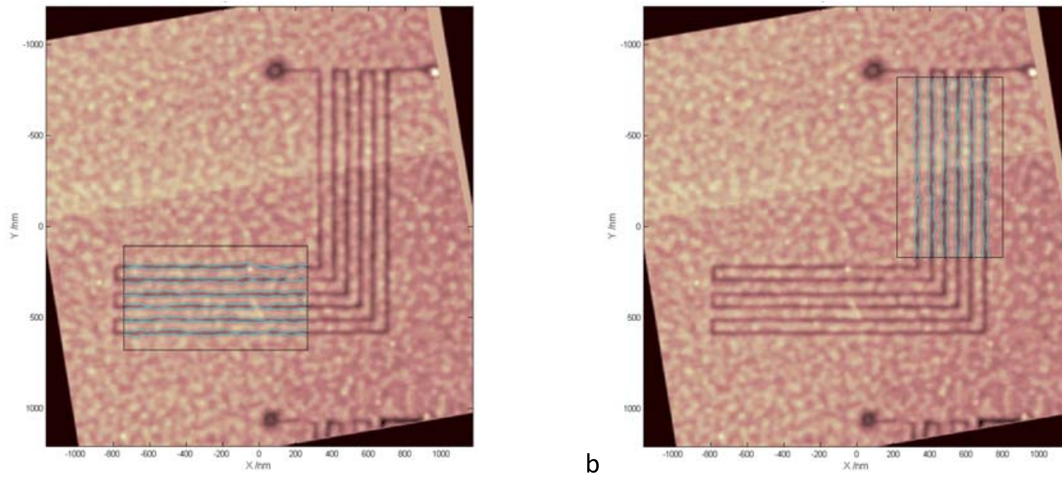

Figure 27. AFM measurement result on corner structure F10. The boxes indicate the areas in which the analysis was performed.

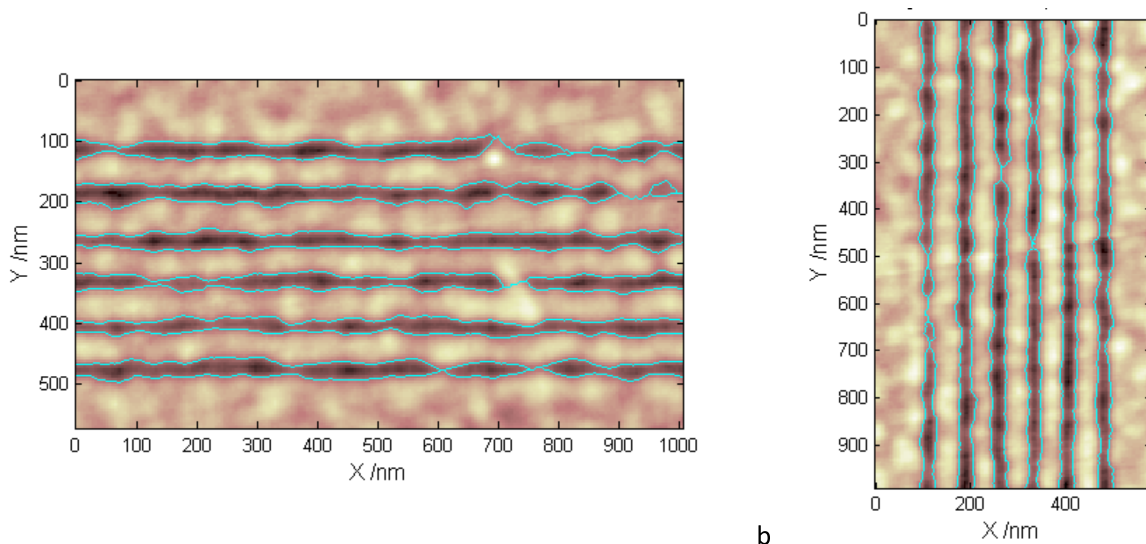

Figure 28. Selected areas on structure F10 for the analysis including the detected edges.

Funded by
the European Union

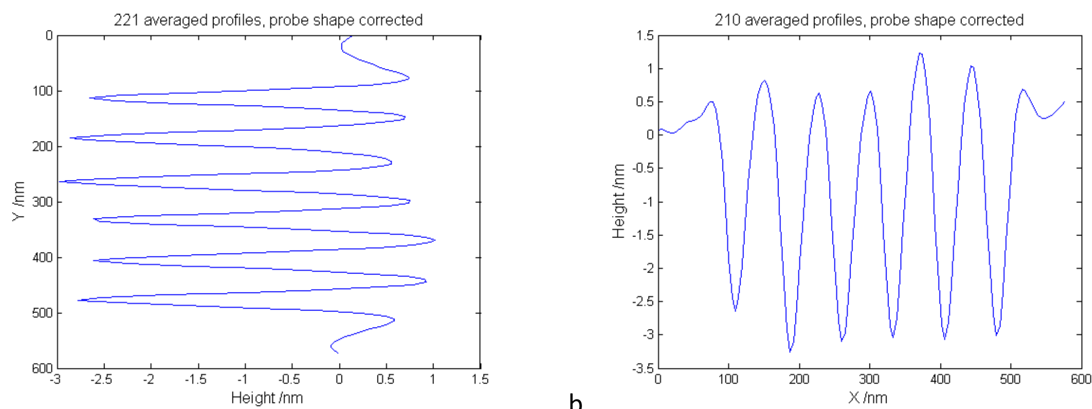

Figure 29. Averaged height profiles for the selected areas on structure F10.

	Line width /nm	LWR /nm	LER edge 1 /nm	LER edge 2 /nm	Line depth /nm
Line 01	21.0	8.4	5.4	6.3	-2.6
Line 02	24.1	9.2	5.0	4.8	-2.8
Line 03	24.0	5.2	3.5	3.2	-2.9
Line 04	21.0	7.6	4.9	3.8	-2.6
Line 05	21.3	5.1	4.0	3.4	-2.6
Line 06	22.4	7.4	4.5	4.2	-2.7

Table 22. Analysis results for the selected horizontal lines of structure F10. Line 01 corresponds to the upper line.

	Line width /nm	LWR /nm	LER edge 1 /nm	LER edge 2 /nm	Line depth /nm
Line 01	21.9	9.7	5.5	5.1	-2.6
Line 02	27.9	5.0	2.8	3.7	-3.2
Line 03	27.2	7.0	5.0	3.5	-3.1
Line 04	25.0	6.3	3.4	3.9	-3.0
Line 05	24.9	6.9	3.0	4.1	-3.0
Line 06	25.6	6.6	3.5	4.1	-3.0

Table 23. Analysis results for the selected vertical lines of structure F10. Line 01 corresponds to the left most line.

3.2.2. Sample SNM_TUIL_BOx7_S6_2ndSPL

Meander structure

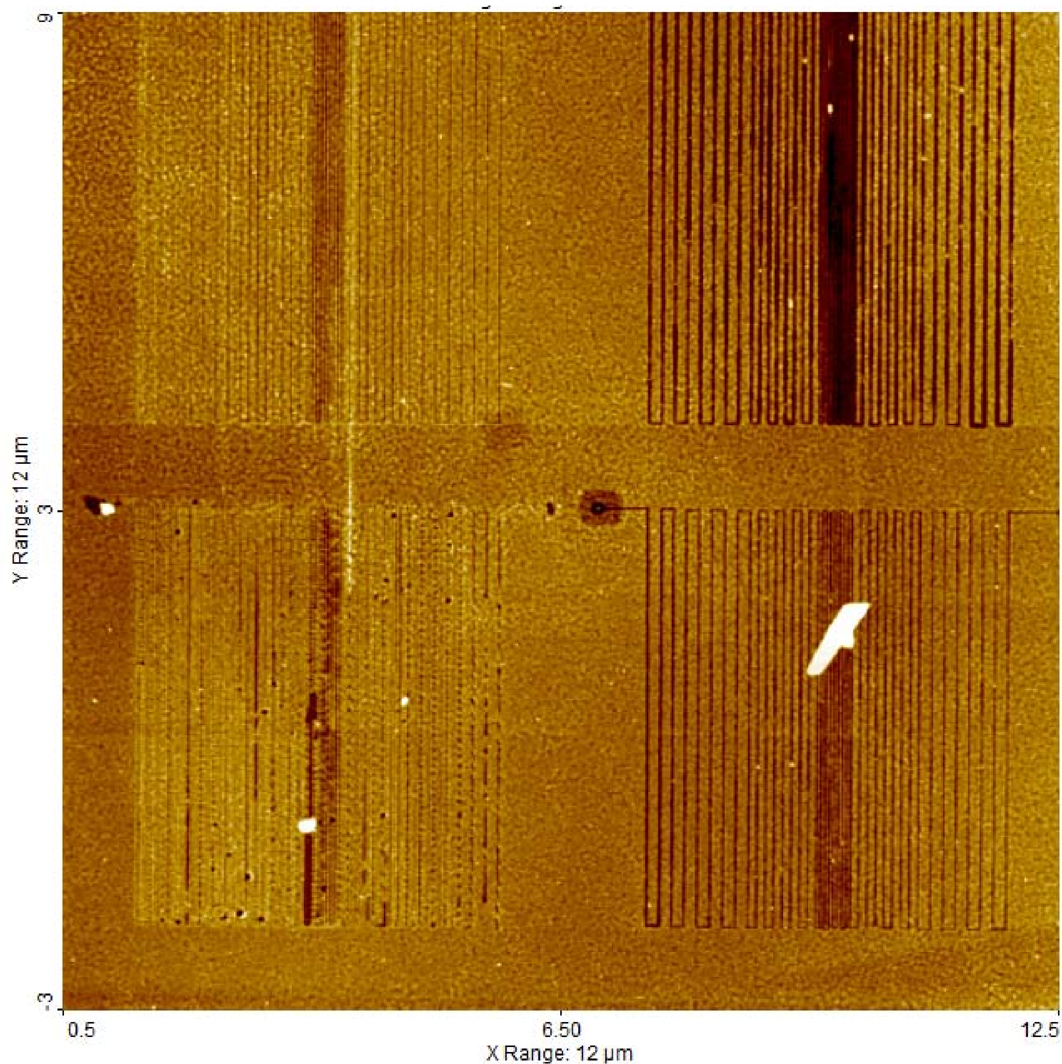

Figure 30. Overview of the second SPL structure that consists of 4 meander fields.

The size of the second SPL structure is about 10 µm x 10 µm as can be seen in Figure 30. In order to capture more detail of the individual fields, scans with areas of nominally 5 µm x 5 µm were taken.

Upper left meander structure

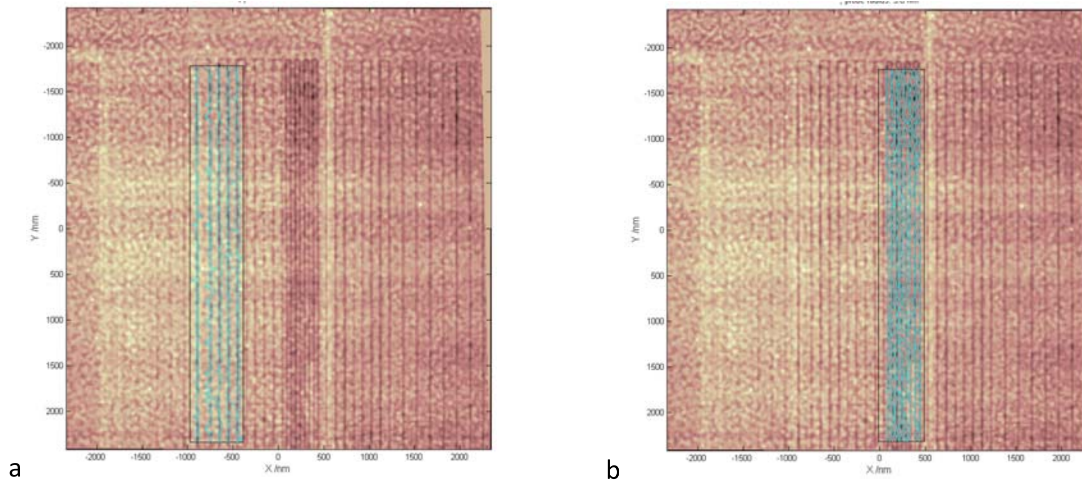

Figure 31. AFM measurement result on the upper left meander structure. The boxes indicate the areas in which the analysis was performed.

The right part of the image field could not be analyzed due to inconsistent edge detection.

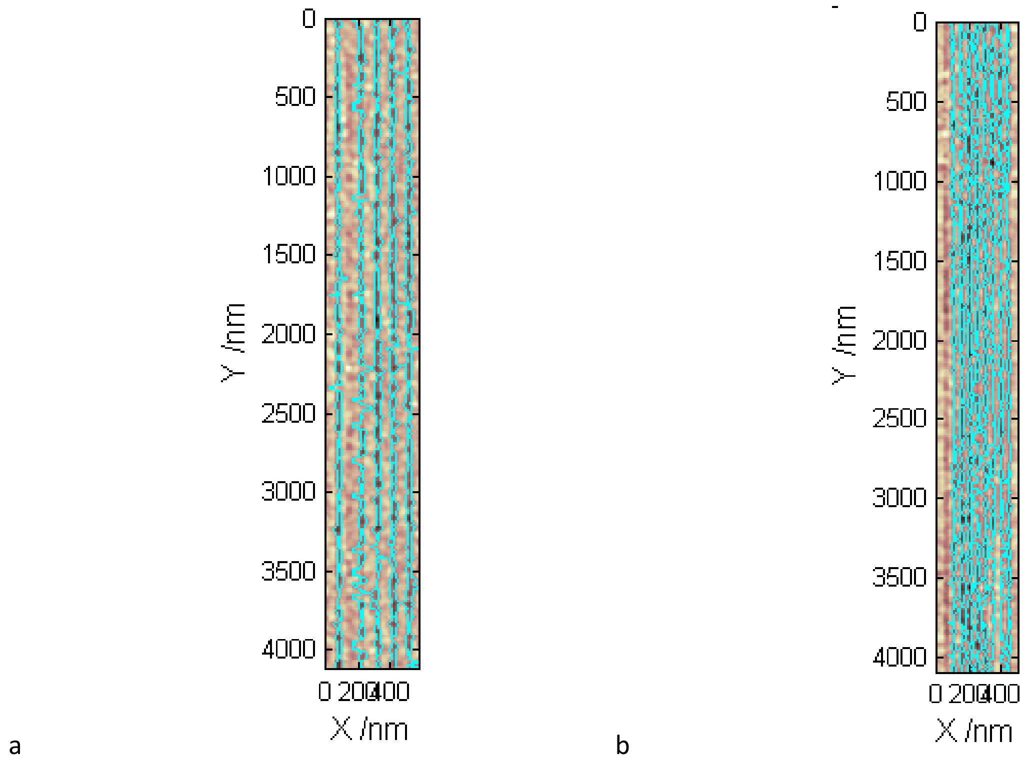

Figure 32. Selected areas on the upper left meander structure for the analysis including the detected edges.

Funded by
the European Union

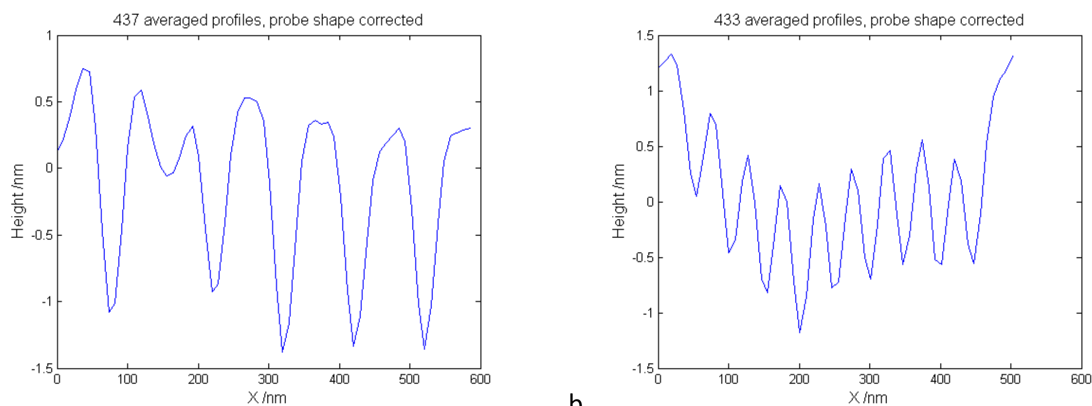

Figure 33. Averaged height profiles for the selected areas on the upper left meander structure. The average profile in b shows that the zero level cannot be defined accurately for this area.

	Line width /nm	LWR /nm	LER edge 1 /nm	LER edge 2 /nm	Line depth /nm
Line 01	19.9	12.0	9.2	9.4	-1.0
Line 02	19.0	14.0	18.8	22.8	-0.9
Line 03	27.2	12.8	8.7	9.0	-1.3
Line 04	28.7	12.9	8.2	9.4	-1.2
Line 05	28.1	13.0	10.0	10.9	-1.2

Table 24. Analysis results for the four selected vertical lines in the upper left meander structure. Line 01 corresponds to the left most line.

	Line width /nm	LWR /nm	LER edge 1 /nm	LER edge 2 /nm	Line depth /nm
Line 01	7.8	9.7	7.4	7.8	-0.4
Line 02	15.7	12.8	10.4	10.4	-0.7
Line 03	23.5	12.0	7.6	7.3	-1.0
Line 04	15.9	12.4	10.5	13.8	-0.7
Line 05	11.7	10.8	9.8	10.1	-0.6
Line 06	8.0	10.6	10.2	10.2	-0.4
Line 07	11.1	11.5	11.0	9.1	-0.5
Line 08	9.0	10.2	6.9	6.6	-0.4

Table 25. Analysis results for the eight selected vertical lines in the centre of the upper left meander structure. Line 01 corresponds to the left most line. Due to the line detection threshold the left The left most dip in the right figure was not qualified as

Upper right meander structure

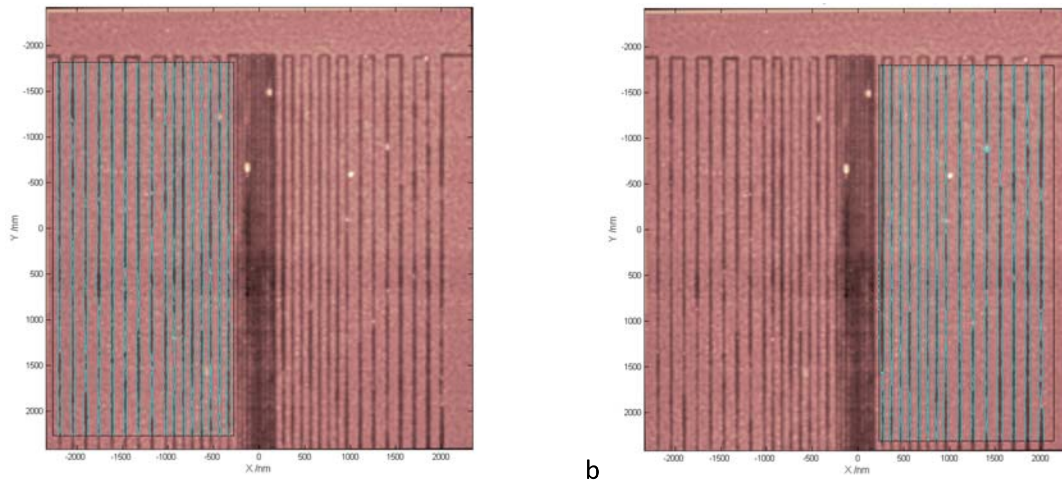

Figure 34. AFM measurement result on the upper right meander structure. The boxes indicate the areas in which the analysis was performed.

The corrugation in the dense region in the centre of the field could not be resolved.

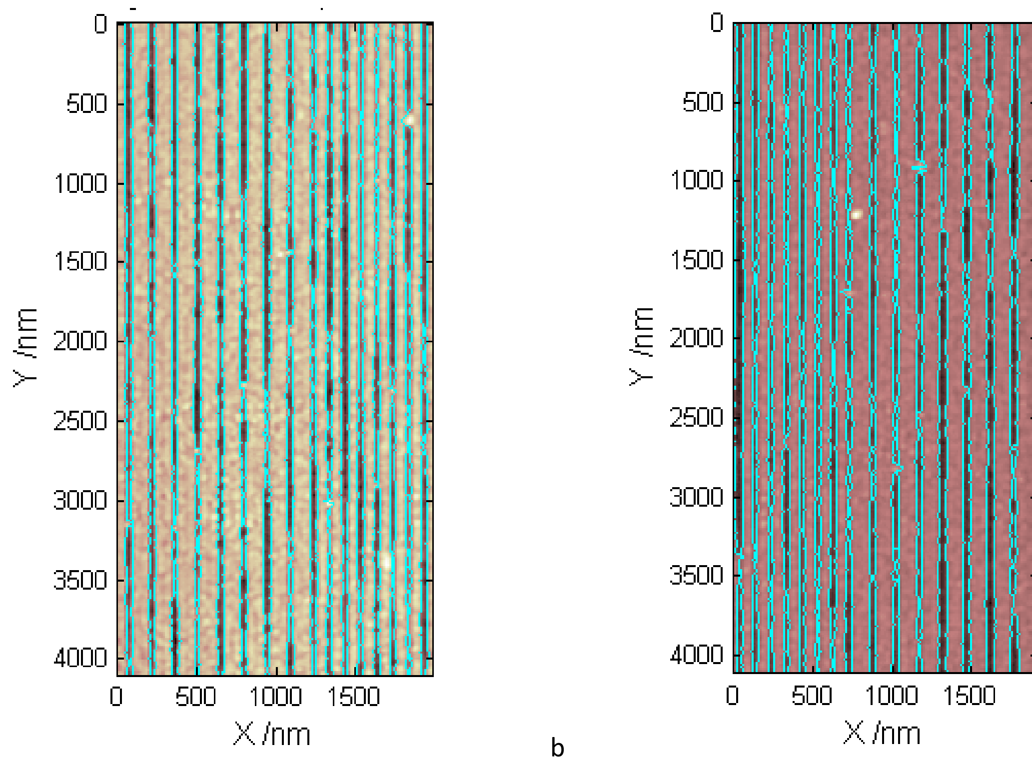

Figure 35. Selected areas on the upper right meander structure for the analysis including the detected edges.

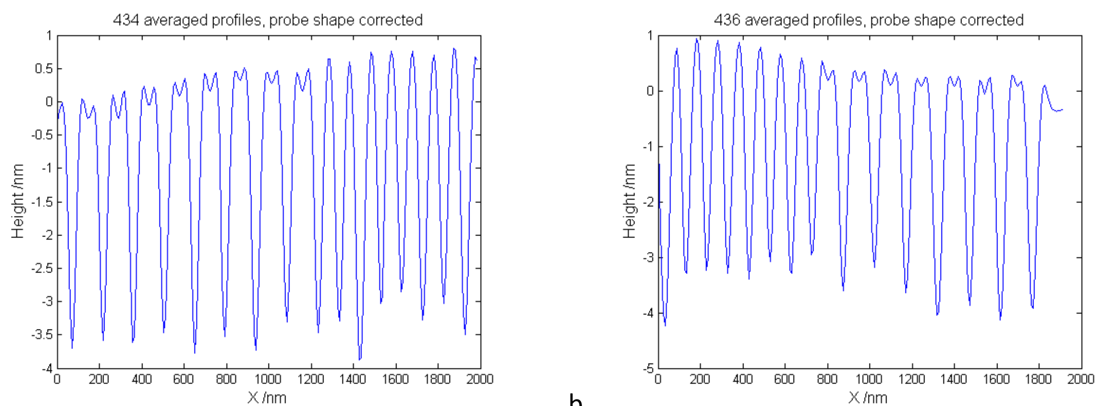

Figure 36. Averaged height profiles for the selected areas on the upper right meander structure.

	Line width /nm	LWR /nm	LER edge 1 /nm	LER edge 2 /nm	Line depth /nm
Line 01	38.2	8.1	4.6	4.1	-3.5
Line 02	36.5	9.6	5.2	5.2	-3.4
Line 03	35.8	8.6	4.1	5.5	-3.5
Line 04	35.1	12.3	6.4	5.9	-3.3
Line 05	36.9	6.2	3.7	3.4	-3.5
Line 06	35.3	11.8	5.8	6.8	-3.4
Line 07	38.5	11.1	5.7	6.0	-3.6
Line 08	31.8	11.7	7.2	6.2	-3.1
Line 09	33.5	9.6	4.6	6.1	-3.3
Line 10	32.1	13.4	7.3	7.2	-3.2
Line 11	42.6	9.1	5.0	4.6	-3.8
Line 12	28.9	11.0	5.8	5.3	-2.9
Line 13	24.7	14.3	5.5	5.8	-2.7
Line 14	32.6	11.6	6.7	6.2	-3.1
Line 15	28.6	12.2	5.1	8.2	-2.9
Line 16	35.4	7.9	4.0	5.2	-3.3

Table 26. Analysis results for the 16 selected vertical lines on the left in the upper right meander structure. Line 01 corresponds to the left most line.

	Line width /nm	LWR /nm	LER edge 1 /nm	LER edge 2 /nm	Line depth /nm
Line 01	45.7	12.5	8.0	5.1	-4.2
Line 02	29.1	10.0	4.8	5.1	-3.2
Line 03	26.9	9.0	4.8	5.0	-3.0
Line 04	28.1	10.4	5.3	5.3	-3.1
Line 05	29.4	4.9	3.0	2.9	-3.2
Line 06	25.2	8.4	3.9	4.7	-2.9
Line 07	31.2	10.5	5.4	6.0	-3.2
Line 08	26.4	13.6	6.8	8.6	-2.9
Line 09	35.0	7.9	4.4	4.5	-3.4
Line 10	28.3	11.9	7.1	5.7	-3.0
Line 11	36.0	12.0	8.4	8.3	-3.6
Line 12	44.5	11.8	5.2	6.2	-4.0
Line 13	38.9	10.2	5.9	5.1	-3.7
Line 14	42.4	13.7	7.0	5.7	-4.0
Line 15	42.2	14.5	6.6	9.1	-3.9

Table 27. Analysis results for the 15 selected vertical lines on the right in the upper right meander structure. Line 01 corresponds to the left most line.

Lower left meander structure

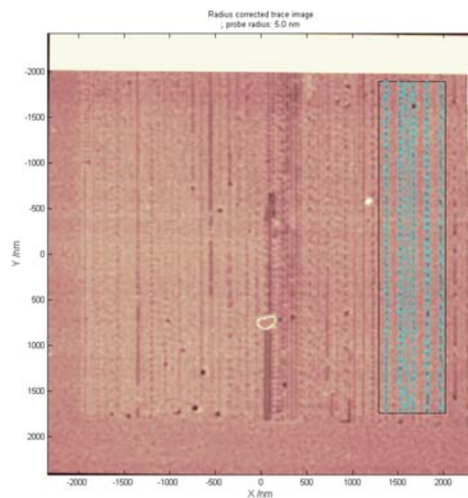

Figure 37. AFM measurement result on the lower left meander structure. The box indicates the area in which the analysis was performed.

Due to the irregular structures in the lower left meander only a small part of the region could be recognized as line-like features.

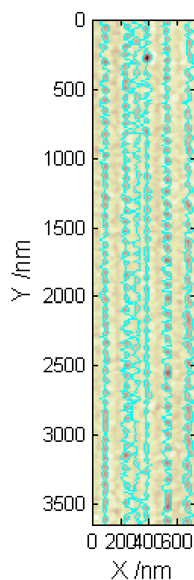

Figure 38. Selected area on the lower left meander structure for the analysis including the detected edges.

Funded by
the European Union

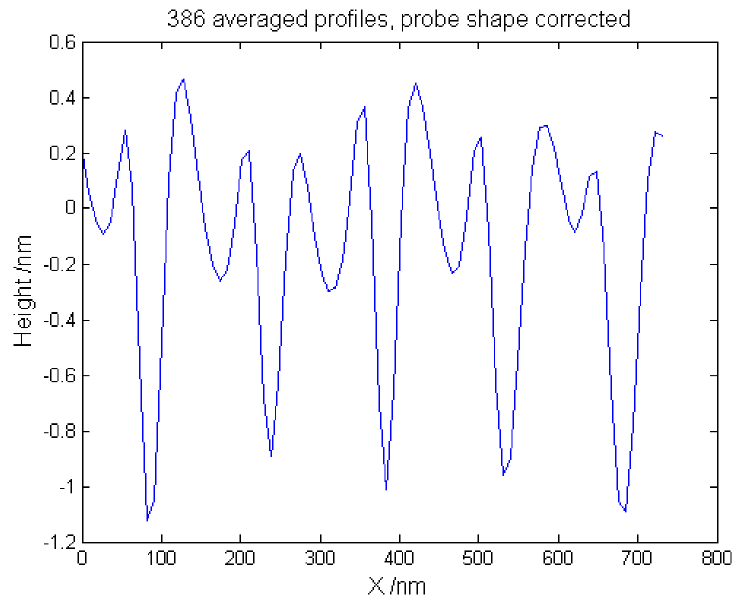

Figure 39. Averaged height profiles for the selected area on the lower left meander structure.

	Line width /nm	LWR /nm	LER edge 1 /nm	LER edge 2 /nm	Line depth /nm
Line 01	24.3	16.6	11.4	16.5	-1.0
Line 02	21.5	19.7	17.9	19.2	-0.9
Line 03	19.4	15.7	10.8	13.1	-0.9
Line 04	24.6	22.1	17.0	21.9	-1.0
Line 05	29.8	17.5	14.4	14.4	-1.2

Table 28. Analysis results for the 5 selected vertical lines on the right in the lower left meander structure. Line 01 corresponds to the left most line.

Lower right meander structure

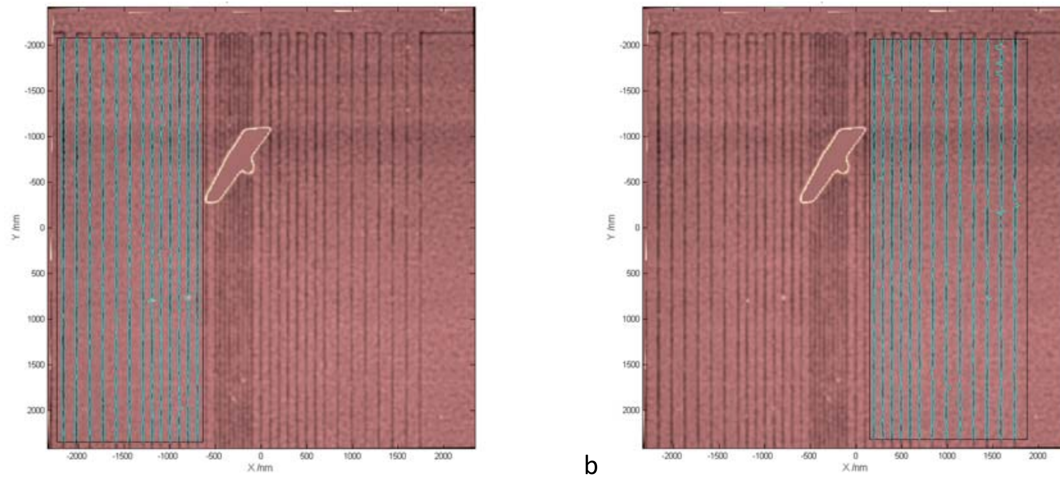

Figure 40. AFM measurement result on the lower right meander structure. The boxes indicate the areas in which the analysis was performed.

The dense region in the centre of the field could not be analyzed.

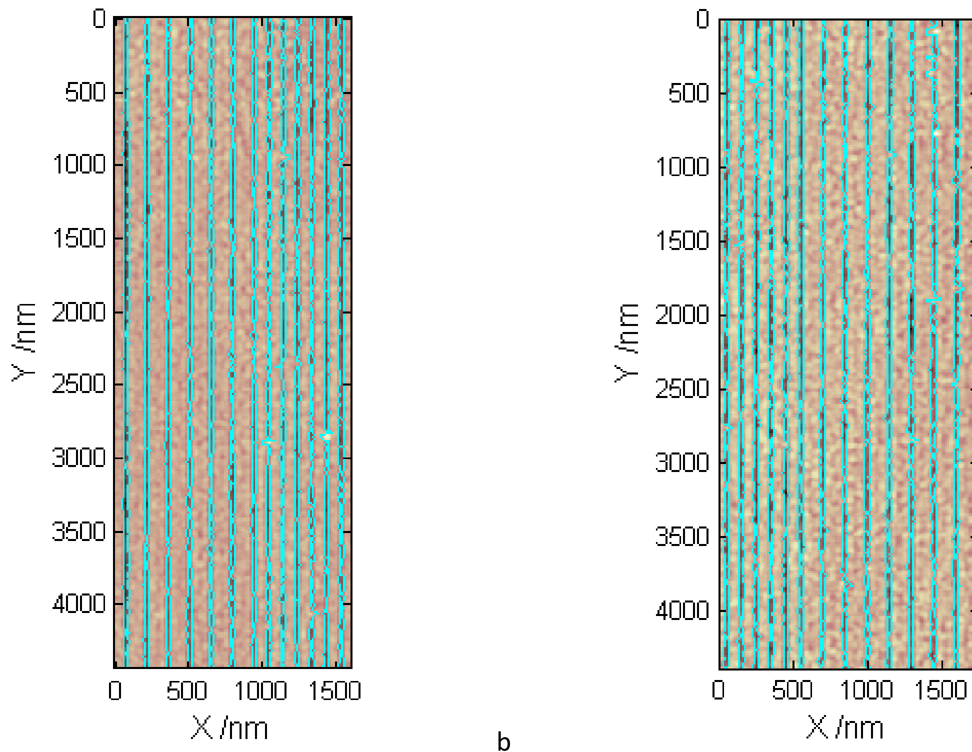

Figure 41. Selected areas on the lower right meander structure for the analysis including the detected edges.

Funded by
the European Union

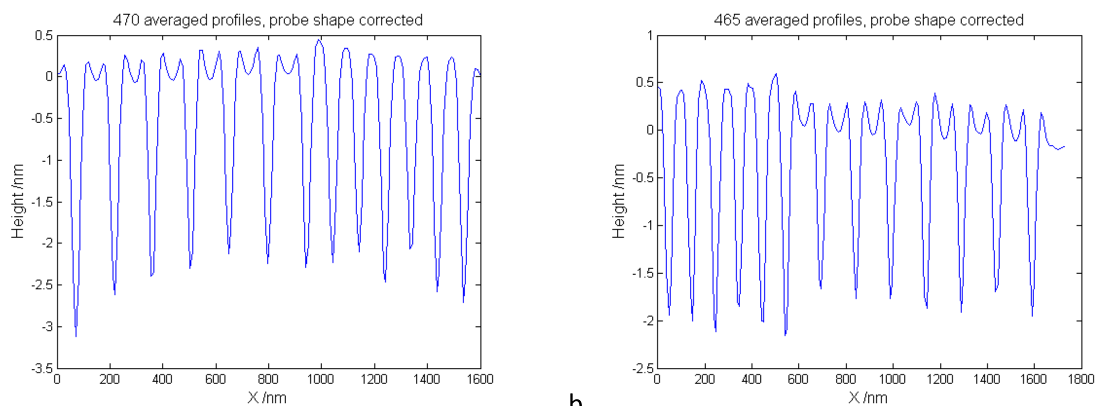

Figure 42. Averaged height profiles for the selected areas on the lower right meander structure.

	Line width /nm	LWR /nm	LER edge 1 /nm	LER edge 2 /nm	Line depth /nm
Line 01	32.9	6.9	4.0	4.3	-2.8
Line 02	27.1	6.4	3.8	3.8	-2.4
Line 03	23.6	7.4	4.3	4.1	-2.2
Line 04	22.0	8.5	4.4	4.9	-2.1
Line 05	18.4	8.8	5.2	4.9	-1.9
Line 06	20.5	10.1	5.9	5.4	-2.0
Line 07	21.3	9.0	4.9	5.1	-2.0
Line 08	20.6	10.5	7.4	7.4	-2.0
Line 09	18.2	9.9	7.2	6.6	-1.9
Line 10	25.4	9.0	6.2	4.4	-2.3
Line 11	18.6	12.4	7.4	7.1	-1.9
Line 12	27.3	8.5	5.5	6.3	-2.4
Line 13	28.7	8.6	4.6	4.7	-2.5

Table 29. Analysis results for the 13 selected vertical lines on the left in the lower right meander structure. Line 01 corresponds to the left most line.

	Line width /nm	LWR /nm	LER edge 1 /nm	LER edge 2 /nm	Line depth /nm
Line 01	26.9	8.9	6.6	5.6	-1.8
Line 02	25.7	9.8	5.6	6.3	-1.8
Line 03	28.4	9.6	6.5	6.7	-1.9
Line 04	25.0	8.8	5.0	5.2	-1.7
Line 05	28.2	9.2	6.1	5.0	-1.9
Line 06	28.9	7.1	3.8	4.1	-2.0
Line 07	22.4	11.5	6.4	6.6	-1.5
Line 08	24.4	9.5	5.5	6.3	-1.6
Line 09	25.2	10.7	5.7	6.8	-1.6
Line 10	26.6	9.7	6.9	6.0	-1.7
Line 11	25.8	11.1	7.1	6.3	-1.7
Line 12	26.0	11.3	9.9	12.3	-1.7
Line 13	28.0	9.8	7.2	6.3	-1.8

Table 30. Analysis results for the 13 selected vertical lines on the right in the lower right meander structure. Line 01 corresponds to the left most line.

3.2.3. Summary

The table below shows a summary of the results on the corner structures and meander structures as averages of the above data. The measurement uncertainty for individual measurements was usually smaller than the dispersion of the data so the standard deviation σ is given to reflect the dispersion of the data. Previously reported data from TUIL with results on the etched features F2, F7 and F10 are replicated below for comparison.

Table 31 Average values of the line width, line width roughness, line edge roughness and depth for the corner features F2, F7 and F10.

Feature	Line width	σ	LWR	σ	LER	σ	Depth	σ
	/nm	/nm	/nm	/nm	/nm	/nm	/nm	/nm
F2	21.8	8.1	6.1	2.2	4.0	2.3	-3.5	0.7
F7	37.9	8.3	5.2	1.3	3.0	0.7	-4.7	0.5
F10	23.8	2.4	7.0	1.5	4.2	0.9	-2.8	0.2

Table 22 Average values of the line width, line width roughness, line edge roughness and depth for four field in the meander structure. UL = upper left, UR = upper right, LL = lower left, LR = lower right.

Feature position	Line width	σ	LWR	σ	LER	σ	Depth	σ
	/nm	/nm	/nm	/nm	/nm	/nm	/nm	/nm
UL	17.3	7.7	11.9	1.3	10.2	3.5	-0.8	0.3
UR	34.1	5.8	10.6	2.3	5.7	1.3	-3.3	0.4
LL	23.9	3.9	18.3	2.6	15.7	3.5	-1.0	0.1
LR	24.8	3.7	9.4	1.4	5.9	1.5	-2.0	0.3

Table 333 Replicated results from report TUIL SNM_Samples_SOI_Box7_S6&7_After Plasma Etching_Metrology at VSL.pdf for the etched features F2, F7 and F10.

Feature	Line width	σ	LWR	σ	LER	σ	Depth	σ
	/nm	/nm	/nm	/nm	/nm	/nm	/nm	/nm
F2							-4.4	
F7							-5.9	
F10							-4.0	

3.2.4. Conclusions

Measurements on the line width, LWR , LER and profile depth and profile shape were performed successfully on the etched SPL pattern from TUIL. Comparison of measurement results on these samples is challenging since the results depend on the exact measurement position and instrumental settings and probe characteristics. Since the TUIL data were provided only for the depth and without measurement uncertainty a quantitative comparison is not possible but the results on the depth measurements are similar.

3.3. AFM measurements on Nanowire sample from UBT

A nanowire sample on a silicon support from SNM partner UBT with identification according to fig. 1 was measured at VSL using a Veeco Dimension 3100 AFM.

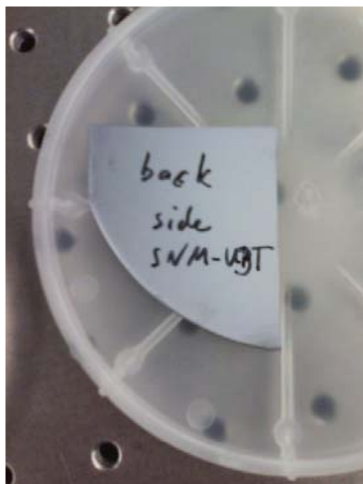

Figure 43. *Sample identification (backside)*

In order to achieve maximum fidelity of the measured profiles, a Nanotools carbon nanotube-like probe was used with the following specifications:

Parameter	Specification
Type	M-CNT-100, High Density carbon tip
Cylinder shape length	100 nm (± 20 nm)
Cylinder diameter	10 nm (± 2 nm)
Nominal resonance	320 kHz

The measurements were performed at an arbitrary location near the centre of the sample in AFM tapping mode. The AFM scanning area was nominally 450 nm × 450 nm and was measured at a scan rate of 1.97 lines/s.

The raw data were processed to minimize effects from drift, noise and sample tilt. The calibration of the lateral scale and the height of the measurement fields was performed using traceable standards.

It was found that the nanowire profile shape as measured with the AFM was strongly dependent on the so-called AFM setpoint parameter that basically controls the interaction height between the AFM probe and the surface. The measurements were therefore performed using different settings of this parameter.

3.3.1. Wide area scan

The sample was first measured over an area of nominally 1.4 µm x 1.4 µm to investigate the density of the deposition and enable the selection of a suitable region for more detailed analysis. The result, Figure 44, shows a collection of nanowires with a coverage of about 20 %. The wires are mostly curved and overlapping with a few isolated wires. The measurement in Figure 44 was acquired with the highest possible setting for the setpoint value before instability of the probe-sample interaction occurred.

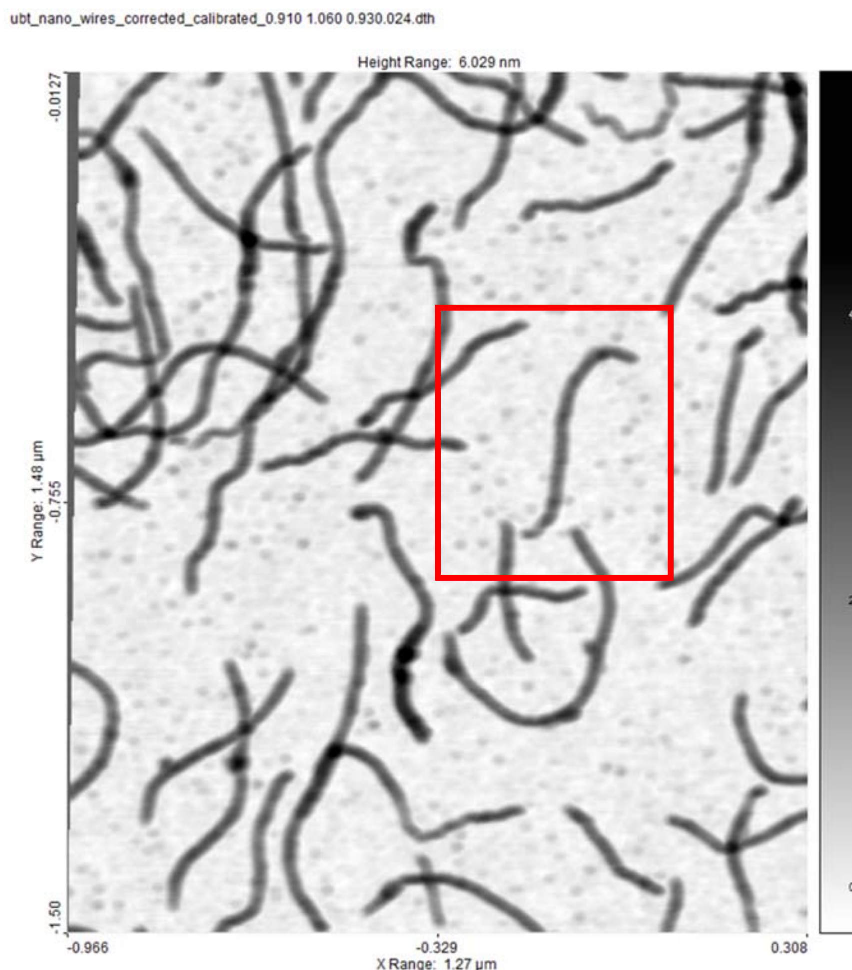

Figure 44. Measurement result on the sample over an area of nominally 1.4 µm x 1.4 µm shown in reversed contrast for clarity. An isolated wire near the centre of the image was selected for more detailed analysis.

In order to illustrate the effect of the AFM tapping mode setpoint parameter value, the indicated area from Figure 44 has been measured for a range of different values. Although the values are related to the details of the interaction between the probe and sample, the absolute value has little meaning and the setpoint may be set to a wide range of values. The range is limited on the lower side because of instabilities in the feedback control below a certain threshold and limited on the higher side because contact between the probe and sample is lost above a certain threshold. In the results below, the setpoint was set to four values spanning the region of stable imaging.

3.3.2. AFM measurements as a function of the tapping mode setpoint parameter

As shown in the Figure 45 to Figure 48, the appearance of the nanowires depends on the value of the setpoint that controls the interaction between the probe and the sample. Since the interaction between the probe and the sample is depending on the probe shape, probe material and sample material the setpoint has to be fine tuned for every situation. The optimum value however depends on what

information is required; the setpoint can be optimized for maximum contrast, highest resolution or best visual appearance.

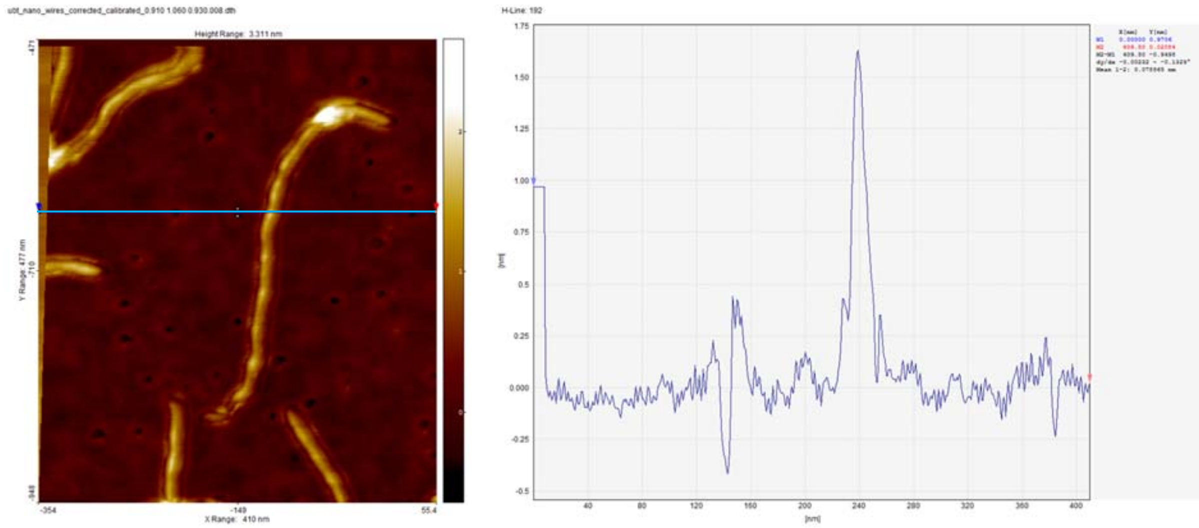

Figure 45. AFM measurement for a setpoint value of 0.6799 and a single profile crossing the nanowire.

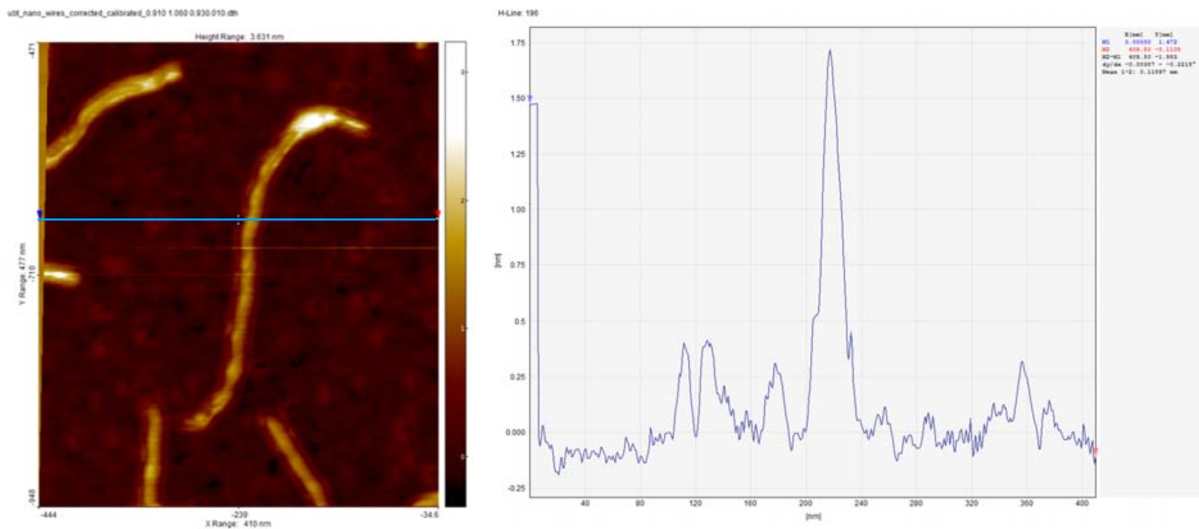

Figure 46. AFM measurement for a setpoint value of 0.7052 and a single profile crossing the nanowire.

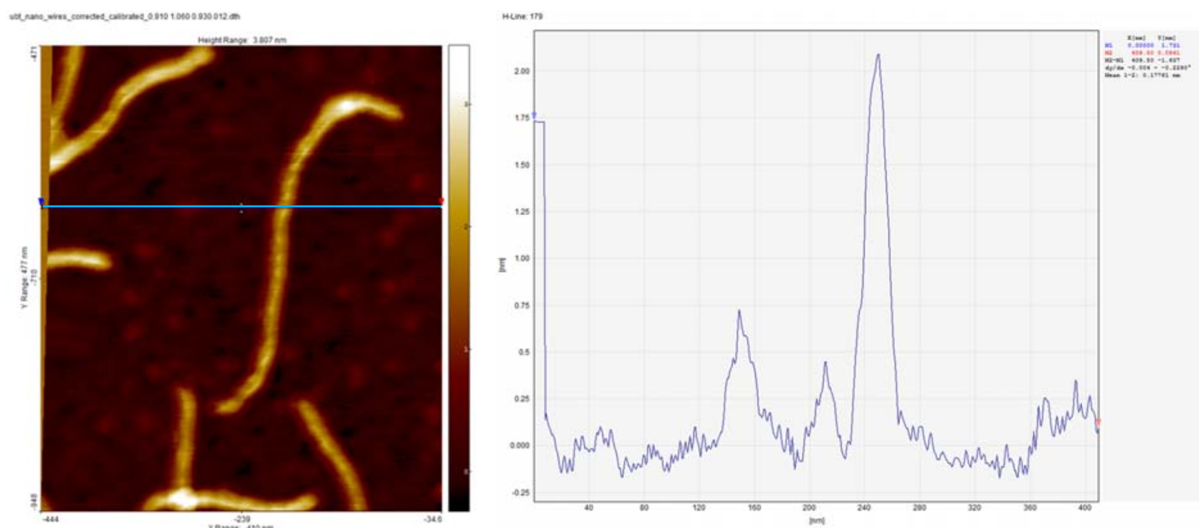

Figure 47. AFM measurement for a setpoint value of 0.7305 and a single profile crossing the nanowire.

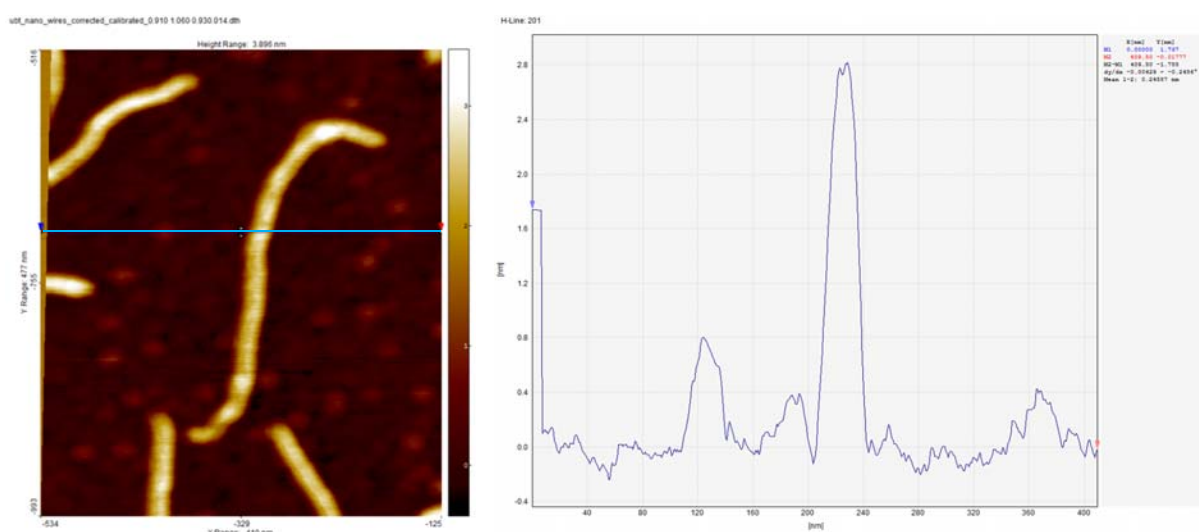

Figure 48. AFM measurement for a setpoint value of 0.7558 and a single profile crossing the nanowire.

The data from Figure 45 to Figure 48 were analysed using the software package SPIP (scanning probe image processor) from Image Metrology.

A more detailed analysis of the height and width along the selected nanowire was performed with a dedicated Matlab script. Because of the corrugated background, the height along the wire was defined as the collection of maxima of each horizontal profile relative to the minimum value in the profile.

An attempt has been made to correct for probe shape effects in the calculation of the width. Although presented below, the results were quite noisy on the selected structure so the quantitative data for the average height and uncertainty were calculated from the uncorrected data.

3.3.3. Height for setpoint parameter value 0.6799 and for 0.7558 (as examples)

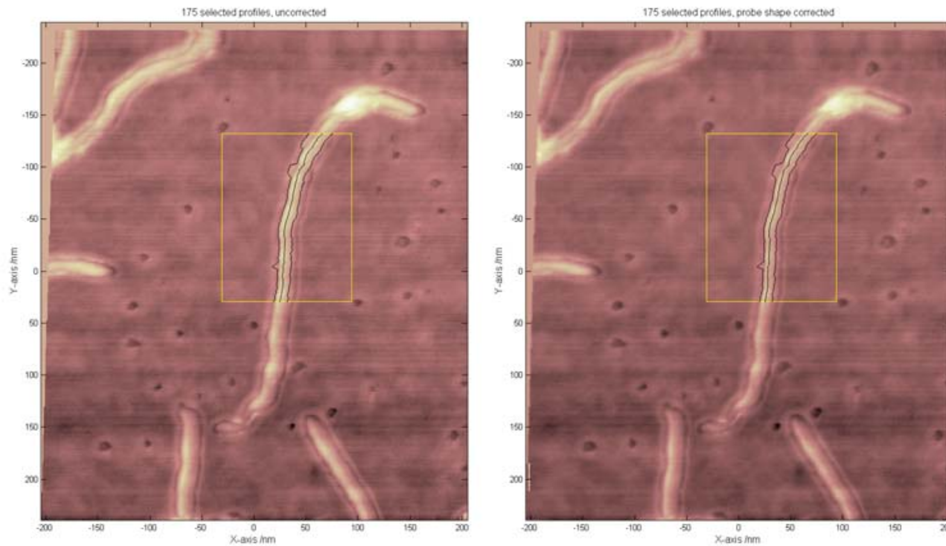

Figure 49. Analysis of the single wire for the lowest setpoint value of 0.6799.

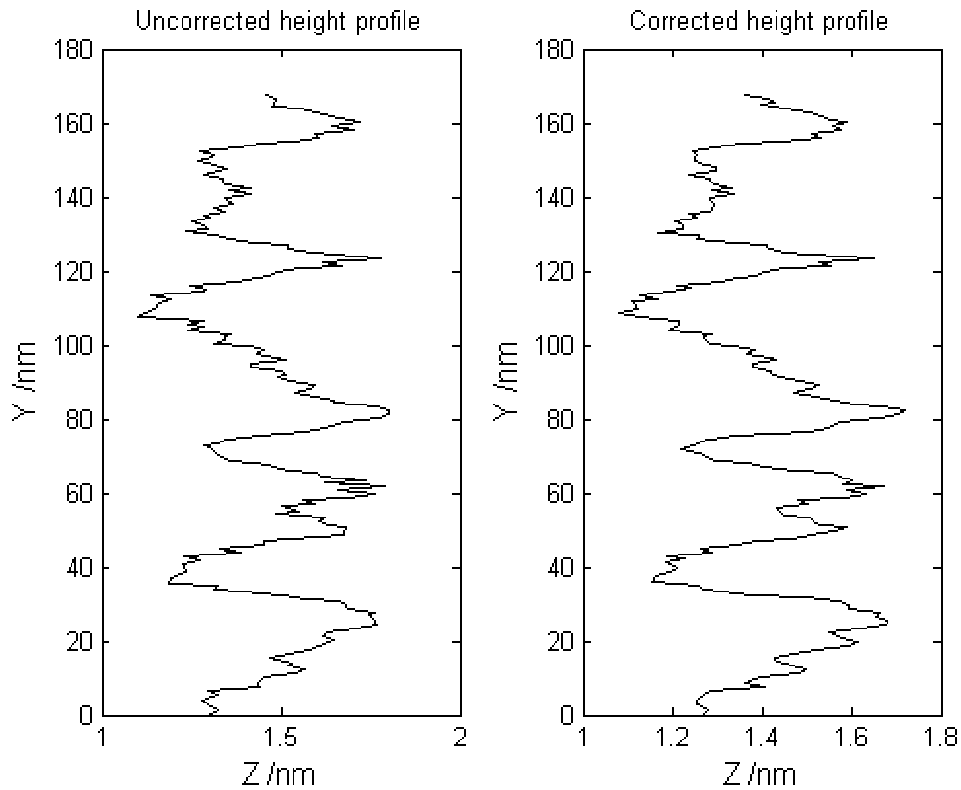

Figure 50. Height profile along the selected wire for the setpoint value of 0.6799.

Average height /nm	Uncertainty (95% coverage) /nm
1.4	0.3

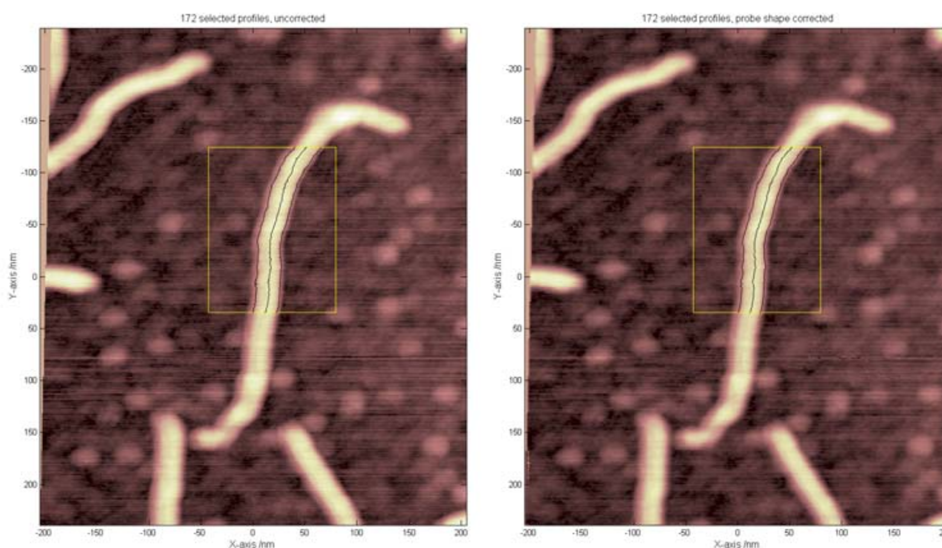

Figure 51. Analysis of the single wire for the setpoint value 0.7558.

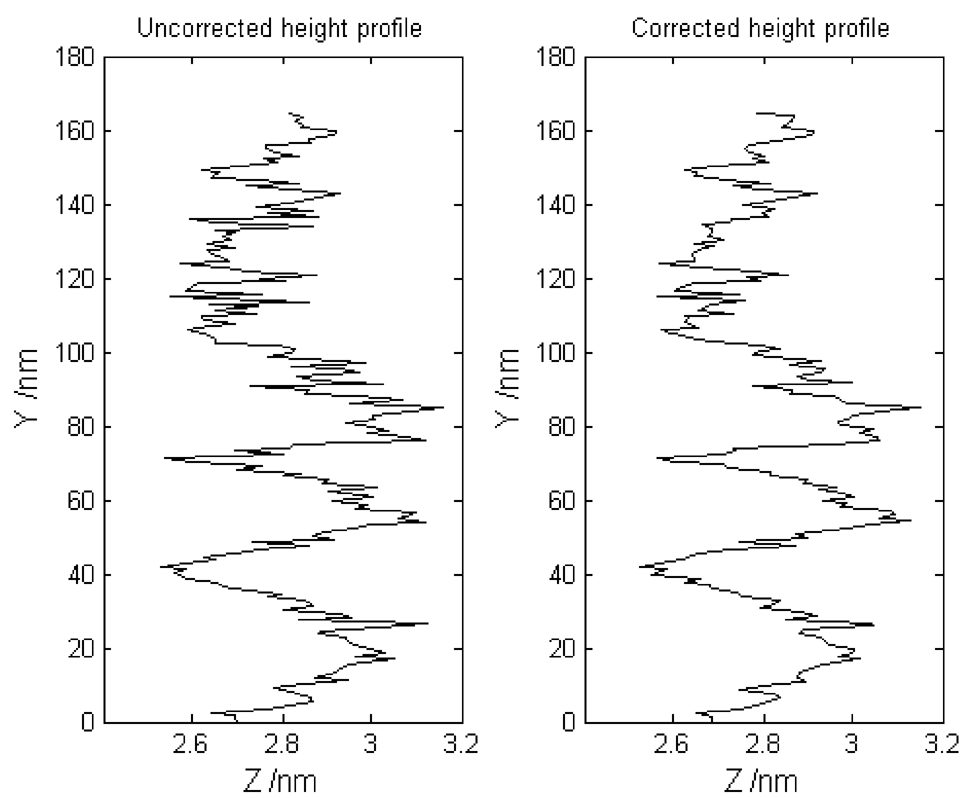

Figure 52. Height profile along the selected wire for the setpoint value of 0.7558.

Average height /nm	Uncertainty (95% coverage) /nm
2.8	0.3

3.3.4. Summary

Table 4 Summary of all height data measured.

Setpoint	Height	U95
/V	/nm	/nm
0.6799	1.4	0.3
0.7052	1.6	0.3
0.7305	2.1	0.3
0.7558	2.8	0.3

The measured height is found to depend strongly on the AFM measurement setpoint.

3.3.5. Conclusion – AFM measurements of the nanowire structure

These measurements were performed to study the potential application of this type of nanowire as reference structures for height and diameter calibration purposes. It was found that the measured height of the nanowire structure is dependent on the measurement settings of the AFM. The apparent height varies between (1.4 ± 0.3) µm and (2.8 ± 0.3) µm for a range of the AFM tapping mode setpoint parameter values that result in stable imaging. Application of these nanowires as reference structures is therefore not very likely since the choice of the setpoint parameter value is arbitrary within the range of stable imaging. It is suspected that the dependence on the AFM setpoint is related to the material (mechanical) properties of the nanowires.

4. OSC: Helium Ion Beam Microscopy (HIM) Measurement of SNM Patterns

4.1. SPL patterned calixarene/Au/Si

OSC's activities in WP7 during year 2 of the project were mainly focused on He Ion Microscope (HIM) evaluation of SPL patterned samples from TUIL. The first samples were 10 nm thick calixarene resist on a thin layer of gold on a single crystal silicon substrate. Images were taken top-down (normal incidence of the He^+ beam) as agreed. Description of the location of the images followed TUIL's test chip registration protocol (see Figures below).

All results were taken at the "best imaging voltage" for these samples of 32.6 kV with a nominal beam current of 0.6 pA; the field of view (FOV) is recorded for each image in addition to the scale bar. It is in the nature of the images that they are largely flat and featureless with the only areas of interest being the exposed trenches in the resist. These contain clusters of gold particles formed in a fluid like agglomeration process from destabilization of the thin gold film which is employed as an anti-charging layer.

Figure 53 shows typical results in which the nominal width of the resist trenches is 57 nm taken from region F33A of the meander lines in the TUIL test pattern. The Au clusters forming in the trenches are sometimes

Funded by
the European Union

self-organized in double file at this width with an indication of segregation to the walls or edges of the trench.

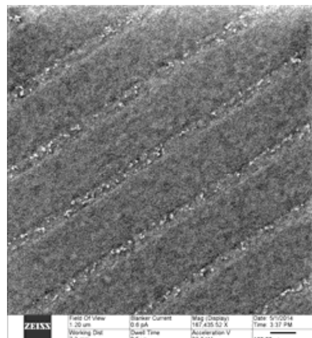

Figure 53. Image OSC3_F33A_02 (FOV 1.2 µm)

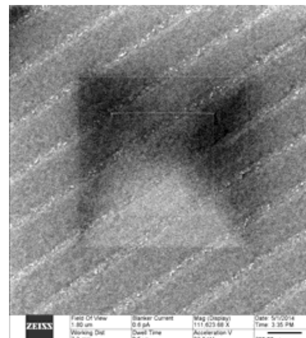

Figure 54. Image OSC3_F33A_02 (FOV 1.2 µm)

Figure 54 shows the same region of the sample at a larger field of view (1.8 µm *cf*. 1.2 µm) in which there is evidence of carbon contamination of the surface. This was caused during HIM by focused ion beam deposition decomposition of surface hydrocarbons present in the vacuum. The hydrocarbon contamination is associated with multiple imaging of the same area during HIM investigation which causes increased local dose. However, it is clear that multiple scanning does not degrade the key features of linewidth, line edge roughness or the appearance of the Au particles.

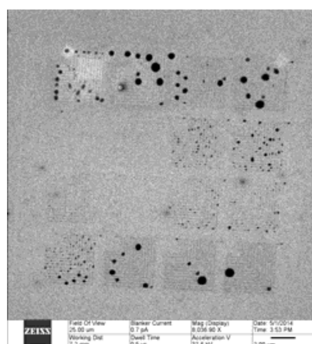

Figure 55. Image OSC3.3_F33C (FOV 25 µm)

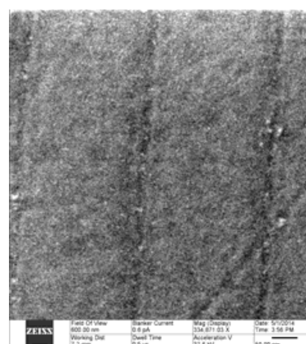

Figure 56. Image OSC3.3_F33C_02 (FOV 600 nm)

Figure 55 shows a general view at larger magnification from which the detail is shown at higher magnification in Figure 56. There is curvature in some trench lines and crossed lines are also present, implying an issue with scanning during the SPM writing process. The lines are rather faint with nominal width 28 nm. At this width (roughly half of those in Figure 53), the gold clusters self- organize in single file instead of the double file seen in Figure 53. This is a significant result, providing insight into the Au cluster formation and alignment processes which need to be investigated further.

The faint nature of the lines is a potentially complex issue and needs further consideration and discussion. In the meantime it is important to recognize that the faintness is not a resolution shortcoming, as the Image resolution estimated from the clearly imaged gold nanoparticles in the right hand image is around 3 nm. Poor secondary electron statistics at small dimensions and probe size combined with low contrast are probably the main contributing factors.

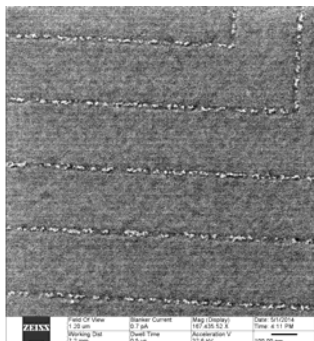

Figure 57. Image OSC3_F33C-05/06 (FOV 1.2μm)

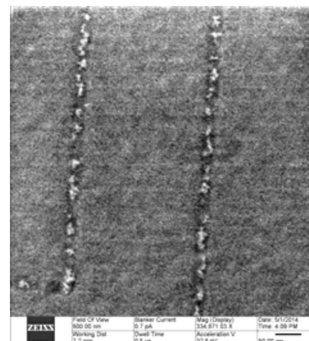

Figure 58. Image OSC3_F33C_07 (FOV 600nm)

Figure 57 shows well delineated clear lines of nominal width 28 nm with single file organization of relatively large clusters which are big enough to fill the width of the patterned channels, hence the single file self - assembly. The clusters are shown in more detail in Figure 58.

Figure 59 shows two new phenomena, one is a purely technical artifact due to the HIM system and the other a more fundamental result of the nature of the He ion beam and its interaction with the resist-on-silicon sample surface:

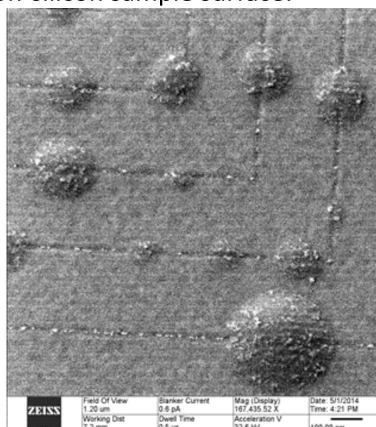

Figure 59. Image OSC3_F33C_07 (FOV 1.2μm)

This image shows areas in which the resist has become domed with what appear to be gold clusters on the surface. How these domes originate is not entirely clear but they may be due to He gas bubble formation which is an established effect in HIM. Alternatively, the protrusions may be due to tiny bubbles of He formed around defects introduced during the resist coating process. The surface of each dome is decorated with Au clusters. This is the only occasion that Au cluster decoration has been seen other than in locations where the resist has been removed. Gold migration through the resist surface is one possibility but for the present this phenomenon is somewhat puzzling and requires further investigation.

There are faint, evenly spaced horizontal lines etched into the surface of the resist. These were not produced during SPL lithography at TUIL but are associated with the image scan system of the HIM which produces X-scan lines spaced vertically by approximately 25 nm. These lines are not an issue at lower magnification but at the higher magnifications required for the current work, they become visible. Reducing this spacing, should be possible, but this will increase the time required to acquire images. For the present, since this artifact does not affect the ultimate resolution and utility of the images, it is not being treated as a priority.

Further experiments were performed using wafers patterned by SPL at TUIL without the Au underlayer. These plain Si samples showed no nanoparticle decoration. It is therefore confirmed that the nanoparticle effects in resist nanotrenches are due to liquid-like cluster formation of the gold underlayer occurring as it is exposed to form a free surface during SPL.

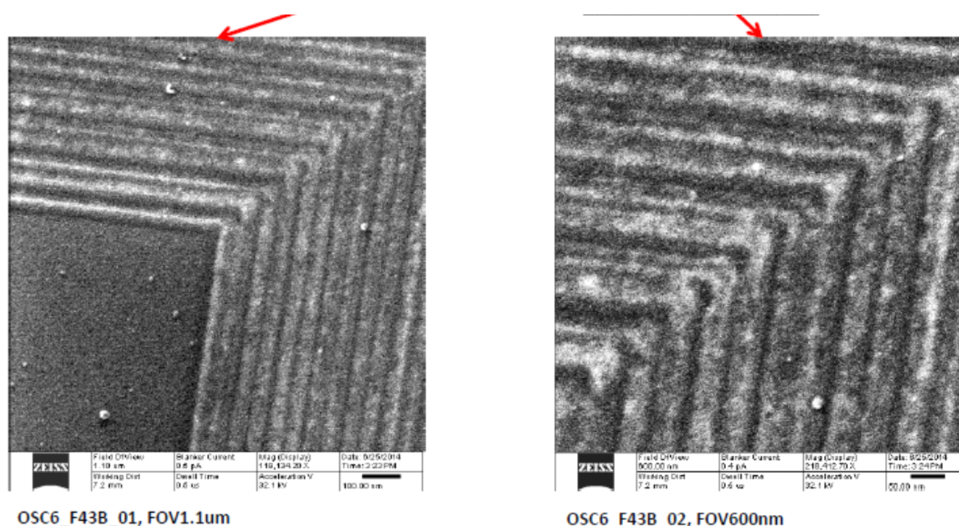

Figure 60. HIM images of SPL patterned calixarene on plane Si wafer surface showing absence of nanoparticles.

Figure 60 shows a typical example in which SPL lithography of calixarene on a plain Si wafer surface show no trace of the nanoparticle clusters seen in the calixarene/Au/Si wafers.

.

4.1.1. Conclusions

In conclusion, the second round of HIM imaging of SPL patterned samples has provided interesting results albeit with some imaging issues but with several areas for further investigation and discussion after SNM. In particular, it has been shown that nanoparticle decoration seen in resist trenches are the result of destabilization of the exposed gold underlayer in SPL patterned calixarene/Au/Si samples leading to liquid-like behavior in the Au film. This is confirmed by the absence of such nanoparticles in the case of plane silicon wafers with SPL patterned calixarene/Si. The presence of the dome structures is an indication of subsurface bubble formation due to implanted He during extensive HIM imaging.

4.2. HIM imaging of sub-10nm patterned Fullerene Resist

Considerable effort in SNM was committed to imaging of nanoscale patterns in the novel resists developed in WP5, in particular the customized fullerene system HM-01 from Irresistible Materials and OSC. Ultra high resolution images were produced using the ORION™ NanoFab Helium ion microscope in naopatterning mode (SHIBL) in WP4 and are reported in detail in deliverable D4.5 and in published form [2]. The results of He^+ ion beam lithography were invariably imaged in the same ORION™ tool operated in scanning microscope mode (HIM) as reported comprehensively in D4.5. A selection of these results is reproduced here.

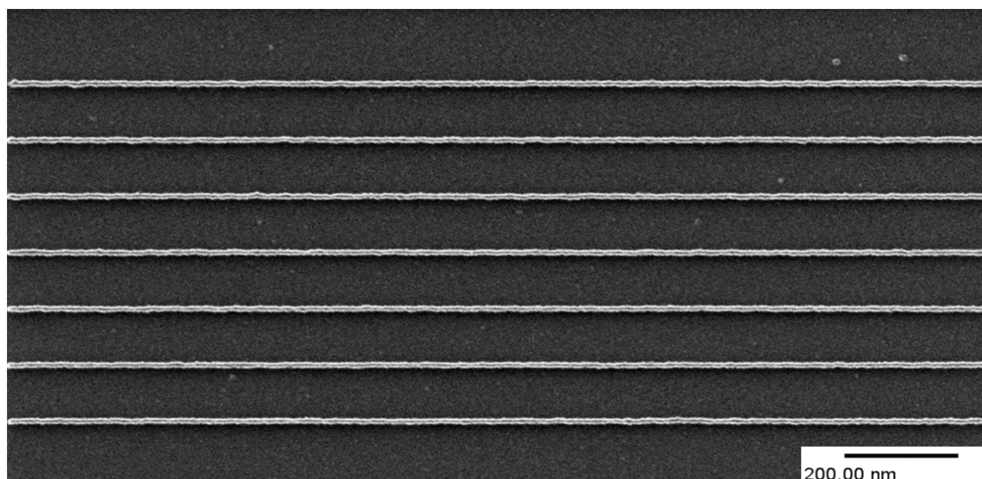

Figure 61. Isolated lines in HM-01 fullerene resist produced by SHIBL and imaged in the ORION™ HIM

The resist pattern in Figure 61 comprises 8nm Isolated Lines in HM01-AN (C_{60} in anisole solvent) produced by single pixel linescan. The HIM imaging conditions were as follows:

- Beam Energy: 30 keV
- Beam current: 0.5 pA
- Beam diameter: ~0.35-0.5 nm
- Number of lines per frame: 128
- Number of frames per image: 1

HIM is capable of resolving fine differences between optimal and sub-optimal resist images, without charging, as seen from this image and the exposure dose matrix in Figure 62. The HIM image is taken at 30keV and shows optimum CD of 7.2nm by resolving fine variations in the sparse line patterns as the line dose varies from underexposure to overexposure with clear identification through imaging of the optimum dose at 0.075nC/cm.

Funded by
the European Union

9.7nm underexposed 7.2nm optimal 8.3nm overexposed

0.045nC/cm 06nC/cm 0.075nC/cm 0.09nC/cm

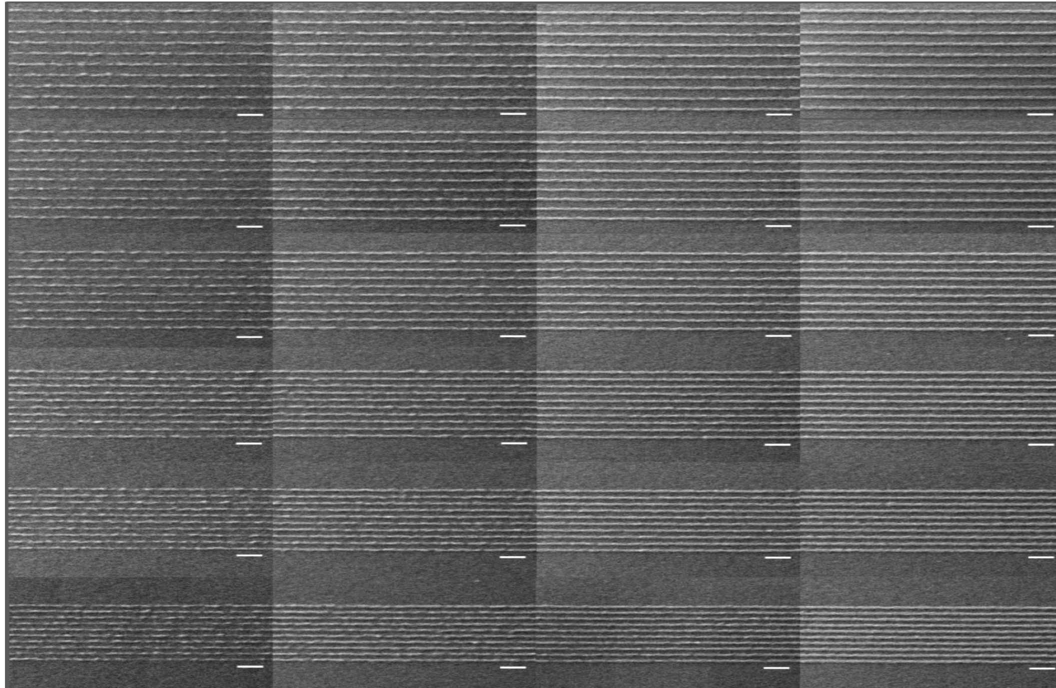

Figure 62. HIM image of line dose optimization matrix using SHIBL with HM01-AN spin coated resist (scale bar 50nm). HIM is capable of distinguishing between optimal and sub-optimal exposures.

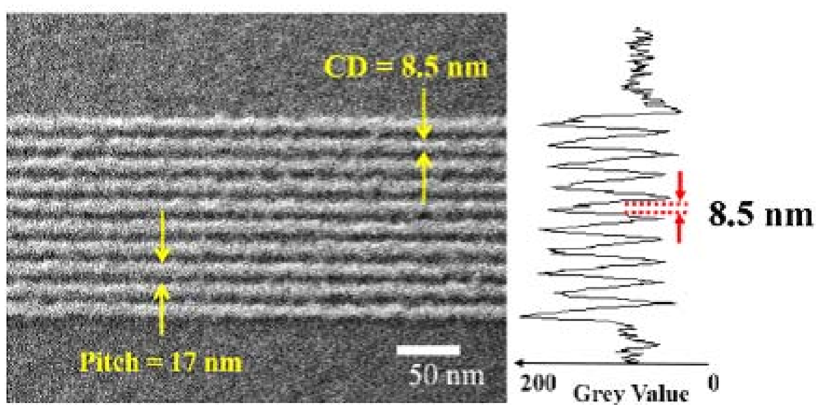

Figure 63. Left: HIM image of dense single pixel features in HM-01 fullerene resist 10nm thick on silicon. Right: Ion induced secondary electron (ISE) contrast measurement reveals 8.5nm lines on 17nm pitch.

Figure 63 is an HIM image of dense features in HM-01 with a pitch of 17nm as measured by the HIM and a linewidth CD of 8.5nm corresponding to a mark/space ratio of 1:1. The figure shows use of the CD measurement capability which utilizes a He^+ probe scan across the lines producing a cross line profile of the ISE signal from which the linewidth CD and line edge roughness (LER) can be extracted using the SUMMIT™ image analysis software from EUV Ltd. While the dense features are well defined at 8.5nm CD, the pattern begins to break up at 6nm CD due to shot noise effects (see D4.5 for a fuller discussion of the lithography process). It is important to note here that HIM has sufficient resolution to identify the missing pixels at 6nm linewidth and 1:1 pattern density, thus identifying the development of shot noise.

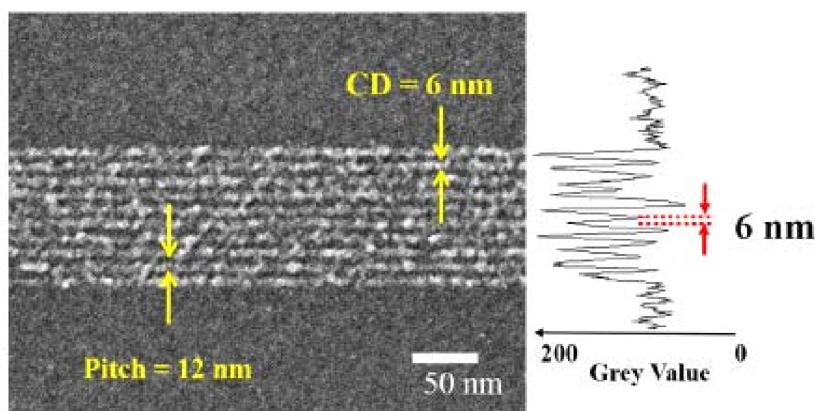

Figure 64. Left: HIM image of dense single pixel features in HM01 fullerene resist produced by SHIBL and imaged by HIM. Right: ISE contrast measurement showing missing pixels due to shot noise at linewidth CD of 6nm (pattern density 1:1).

The SUMMIT™ software package has been used in conjunction with HIM to measure CD and LER of these patterns with results as summarized in Table 1

Line Dose (nC/cm)	0.045	0.06	0.075	0.09
CD (nm)	6.77±1.73	7.68±2.2	7.3±1.3	8.3±1.2
LER (nm)	4.82±0.22	3.66±0.12	2.95±0.06	2.65±0.08

Table 1. HIM measurements of CD and LER as a function of line dose for SHIBL in HM01 fullerene resist using SUMMIT™ software with ISE profile.

In conclusion: the ORION™ tool as a dual purpose lithography and microscopy system has been used to investigate the limits of scanning He^+ ion beam lithography through its complementary nanolithography and high resolution microscopy capabilities. The dual function nature of the HIM tool ensures close tailoring of the metrology to the pattern generation capabilities by selection of identical ion probe characteristics for writing and imaging (30keV beam energy, ~0.4nm beam diameter, 0.5pA beam current). Then for writing lines, as for device gates, the beam is vector scanned at a typical line writing speed of 1nm/16µs, determined by the resist sensitivity. For imaging and metrology of the pattern produced, exactly the same beam settings are used to scan a single image frame of 128 horizontal lines at an acquisition rate determined by the sensitivity of the secondary electron detector unit.

The method has been used to write, image and measure HM-01 fullerene resist lines down to the shot noise limit of 6nm.

References

[1] Gregor Hlawacek, Vasilisa Veligura, Raoul van Gastel and Bene Poelsema J. Vac. Sci. Technol. B **32** (2014) 020801

[2] Xiaoqing Shi, Philip Prewett, EjazHuq, Darren M Bagnall, Alex P G Robinson and Stuart A Boden Microelectron Eng **15** (210) 74-78

5. TUIL: AFM measurements

5.1. Surface roughness measurement for characterization of resist materials

TUIL examined the resist surface of freshly prepared samples and of stored samples (3-11 months after receiving) to conclude on their stability and to investigate if aging effects occur. The surface roughness (Rq & Ra values) were measured by AFM using a defined tip (tip radius of curvature <5nm) as well as standardized protocol (1024 points/lines, 10x10 as well as 1x1 μm^2 scan area) in order to ensure a high comparability between the different measurements conducted during the 4 year project periods. Since TUIL has investigated more than 20 different resist materials, resist combinations and associated preparation methods we refer to D1.3 report or WP5 reports (D5.1, D5.2, D5.3, D5.4), wherein the gained surface roughness measurements are linked with decisive conclusions.

5.2. Regular AFM characterization of FE-SPL patterned features

AM-AFM topographic measurements of samples were carried out in order to characterize (a) the lithographic processes, (b) the resist materials as well as (c) the pattern transfer processes.

Since radiation-sensitive ultra-thin (typically sub-20 nm) resist films are applied for FE-SPL, SEM investigations prior a successful pattern transfer are not aimed [SEM exposure leads to crosslinking of the resist; In addition, in order to have a good topographic contrast coating with a thin metal layer is required, which inhibits further applications, e.g. for pattern transfer.]. Thus, analysis and evaluation of the lithographic processes itself was only possible by AFM methods. In this context, only AFM measurements were applied prior pattern transfer, whereas after a successful pattern transfer also SEM as well as xTEM (not carried out regularly since our access to xTEM at Imec was limited) are applied (ref. report section comparison between AFM, SEM and XTEM measurements).

Within the typical measurement process the sample is measured directly after exposure (=imaging of the positive tone self-development patterns), after wet developed (if applied in order to image the negative tone patterns), as well as after the applied pattern transfer processes (all plasma etching techniques applied during the entire project period) by using AM-AFM technique. The developed active cantilevers were applied. The AFM systems were calibrated prior the SNM benchmark by purchasable reference samples (e.g. Gratings as well as natural standards like HOPG). After the SNM benchmark, led by VSL, the systems were re-calibrated by using the SNM benchmark result. Limitations of the measurement caused by the tip (limitations of the measurement depth / errors in width measurement) are taken into account by calculation of the limitations and errors as function of tip and targeted geometric measurement range.

In this context, prior AFM imaging the tips are inspected by using SEM in order to ensure a tip radius of curvature suited to the features to be imaged (e.g. for sub-20nm features a tip radius of curvature of <10nm are required). Since typically a large amount of features are analyzed (e.g. features are patterned at different exposure parameters, different transfer steps are tested, etc.), an AFM pattern analysis program for automatic extraction of geometric feature data (line width, pitch, line depth, etc.) was developed. Here, directly after image acquisition the AFM topography image is sectioned and each section is analyzed, respectively. All geometrical feature data are recognized and the statistical mean value plus the standard deviation of the geometric data is determined, e.g. the line width or the line depth/height of a feature. Using the feature analysis software module the large amount of measurement data were analyzed required for lithographic performance evaluation of resist materials in frame of WP1 & WP5, analysis of pattern transfer processes in frame of WP1 & WP6, or analysis of patterned devices in frame of WP1 & WP8/9/10. Examples of AFM-based metrology applied at TUIL are summarized in Figure 70 and 71, respectively, showing the characterization of lateral as well as vertical dimensions of fabricated features.

Furthermore, during the entire project time TUIL has done standard AFM topographic investigations of diverse nanoscale lithographic features. Examples of different cases, wherein AFM metrology and analysis were applied, are summarized in Figure 66. The LER of lines was not investigated by using AFM methods since no standard protocols/routines at TUIL therefore were so far implemented. In the frame of the project LER investigations of FE-SPL patterned features were carried out by VSL.

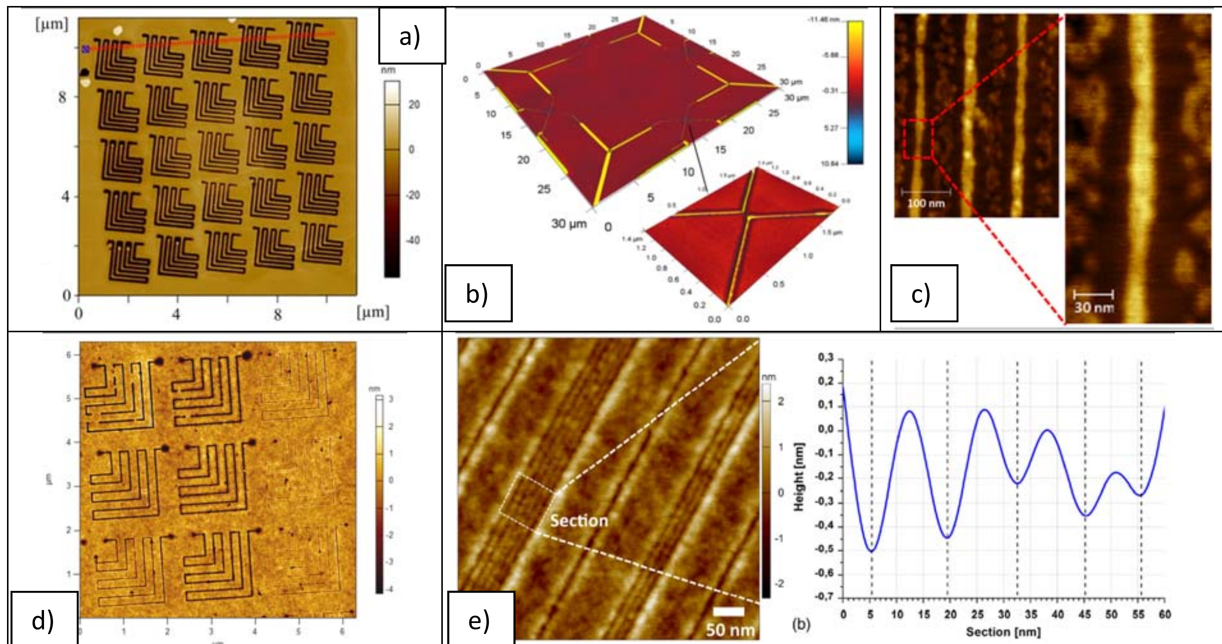

Figure 65. Excerpt of standard AFM topographic metrology carried out by TUIL during the entire project frame for: (a) Characterization of pattern transfer processes (in the example corner features transferred by cryogenic plasma etching); (b) Characterization of SET devices patterned by FE-SPL and transferred by cryogenic plasma etching; (c) Characterization of MoS2 patterns and devices patterned by FE-SPL; (d) Evaluation of dose tests, e.g. required for resist investigations; (e) Measurement of high resolution patterns (e.g. 7 nm hp pattern).

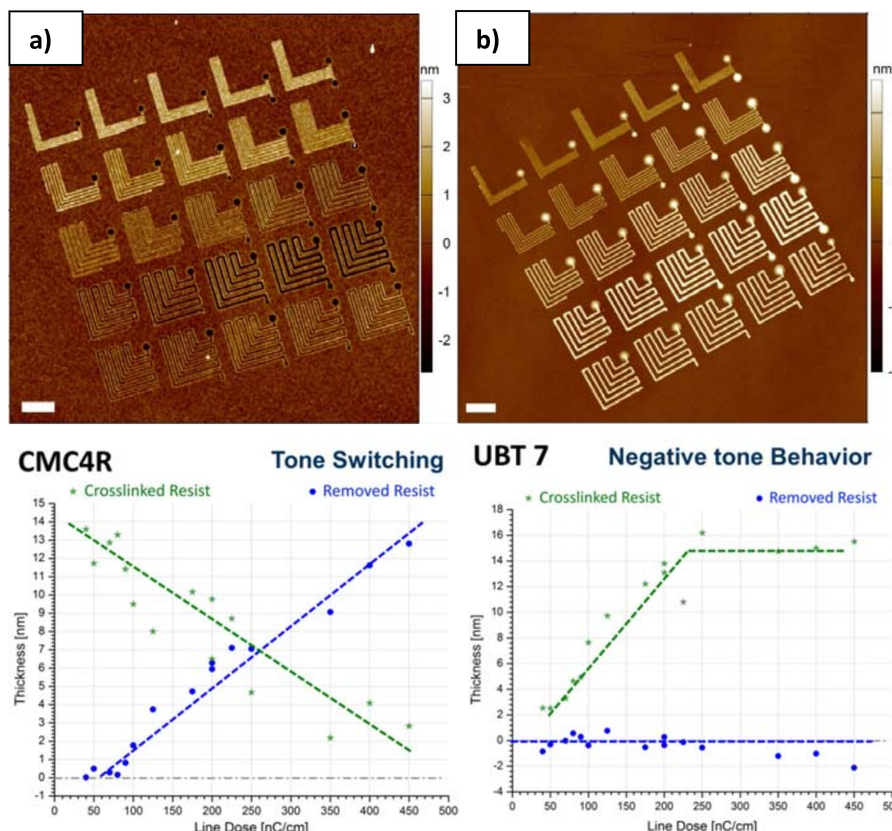

Figure 66. AFM metrology applied for measurement of resist thickness as function of exposure dose. Example of an exposure dose test using AFM metrology and subsequent automatic feature analysis in order to compile resist thickness vs. line dose graphs for evaluation of resist materials.

5.3. AFM measurement of 10 nm hp dense line/space features, patterned by FE-SPL, for AFM measurement comparison between TUIL & VSL (ref. section 2.2 for description of VSL measurements)

5.3.1. Sample description and lithographic definition of the 10 nm hp pattern:

A test chip with 10 nm half-pitch (hp) dense line/space patterns was prepared by TUIL. In particular, a test chip [FDSOI chip (15x15 mm); SOI layer thickness 12+/-1 nm, <100>, p-doped 9-15 Ωcm] was PVD-coated by SNM project partner UBT (WP5) with a 10 nm thick uniform resist layer. In particular, the novel two-component molecular glass resist UBT8+C60 was applied, which was identified as one of the most promising ultra-thin resist material combination (collaboration between WP1-WP5-WP6). The resist layer was prepared via co-evaporation in a ratio of 1:1 (UBT8:C60). As found out, this material combination gives highest lithographic resolution, a long-term stability as well as excellent plasma etching durability. Details on the performance capability are summarized in deliverable report D1.3, D1.6, D5.1, D5.2, D5.3, respectively. The prepared two-component molecular glass resist thin films give ultra-smooth surfaces verified via AFM roughness measurements.

By field emission scanning probe lithography (FE-SPL) [details are provided in WP1-reports] 10 nm hp features were patterned directly into the resist layer using the positive tone, development-less scheme

developed at TUIL (development-less, or also called self-development mode, ref. deliverable report D1.3). Since the patterning scheme is self-developing no subsequent development step was applied. A pattern transfer of the features was not carried out since the characterization of the resist features itself was targeted.

5.3.2. AFM measurement at TUIL

Directly after patterning the 10 nm hp features were characterized by AFM at TUIL. The home-built FE-SPL technology platform system based on the active cantilever technology (thermally actuated with piezoresistive readout, ref. WP1) was applied for in-situ AFM measurements. The measurements were carried out directly after patterning by using the same cantilever as applied for lithography (closed loop FE-SPL scheme).

Active cantilever characteristics:

Cantilever type	Active cantilever developed and fabricated at TUIL
Tip height	4-6 µm
Tip radius	<10 nm
Nominal resonance	~100 kHz
Tip shape	Pyramidal

The FE-SPL technology platform developed in WP1 was calibrated via standard samples (height and pitch standards) purchased from commercial companies (e.g. nano and more Germany). The SNM benchmarking test among all SNM project partners was carried timely after the 10 nm hp patterning test. Thus, re-calibrations as a result from the benchmarking test were not included herein. The measurements were performed in ambient conditions (temperature: 26 +/-1 °C, humidity: 31.5% r.h. +/- 2% r.h.). Imaging was carried out in AC-AFM mode with closed loop in X-, Y- and Z- direction.

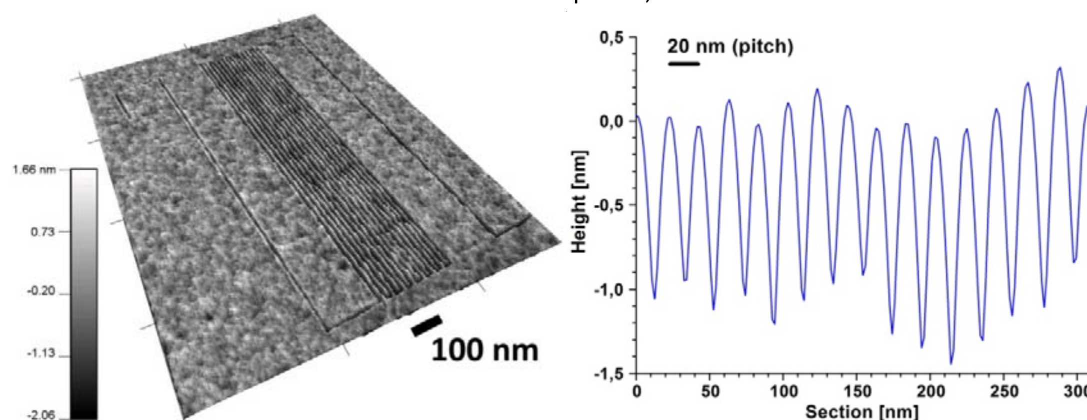

Figure 67. AFM topographic image of the 10 nm hp feature with corresponding section graph (section: perpendicular to the line/space pattern; averaging over 420 single lines; no tip deconvolution algorithm / tip shape correction was applied).

The fast scan axis was perpendicular orientated to the line features. The topographic AFM image with corresponding section perpendicular to the line/space pattern is shown in Figure 67. An image of 1.85 x 1.85 µm with a resolution of 1024 points & lines was taken, which gives a measurement resolution of 1.8 nm. A scan rate of 1 Hz (= 4.5 µm/s scan speed) was used.

5.3.3. Data evaluation

The raw AFM image was flattened. No further post-processing actions like averaging or filtering were carried out. No deconvolution algorithm / tip shape correction was applied. The section profile was averaged over 420 single line sections. Afterwards, the line (=groove) width, the line pitch as well as the line (=groove) depth were calculated from the averaged profile using the automatized AFM feature analysis software (explained prior). The line depth was measured from topmost side points of the line and the local minima. The line width was measured at 50% (FWHM) of the particular line depth of each single line. The line-to-line distance (averaged = pitch) was measured from the actual line minima to the neighboring line minima. LWR and LER could not be determined since the measured groove depth is, compared to the surface roughness, too small. An automated detection of the line edges with respect to the surrounding area has failed.

5.3.4. Measurement results and discussion

The measurement results are summarized in the following table:

Line	Groove Width (FWHM)	Line Pitch	Groove depth
[#]	[nm]	[nm]	[nm]
1	8.32	21.78	1.08
2	7.88	18.15	0.94
3	8.00	19.97	1.17
4	7.61	19.97	1.08
5	8.02	19.97	1.23
6	7.87	19.97	1.20
7	8.29	19.97	1.10
8	7.91	19.97	0.94
9	7.88	19.97	1.24

10	7.90	18.15	1.29
11	8.05	21.78	1.37
12	8.58	19.97	1.30
13	8.80	21.78	1.30
14	8.59	21.78	1.38
15	7.87		1.04
Average	**8.10**	**20.22**	**1.18**
Standard Deviation	**0.34**	**1.20**	**0.14**

An average FWHM of the lines of 8.10+/-0.34 nm was measured. The line pitch is determined with 20.22+/-1.2 nm, which agrees very well with the targeted pitch of 20 nm. A groove depth of 1.18+/-0.14 nm was measured. Taking into account a probe tip radius from 5-10 nm, the groove depth (10 nm resist) cannot be reached and thus quantified. For example, in Figure 68 the tip-sample geometrical depth measurement limitation is calculated for various tips. By a red circle our measurement area is marked, respectively, showing that at 10 nm hp dense line/space features the measurement depth is limited in the order of 1-3 nm (depending on the exact tip shape and tip characteristics). Thus, we are working at the geometrical measurement limit of the tip. This is also indicated by the groove width versus depth plot, Figure 69.

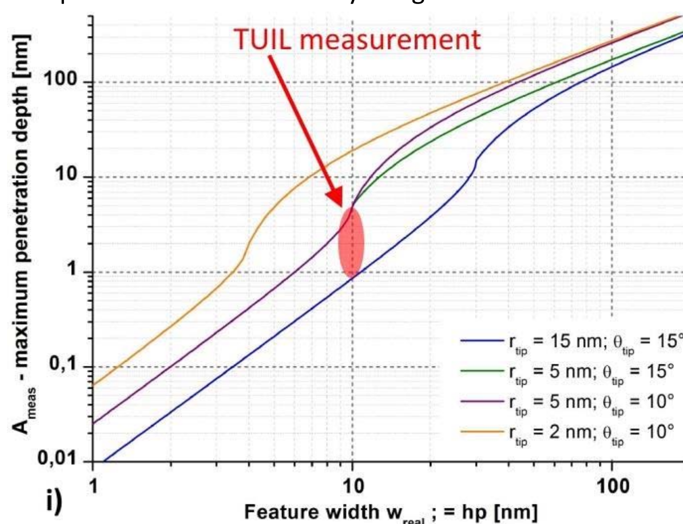

Figure 68. Geometrical limitation in line depth measurement. The maximum penetration depth is calculated as function of feature pitch for diverse tip properties (tip radius and cone half angle).

Funded by
the European Union

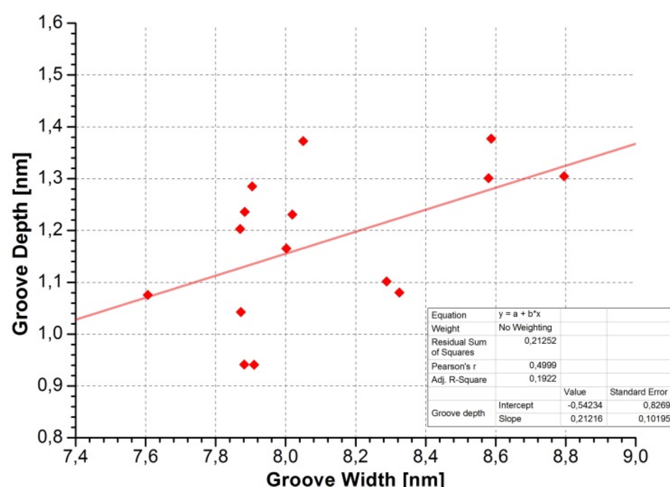

Figure 69. Groove depth vs. width (FWHM) of the lines measured by AFM (Figure 67).

5.4. AFM vs. SEM vs. XTEM measurements of FE-SPL patterned and by ALE transferred line features

Three measurement samples were prepared by FE-SPL (TUIL, WP1) and subsequent etched with either ALE at OINT (sample number 1 and 2) or cryogenic plasma etching at TUIL (sample number 8). AFM images were obtained after FE-SPL, ALE and resist strip at TUIL using a commercial calibrated AFM system. Cantilever with a guaranteed tip radius of curvature of less than 5 nm (typical tip radius of curvature of 2 nm specified) were applied in order to ensure highest measurement resolution. SEM images were acquired after resists strip with a Helios 600i system at TUIL (SEM imaging prior pattern transfer was not carried out since the resist material is radiation sensitive). After resist strip and final measurements (AFM & SEM) at TUIL, xTEM measurements were acquired at IMEC. AFM images were analyzed using profile function of Gwyddion. Line widths of SEM images were measured with the Helios analysis software. xTEM images were analyzed using ImageJ.

Only for sample 1 a comparison of all three measurement methods was possible. The patterned field on sample 1 is shown by SEM and AFM in Figure 70. On the other samples the identification of patterns in xTEM measurements was not clear (most probably not the same patterns were imaged).

SEM image of sample 1 pattern	AFM image of sample 1 pattern

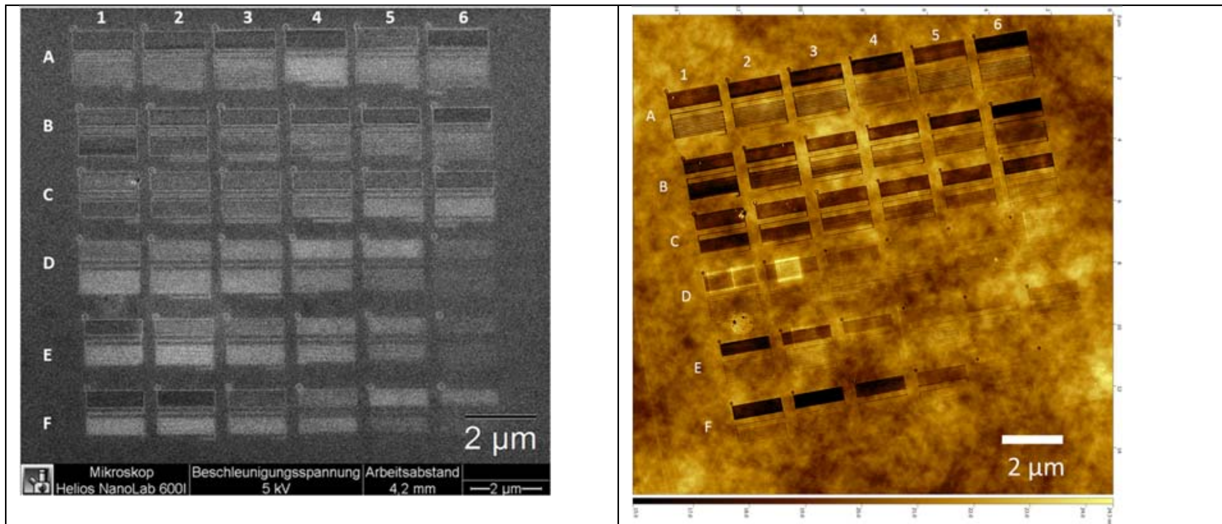

Figure 70. SEM and corresponding AFM topographic image of sample 1 features patterned via FE-SPL (TUIL) and transferred by atomic layer etching (OINT).

Three fields were measured in higher resolution. The SEM and AFM images of the in detail analyzed patterns are summarized in Figure 71. The corresponding xTEM measurements (IMEC) of the 30 nm (D-features) and 25 nm pitch (E-features) patterns are shown in Figure 72.

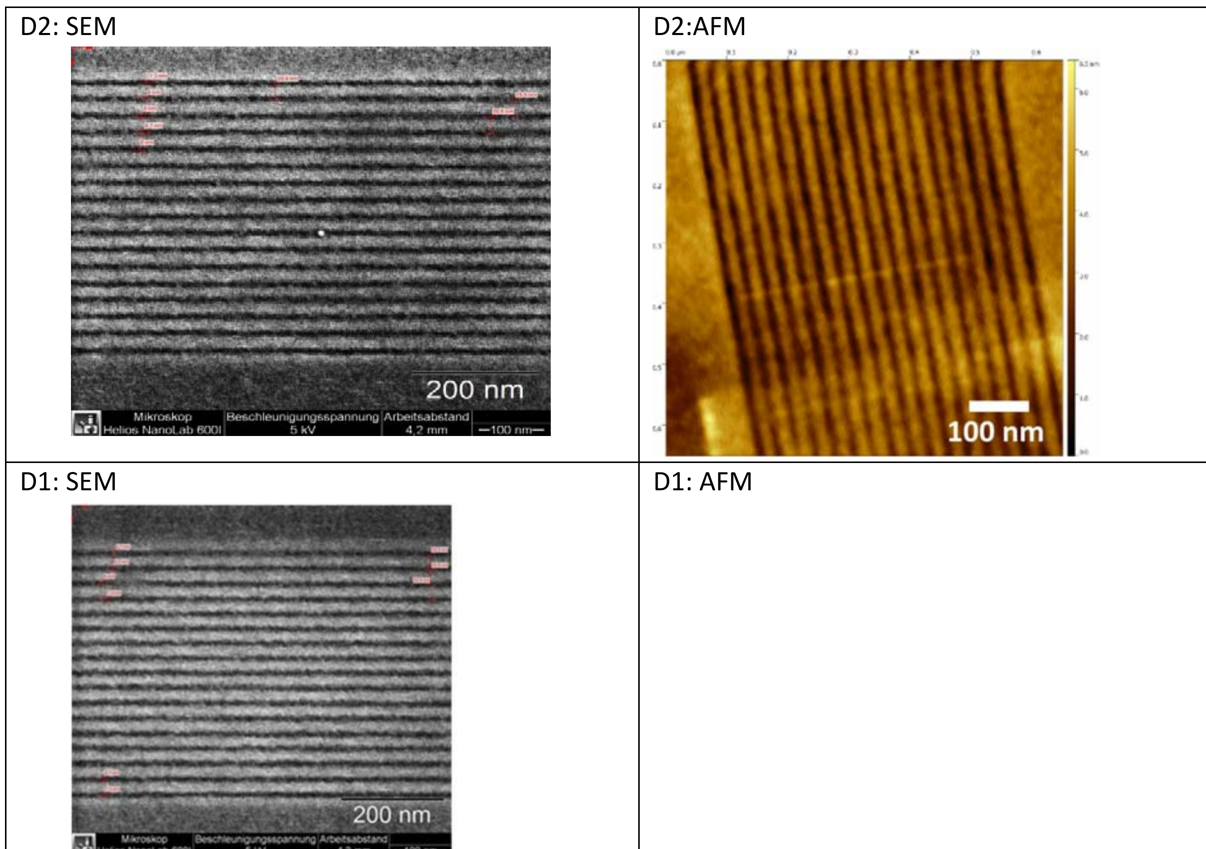

Funded by
the European Union

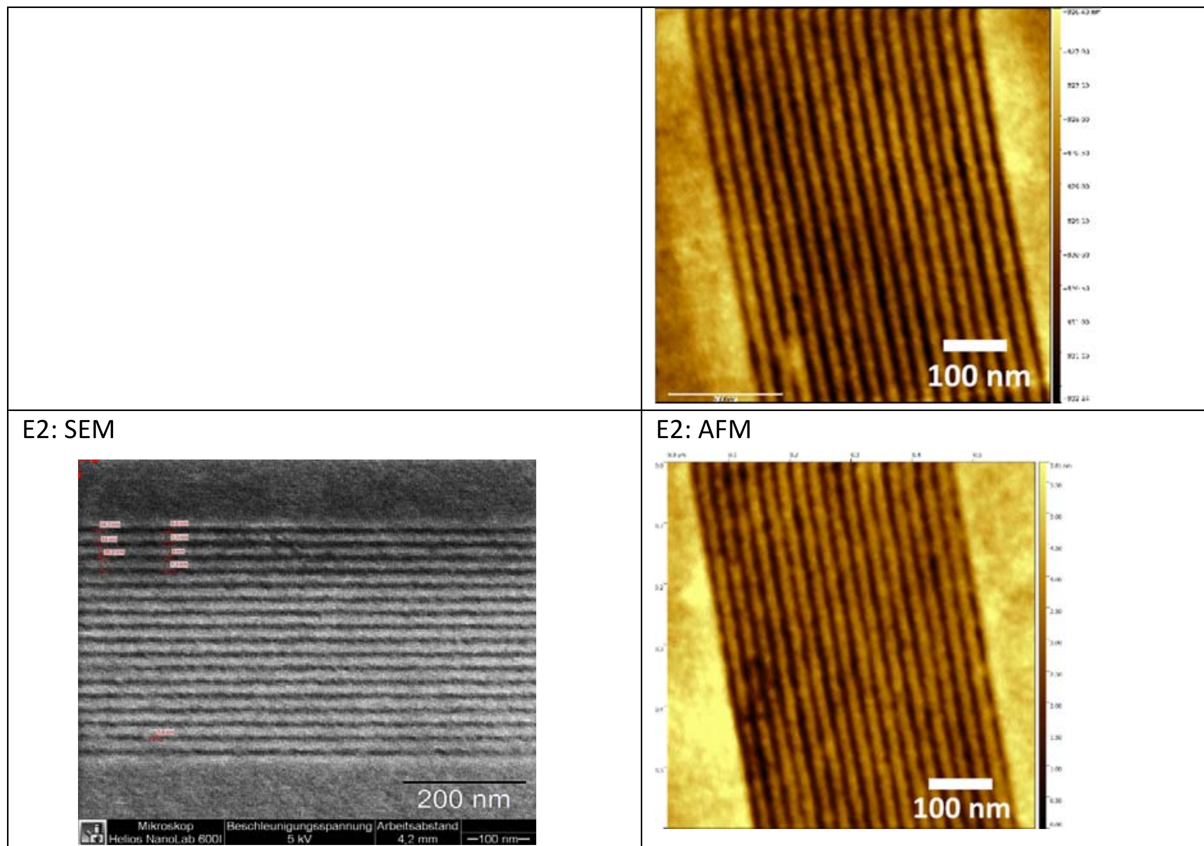

Figure 71. SEM (left column) and AFM topographic (right column) images of the in detail analyzed patterns D2, D1 and E2.

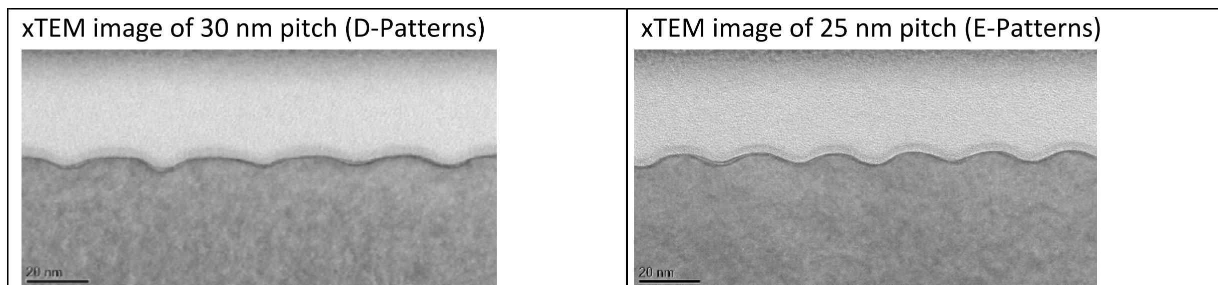

Figure 72. Corresponding xTEM measurement (by IMEC) of the 30 nm and 25nm pitch patterns of sample 1.

Summary of the measurement results:

- *Comparison of pitch measurements*: Values for pitch measurements are comparable within uncertainty with largest standard deviation (SD) of measurements for SEM (measurement values in [nm]):

Field	***D2 (30nm)***	***D2 (30nm)***	***D1 (30nm)***	***D1 (30nm)***	***D (30nm)***	***D (30nm)***	***E2 (25nm)***	***E2 (25nm)***	***E (25nm)***
Meas. No.	**Pitch (SEM)**	**Pitch (AFM)**	**Pitch (SEM)**	**Pitch (AFM)**	**Pitch (xTEM)**	**Pitch (xTEM)**	**Pitch (SEM)**	**Pitch (AFM)**	**Pitch (xTEM)**
Mean	29.563	30.784	28.856	30.685	30.411	30.640	24.386	25.206	25.661
SD	2.047	1.828	2.709	1.209	1.113	1.647	1.677	0.768	0.476

Min	26.763	27.779	23.806	29.036	29.315	28.188	21.484	23.613	25.172
Max	32.904	34.243	32.528	32.835	31.781	33.237	26.953	26.155	26.259

- *Comparison of line width measurements*: Values for line width measurements are comparable within uncertainty for SEM and xTEM for patterns with 30 nm pitch (D-features), as well as for SEM, AFM and xTEM for patterns with 25 nm pitch (E-features). The line width is enlarged in case of AFM measurements for structure D2 whereas for pattern D1 and E2 the obtained line width is similar to the xTEM and SEM results. This could be attributed to tip convolution effects (no deconvolution routine applied) or measurement error. The line width was measured at 50% of maximum peak height (FWHM value). Smallest line width values were measured with SEM (5.8 nm). Largest standard deviation of measurements was observed again for SEM measurements. This could be caused by the smaller resolution of the taken images.

Field	***D2 (30nm)***	***D2 (30nm)***	***D1 (30nm)***	***D1 (30nm)***	***D (30nm)***	***D (30nm)***	***E2 (25nm)***	***E2 (25nm)***	***E (25nm)***
	LW (SEM)	LW (AFM)	LW (SEM)	LW (AFM)	LW (xTEM)	LW (xTEM)	LW (SEM)	LW (AFM)	LW (xTEM)
Mean	10.636	14.462	14.002	14.321	10.932	11.247	10.796	12.222	11.837
SD	2.867	1.281	3.213	1.169	1.013	0.960	3.114	1.604	1.082
Min	5.875	12.178	9.804	12.378	10.000	9.420	7.432	9.276	10.340
Max	17.239	16.368	20.612	15.721	12.603	13.087	17.969	14.991	13.334

- *Comparison of line depth measurements:* Line depth was measured by AFM and xTEM. Values for Line depth are comparable for AFM and xTEM measurements.

Sample – feature	**Line depth AFM [nm]**	**Line depth xTEM [nm]**
S1 - 25nm pitch	2-2.5	3-3.5
S1 - 30nm pitch	2.6-3.2	2.5-3

A comparison between the measurement methods for the other two samples (sample number 2 and 8) could not be obtained since either different structures were imaged by xTEM (no high-resolution AFM/SEM for this region are taken – in case of sample 2) or no pattern was detected within the xTEM image (in case of sample 8).

5.4.1. Conclusion

Concluding, SEM, xTEM and AFM yielded comparable results regarding pitch, line depth and line width measurements. SEM measurements exhibited a larger variation in line width and pitch values, which could be caused by the lower resolution of the images or the larger amount of measurements (values extractable from profiles) in case of SEM images. In xTEM measurements, only 4-6 values for the line width, pitch and line depth could be obtained. As outcome of this study TUIL has verified its measurement results obtained by AFM and SEM by xTEM measurements at Imec. In this context, since xTEM is destructive, time-consuming and TUIL has only limited access, AFM and SEM are applied as standard metrological tools at TUIL.

6. IBM: line edge roughness in t-SPL processed samples.

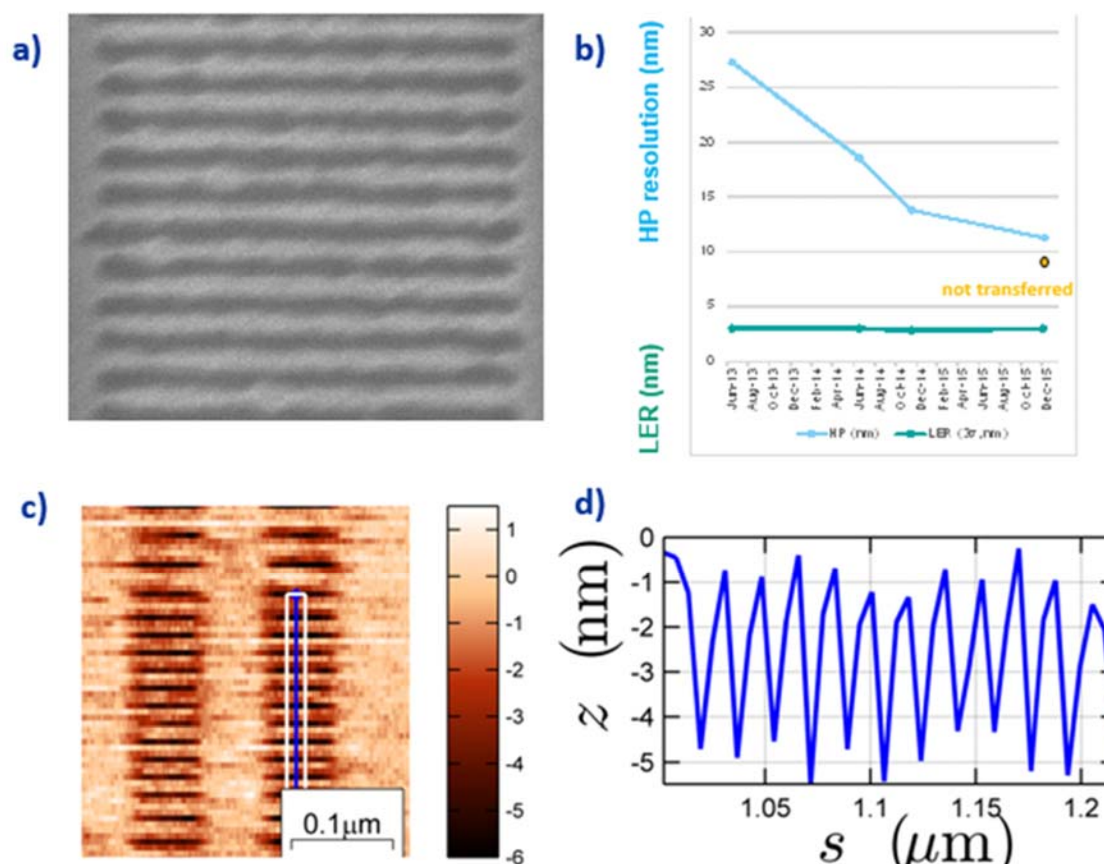

Figure 73: a) SEM image of the 11 HP line pattern after transfer into 20 nm of HM8006. b) Half-pitch density of transferred patterns and line edge roughness (3σ) as a function of time. c) AFM image recorded in tSPL tool of 8.9 nm half-pitch pattern written in a 5 nm thick PPA layer. d) Line cross-section showing uniform patterning depth corresponding to the PPA layer thickness.

Figure 73 shows the state of the art t-SPL patterning achieved during this project. For IBM the emphasis was the characterization of transferred patterns. Figure 73 a) shows the record density result of a transferred pattern. A half-pitch density of 11 nm Full into the HM8006 polymer mask layer was achieved. The measured line edge roughness in this image was approximately 3 nm (3σ). Figure 73 b) shows the evolution of the patterning density and line edge roughness (3σ) over the past 3 years, see also Ref [1]. 2013 and 2014 were characterized by a fast rate of density improvement by nearly a factor of two per year. It looks now that we have reached saturation of the progress approaching 10 nm half-pitch density in transferred patterns. Interestingly, the line edge roughness has remained at a constant level of approximately 3 nm (3σ) indicating that it is limited by a fundamental property of the polymer most likely related to the chain structure itself.
Even higher resolution could be achieved in the polymer resist. Figure 73c) shows the surface topography of a deeply structured PPA film at half-pitch density of 8.9 nm. The corresponding line cross-section, Figure Figure 73d), demonstrates that excellent patterning has been achieved resulting in a uniform topography contrast at such densities.
The measurement procedure for the line edge roughness assessment is mentioned in Ref. [2]. The line edge roughness is determined from SEM images of straight trench patterns. The line edge contour inside

a trench is set to the pixel positions at 80% of the maximum intensity level. The pixel contour is fit to a straight line and the rms deviation corresponding to the 1σ roughness value is calculated numerically. The roughness is obviously strongly correlated as can also be seen in the power spectrum, Figure 81, and long wave length roughness components clearly dominate. The white noise background level arises from the intrinsic noise in the SEM image and has no physical significance.

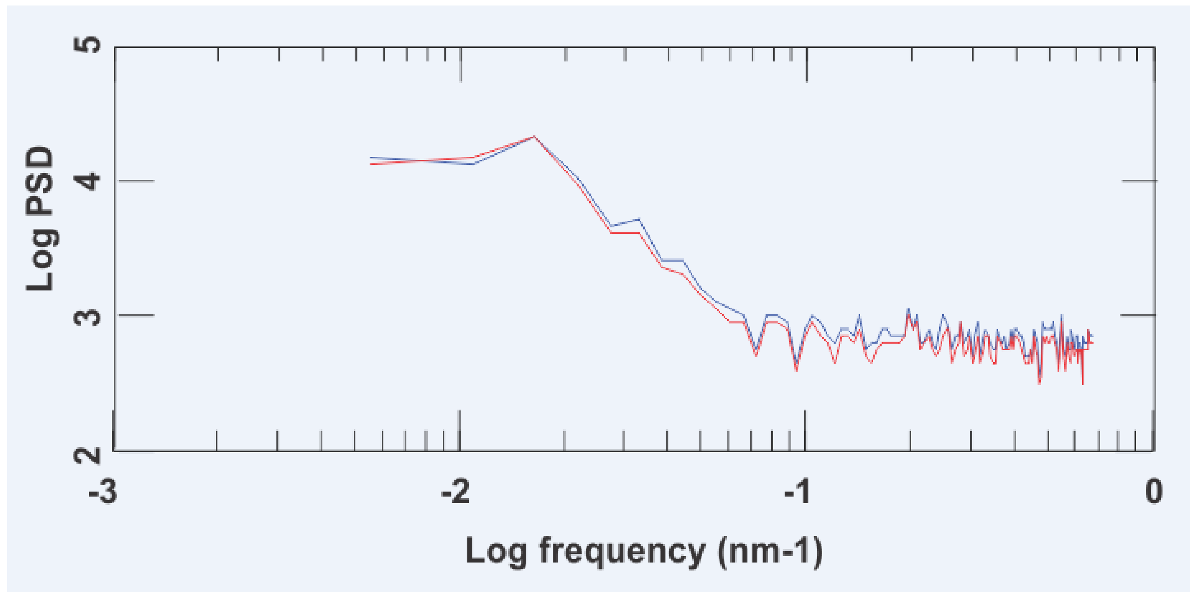

Figure 74: Typical power spectrum of the line edge profile determined from SEM images of transferred structure.

We found that the measured line edge roughness after transfer depends on the process. Best results were obtained for ion-milling of high resolution structures into thin (20 nm) gold layers, see Figure 75. Dense lines of 17.6 nm half pitch were written on the high resolution stack (20 nm HM8006, 2.5 nm SiO_2, 2.5 nm PMMA and 7 nm PPA) and transferred from the HM8006 mask into the gold layer by Ar^+ ion milling. The line edge roughness was found to be lower than in the typical silicon transfer results. We measured an average line edge roughness of 2.1 ± 0.4 nm, the error is given by the standard deviation of the LER values of the individual lines. The measured CD was 17.6 nm for the lines.

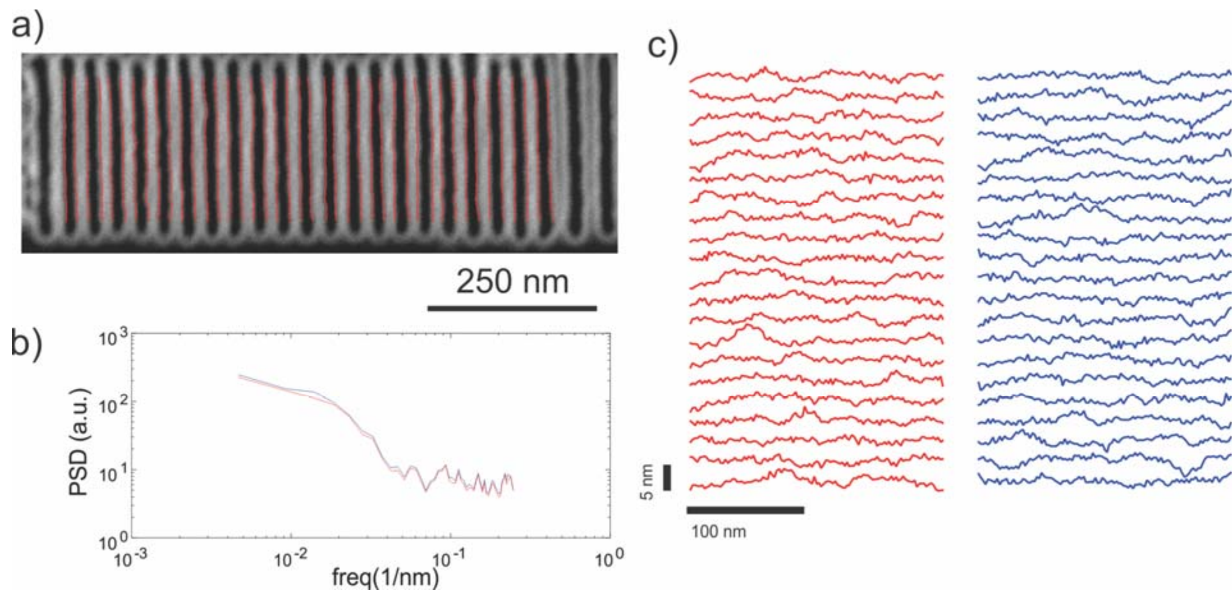

Figure 75: Line edge roughness analysis for the ion milling process: The resulting LER was 2.1 ± 0.4 nm. a) SEM image of the fabricated dense lines. Contour lines of the edge detection are overlaid in red. b) Average power spectral density (PSD) of the lines (red and blue denote the left and right side of the lines). c) All contour lines measured in the process. Red and blue denote left and right edges of the lines.

6.1. STEM cross sections

Patterns were written by tSPL at 13.7 nm half pitch and transferred into the silicon layer of the IMEC SNM chips. A 45 nm thick layer of SiOx was deposited by PECVD. After Pt deposition, a 50-100 nm thick lamella was cut out by FIB. The lamella was inspected by STEM (JEOL ARM200F double corrected microscope operated at 200 kV), see Figure 4. The observed spacing is consistent with the targeted tSPL half pitch values. The close-up of the silicon lines reveals the atomic lattice of silicon. The height of the structures was approximately 7.7 nm. The line width was approximately 7 nm with a variation consistent to our observed line edge roughness of 3 nm (3 sigma).

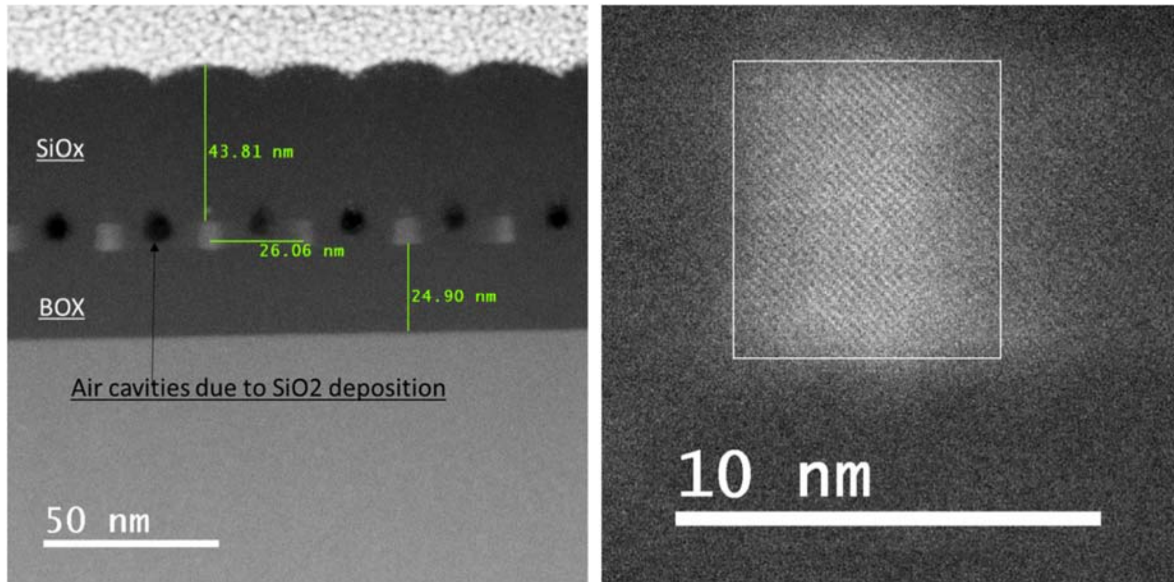

Figure 76: STEM images of the fabricated 13.7 nm half pitch silicon lines.

References:

[1] H. Wolf *et al.*, *J. Vac. Sci. Technol. B*, 33, 02B102 (2015)
[2] Cheong et al., *Nano Lett.* 13, 4485 – 4491 (2013)